



8-2001

**Advanced off-column technologies for capillary electrophoresis :
microfluidic deposition, two-dimensional separations, and
surface-enhanced Raman scattering-based detection**

Gerald Lynn DeVault

Follow this and additional works at: https://trace.tennessee.edu/utk_graddiss

Recommended Citation

DeVault, Gerald Lynn, "Advanced off-column technologies for capillary electrophoresis : microfluidic deposition, two-dimensional separations, and surface-enhanced Raman scattering-based detection. " PhD diss., University of Tennessee, 2001.
https://trace.tennessee.edu/utk_graddiss/8490

This Dissertation is brought to you for free and open access by the Graduate School at TRACE: Tennessee Research and Creative Exchange. It has been accepted for inclusion in Doctoral Dissertations by an authorized administrator of TRACE: Tennessee Research and Creative Exchange. For more information, please contact trace@utk.edu.

To the Graduate Council:

I am submitting herewith a dissertation written by Gerald Lynn DeVault entitled "Advanced off-column technologies for capillary electrophoresis : microfluidic deposition, two-dimensional separations, and surface-enhanced Raman scattering-based detection." I have examined the final electronic copy of this dissertation for form and content and recommend that it be accepted in partial fulfillment of the requirements for the degree of Doctor of Philosophy, with a major in Chemistry.

Michael J. Sepaniak, Major Professor

We have read this dissertation and recommend its acceptance:

Kelsey Cook, Ziling Xue, Gary Sayler

Accepted for the Council:

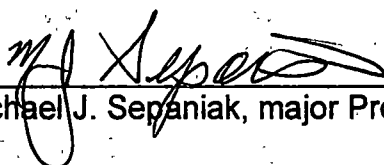
Carolyn R. Hodges

Vice Provost and Dean of the Graduate School

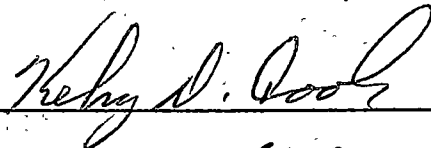
(Original signatures are on file with official student records.)


To the Graduate Council:

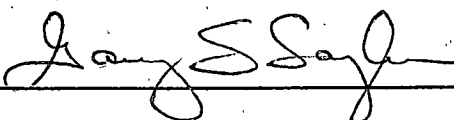
I am submitting herewith a dissertation written by Gerald Lynn DeVault entitled "Advanced Off-Column Technologies for Capillary Electrophoresis: Microfluidic Deposition, Two-Dimensional Separations, and Surface-Enhanced Raman Scattering-Based Detection." I have examined the final copy of this dissertation for form and content and recommend that it be accepted in partial fulfillment of the requirements for the degree of Doctor of Philosophy, with a major in Chemistry.


Michael J. Sepaniak, major Professor

We have read this dissertation
And recommend its acceptance:







Accepted for the Council:



Interim Vice Provost and
Dean of the Graduate School

**ADVANCED OFF-COLUMN TECHNOLOGIES
FOR CAPILLARY ELECTROPHORESIS:
MICROFLUIDIC DEPOSITION,
TWO-DIMENSIONAL SEPARATIONS, AND
SURFACE-ENHANCED RAMAN SCATTERING-
BASED DETECTION**

A Dissertation

Presented for the

Doctor of Philosophy

Degree

The University of Tennessee, Knoxville

Gerald Lynn DeVault

August, 2001

Dedication

This dissertation is dedicated to my family

Lori and Jack DeVault

and to my parents

Barbara and Clyde DeVault

for their support, encouragement, and understanding.

Acknowledgements

While attending graduate school, I maintained a full-time job with Lockheed Martin in Oak Ridge. Obtaining a Ph.D. in this manner would not have been possible without the support of my colleagues and mentors. Foremost, I would like to acknowledge Professor Michael Sepaniak. What I have learned under the direction of Dr. Sepaniak, both technical and professional, will be a valuable source for the remainder of my career. I also wish to thank my other committee members: Professors Kelsey Cook, Ziling Xue, and Gary Sayler.

In addition, I have many people to thank at Lockheed Martin. First, I would like to thank my supervisor, Dr. Ray Hinton. He has always supported my career, sometimes in less than ideal circumstances. I owe a great deal of gratitude to Dr. Robert Smithwick, his breadth of technical knowledge never ceases to amaze me. I would also like to thank Sam and Dr. Linda Lewis for their advice throughout this process. Dr. Bill Partridge and Dr. John Storey of Oak Ridge National Laboratory have offered continued support with technical advice and equipment that made much of the work reported herein possible.

Last but not least, I would like to thank the graduate students who have been a part of the Sepaniak Group for my tenure at UT. It has been a truly enjoyable experience to be a part of this group.

Abstract

Capillary electrophoresis (CE) is a widely accepted technique for performing high-efficiency liquid separations. The utility of CE separations could be increased by comprehensively depositing the capillary effluent onto a planar substrate, thus essentially preserving the separation to allow the application of off-column technologies. Electrospray is a convenient technique for continuously transferring column effluent from capillary-to-planar format. Conditions are optimized to produce a narrow ($\sim 20 \mu\text{m}$) liquid filament (electrofilament), which is capable of depositing spatially focused bands with track widths that are routinely $100\text{-}200 \mu\text{m}$. A fiber optic-based laser-induced fluorescence cell is employed to monitor the separation on-column while the separated bands are deposited onto a moving substrate. The electrofilament (EF) technique is evaluated based on its ability to deposit spatially focused bands, which preserve the on-column separation performance.

The EF technique was used to couple CE with thin-layer chromatography (TLC) to demonstrate a convenient technique for performing two-dimensional microseparations. The TLC plate stores the separation from the CE capillary in the first dimension and then serves as the stationary phase for the separation in the second dimension. To demonstrate this technique, dansylated derivatives of select amino acids are separated in the first dimension by micellar electrokinetic chromatography, and in the second

dimension their enantiomers are separated by reversed-phase TLC using a mobile phase that contains cyclodextrins as a chiral reagent. Prior to TLC development, off-column CE efficiencies of 130,000 to 190,000 plates per meter were obtained. The enantiomers of four DNS-amino acids are baseline resolved and a significant improvement in peak capacity over the one dimensional separation is demonstrated.

Surface-enhanced Raman scattering (SERS) is employed to obtain distinctive spectra for compounds that are separated by CE and EF deposited onto planar SERS-active substrates. A simple method is described that explains how to prepare SERS-active substrates by depositing a silver-colloid solution onto frosted-glass microscope slides. Scanning electron micrographs reveal a layered coating of fairly uniform-sized, 100-nm silver nanoparticles with interstitial spaces ranging from a few to tens of nanometers. The test compounds used to demonstrate this technique include compounds of biological significance: benzyloxyresorufin, riboflavin, and resorufin. Characteristic spectra with major Raman bands exhibiting signal-to-noise of greater than 3 were obtained for a 3.2-nL injection of 10^{-6} M (706 fg) resorufin. Forming a self-assembled monolayer on the substrate increases the sensitivity of the SERS technique and decreases the on-substrate broadening of deposited bands.

Preface

One valuable aspect of my graduate work has been my introduction to scientific literature. Every month, there are a tremendous number of published articles relating to all aspects of science. Analytical chemistry is a cornerstone of many of these articles. Whether the research involves organic synthesis, fundamental study of chemical principles, or the introduction of new pharmaceutical drugs, analytical chemistry provides the means by which research is verified. Therefore, it is extremely important to continually push the boundaries of analytical instrumentation. Since I have been at the University of Tennessee, the goal of my research has been to expand the applicability of capillary electrophoresis beyond that which is attainable with conventional instrumentation.

This dissertation is arranged into four chapters. The first chapter is an introduction into the technology that is relevant to the presented research, specifically capillary electrophoresis and various detection methods. Although this is not a comprehensive review, it covers the basics that will allow the reader to better understand the proceeding research chapters. The next three chapters are modified versions of the following research articles:

Nirode, W.F.; DeVault, G.L.; Sepaniak, M.J. *Anal. Chem.* **2000**, *72*, 1866.

DeVault, G.L.; Sepaniak, M.J. *Electrophoresis* **2000**, *21*, 1320.

DeVault, G.L.; Sepaniak, M.J. J. Microcolumn Separations **2000**, 12, 419.

DeVault, G.L.; Sepaniak, M.J. Electrophoresis **2001**, in press.

Certain areas have been expanded to increase the readers' understanding and other areas have been reduced to eliminate repetitiveness.

Table of Contents

Chapter 1. CAPILLARY ELECTROPHORESIS.....	1
Introduction	1
Separation Theory	4
<i>Electrophoresis</i>	<i>6</i>
<i>Electroosmotic Flow.....</i>	<i>7</i>
Analytical Parameters	10
<i>Migration Time</i>	<i>10</i>
<i>Resolution</i>	<i>12</i>
<i>Efficiency</i>	<i>13</i>
Select Modes of CE	15
<i>Capillary Zone Electrophoresis</i>	<i>16</i>
<i>Micellar Electrokinetic Chromatography</i>	<i>16</i>
<i>Cyclodextrin Capillary Electrophoresis</i>	<i>20</i>
Injection Techniques	23
<i>Hydrodynamic Injection</i>	<i>24</i>
<i>Electrokinetic Injection</i>	<i>25</i>
Detection Techniques	26
<i>Ultraviolet and Visible Absorption</i>	<i>31</i>
<i>Laser-Induced Fluorescence</i>	<i>34</i>
<i>Raman</i>	<i>36</i>

	CE Research and Development Needs	41
Chapter 2.	DESIGN AND OPTIMIZATION OF ELECTROFILAMENT DEPOSITION	43
	Introduction	43
	Deposition Techniques for Column Chromatography	44
	Description of the Electrofilament Process	46
	Experimental	47
	<i>Chemicals and Materials</i>	47
	<i>CE Separations</i>	49
	<i>EF Deposition</i>	51
	<i>Off-Column LIF Detection Instrumentation</i>	54
	Results and Discussion	56
	<i>Evaluation of the Electrofilament</i>	56
	<i>Electrofilament Effects on the On-Column Separation Performance</i>	57
	<i>Optimization of Deposition Conditions</i>	66
	<i>Comparison of On- and Off-Column Electropherograms</i>	71
Chapter 3.	TWO-DIMENSIONAL CAPILLARY ELECTROPHORESIS / THIN-LAYER CHROMATOGRAPHY	76
	Introduction	76
	CE Two-Dimensional Separations	79

Thin-Layer Chromatography81
Chiral Amino Acid Separations84
Experimental85
<i>Chemicals and Materials</i>85
<i>CE Separations and EF Deposition</i>86
<i>TLC Separations</i>87
<i>CCD LIF Imaging Instrumentation</i>88
Results and Discussion88
<i>One-dimensional CE Separation of Amino-Acid Enantiomers</i>88
<i>Comparison of On- and Off-Column Electropherograms</i>93
<i>Two-Dimensional Separation of Amino-Acid Enantiomers</i>98

Chapter 4. SURFACE-ENHANCED RAMAN SCATTERING FOR OFF-COLUMN DETECTION IN CAPILLARY ELECTROPHORESIS106
Introduction106
Theoretical Aspects of SERS107
<i>Electromagnetic enhancement</i>108
<i>Chemical enhancement</i>109
SERS Substrates110
Applications of SERS111
SERS-Based Detection for Chromatography112

Experimental	113
<i>Chemicals and Materials</i>	113
<i>CE Separations and EF Deposition</i>	114
<i>SERS Substrates</i>	114
<i>SERS Detection Instrumentation</i>	117
Results and Discussion	119
<i>Development of SERS-Active Substrates</i>	119
<i>Optimization of CE and Raman Conditions</i>	125
<i>Evaluation of CE/SERS Technique</i>	129
Chapter 5. SUMMARY AND FUTURE STUDIES	139
References	142
Vita	155

List of Figures

FIGURE	PAGE
1.1 General schematic of a CE instrument	5
1.2 Schematics describing electroosmotic and laminar flow	8
1.3 Schematic depicts the affect of EOF on separation	11
1.4 Differential-solute migration in CZE:	17
1.5 Illustrations of MEKC:	19
1.6 Illustrations of cyclodextrin CE:	22
1.7 Jablonski diagram	29
1.8 Energy-level diagram	30
2.1 Images of electrospray operating under normal and EF conditions	48
2.2 Images of fused-silica capillary used for EF deposition:	50
2.3 Schematic of the EF deposition apparatus	52
2.4 Schematic diagrams of the off-column instrumentation used to detect the deposited analytes	55
2.5 Electropherogram showing the effect of the EF voltage on the LIF on-column performance	58
2.6 Effect of inlet reservoir height on peak height and	

	asymmetry factor of kiton red when an EF voltage of 2 kV is applied	63
2.7	On-column electropherograms during EF deposition with the Inlet-buffer reservoir level with outlet and with it 10-cm above the outlet	67
2.8	Electropherograms of kiton red and fluorescein comparing the on- and off-column LIF detection	72
2.9	Calibration curve for kiton red deposited on a RP-TLC plate and detected using the PMT scanning instrument	75
3.1	Theoretical 2D separations:	78
3.2	Illustrations depicting the TLC experimental set-up and the nomenclature used to define the R _f value in Equation (3.3).....	83
3.3	Schematic diagram of the fiber-optic LIF off-column instrumentation used to detect the deposited analytes.....	89
3.4	Comparison of one-dimensional separations of DNS- AAs:	91
3.5	Comparison of one-dimensional separations of the enantiomers of DNS-AAs using β-CD:	92
3.6	Comparison of one-dimensional separation of the enantiomers of DNS-amino acids	94
3.7	Electropherograms of Val, Norv, Leu, and Norl comparing the on- and off-column detection while electrospray depositing	96
3.8	Electropherogram demonstrating the off-column LIF detection	

	limit obtained by using the CCD camera to image the RP-TLC plate	99
3.9	CCD images of the two-dimensional CE-TLC separations	100
4.1	Images of the high-efficiency nebulizer used to deposit the silver colloid :	116
4.2	Schematic diagram of the confocal-Raman instrument used for obtaining SERS spectra and reconstructing the off-column electropherograms	118
4.3	Images of the SERS substrate:	121
4.4	Background spectra of SERS substrate:	123
4.5	Graph showing XPS data before and after washing SERS substrate with water	124
4.6	SERS spectra of 10^{-5} M erythrosin B injected and EF deposited onto the SERS-substrate	126
4.7	SERS spectra of rhodamine-6G:	128
4.8	The structures of benzyloxyresorufin and resorufin used in the SERS experiments	130
4.9	Electropherograms of 10^{-5} M mixture of BzRes, Riboflavin, and resorufin:	132
4.10	The full SERS spectra obtained at the maximum of the CE peaks in Figure 4.9b	133
4.11	Plots of concentration and reaction time for the dodecanethiol self-assembled monolayer formation	135

4.12 Calibration curves for resorufin EF deposited onto plain-
and dodecane-SERS substrates137

List of Tables

TABLE	PAGE
1.1 LODs for different CE detection techniques	27
1.2 Cross-sections for various photophysical processes	37
2.1 Equation (2.1) solved as function of inlet reservoir height over the outlet reservoir for kiton red.	65
2.2 Effects of substrate temperature, during analyte deposition, on detection and separation parameters.....	70
2.3 Effects of substrate translation rate on detection and separation parameters.	70
2.4 Comparison of reproducibility for on- and off-column detection of kiton red.	73
3.1 Comparison of efficiency for on- and off-column detection using electrofilament deposition.	97
3.2 Comparison of resolution for on- and off-column detection using electrofilament deposition.	97
3.3 TLC separation data for DNS-amino acids	102

Abbreviations

Ar	argon (in reference to argon-ion laser)
AS	anti-Stokes Raman scattering
BzRes	benzyloxyresorufin
CAPS	3-cyclohexylamino-1-propanesulfonic acid
CCD	charge-coupled device
CD	cyclodextrin
CE	capillary electrophoresis
CGE	capillary gel electrophoresis
CHES	2-(cyclohexylamino)ethanesulfonic acid
CIEF	capillary isoelectric focusing
CITP	capillary isotachopheresis
cm	centimeter
CMC	critical micelle concentration
CZE	capillary zone electrophoresis
DAD	diode-array detector
DNA	deoxyribonucleic acid
DNS	5-dimethylaminonaphthalene-1-sulfonyl
2D	two-dimensional
EF	electrofilament
EOF	electroosmotic flow

ESI	electrospray ionization
ES	electrospray
fg	femtogram
FTIR	Fourier-transform infrared spectroscopy
HPLC	high-performance liquid chromatography
i.d.	internal diameter
IR	infrared absorption
kcal	kilocalorie
kV	kilo-volts
Leu	leucine
LIF	laser-induced fluorescence
LOD	limit-of-detection
LUMO	lowest unoccupied molecular orbital
M	molar (moles / liter)
MALDI	matrix-assisted laser desorption ionization
MECC	micellar electrokinetic capillary chromatography
MEKC	micellar electrokinetic chromatography
min	minutes
MS	mass spectrometry
μm	micrometer
mm	millimeter
mM	millimolar
mW	milliwatts

nL	nanoliter
nm	nanometer
Norl	norleucine
Norv	norvaline
o.d.	outer diameter
OHP	outer Helmholtz plane
PC	personal computer
PMT	photomultiplier
ppm	part per million
RP	reverse phase
RR	resonance Raman
RSD	relative standard deviation
S₀	ground singlet state
S₁	first singlet excited electronic energy level
S₂	second singlet excited electronic state
SAM	self-assembled monolayer
SDS	sodium dodecyl sulfate
sec	second
SEM	scanning electron microscopy
SERS	surface-enhanced Raman scattering
SERRS	surface-enhanced resonance Raman scattering
S/N	signal-to-noise

SIMS	secondary ion mass spectrometry
SS	stainless steel
T₁	first triplet excited electronic energy level
TLC	thin-layer chromatography
TRIS	tris(hydroxymethyl)aminomethane
UV/Vis	ultraviolet/visible
Val	Valine
XPS	X-ray photoelectron spectroscopy

Symbols

A	absorbance
α	polarizability
	Ratio of retardation factors in TLC
b	detection pathlength
c	velocity of light
C	sample concentration
d	capillary inside diameter
D	diffusion coefficient
E	applied electric field
ϵ	molar absorbtivity
	dielectric constant
F	force
	Fluorescence intensity
ϕ_F	fluorescence efficiency
ϕ_R	radiant power of Raman scattering
f(θ)	geometrical factor (solid angle of fluorescing radiation subtended by the detector)
g	gravitational constant
g(λ)	intensity of detector as function wavelength
H	plate height
	height sample for CE injection

I	intensity of radiation emergent from the sample
I_0	intensity of radiation incident upon the sample
η	viscosity
k	Boltzman constant
l	effective pathlength (to the detector)
L	length of column
λ	wavelength
μ	oscillating dipole
μ_a	apparent electrophoretic mobility
μ_{avg}	average electrophoretic mobility
μ_e	electrophoretic mobility
μ_{eof}	mobility of electroosmotic flow
N	efficiency (theoretical plate count)
n_c	peak capacity
n_i	number density in state i
ΔP	pressure difference across capillary
P	polarizability
q	charge of an ion
Q	quantity injected
r	ion radius
	capillary radius
R_f	retardation factor

R_s	resolution
σ^2	variance
t	retention time
t_o	void volume
t_M	migration time of micelle
V	applied voltage
v	velocity of ion
v_{eof}	electroosmotic flow
v_p	hydrodynamic flow velocity
w	width of peak at baseline
$w_{1/2}$	width of peak at half-height
ζ	zeta potential
Z_f	distance traveled by mobile phase in TLC
Z_o	distance from sample origin to the origin of the mobile phase in TLC
Z_x	distance traveled by sample in TLC

Chapter 1. CAPILLARY ELECTROPHORESIS

Introduction

Since the emergence of modern capillary electrophoresis (CE) nearly 20 years ago, the technique has matured into the foremost analytical technique for performing high-efficiency liquid-phase separations. CE has made major contributions to a wide variety of research. Most recently, it played an instrumental role in the sequencing of the human genome, which is considered one of the most significant scientific achievements in the last century [1-3].

Bearing in mind the implications of this work to the basic understanding of the chemistry of life, and to genetic disease diagnosis and therapy, arguably CE is one of the most important analytical tools used today. Research and development involving CE shows no signs of slowing down as evident from the approximately 1900 reviewed research articles in the year 2000. Additionally, CE technologies have been adapted to the "lab-on-a-chip" format, which promises to be the next generation of analytical instrumentation [4,5].

Potentially, due to the need for efficient ultra-fast separations in areas such as genomics, proteomics, and combinatorial chemistry, CE could be involved in some of the most exciting and important research of the next decade [6-10].

Electrophoresis occurs when an electric field is applied across a conductive fluid medium; the electric field causes the charged solutes to migrate through the medium. The rate and direction of the solute migration depend on

the solute charge and size. Historically, the term “electrophoresis” can be traced back to 1909 when Michaelis separated proteins based on their isoelectric points [11]. In the late 1930s, Tiselius performed moving boundary experiments on the separation of human serum proteins, albumin, and α -, β -, γ -globulins. For his work in electrophoresis, Tiselius was awarded the Nobel Prize in Chemistry in 1948 [12].

An inherent limitation of electrophoretic methods is Joule heating, which is heating caused by the passage of an electric current through a conductive medium [13]. Joule heating causes thermal convective flow that results in decreased separation performance. To reduce the effects from this heating, electrophoresis was initially performed in a slab of gel immersed in a conductive medium. The gel, which has a high area-to-volume ratio, effectively dissipates any heat that is generated. This technique, known as slab gel electrophoresis, has been widely used for the separation of large biological molecules such as proteins and oligonucleotides [14]. Although slab techniques are still used today [15,16], the full potential of electrophoresis was not realized until capillaries were employed as migration channels, which put electrophoretic separations on the same instrumental level as high-performance liquid chromatography (HPLC).

When employing tubes or capillaries for electrophoresis, the convective flow from Joule heating is reduced as smaller internal diameter (i.d.) capillaries are employed. Additionally, analogous to gel in slab-electrophoresis, the high area-to-volume ratio inherent to the capillaries will serve to dissipate heat that is generated. Initially, Hjerten performed separations of inorganic ions and proteins

in 3-mm tubes [17]. Following this work, Virtanen used smaller internal diameter (0.2 mm) Pyrex tubes [18]. In the late 70s, Mikkers et al. sought to solve the Joule heating problems through the use of narrow-bore (200 μm) Teflon tubes [19]. However, it was not until Jorgenson and Lukacs demonstrated electrophoresis in glass capillary tubes that modern CE started to take shape.

In this initial work, electrophoresis was conducted in open-tubular glass capillaries of 75- μm internal diameter and with applied voltages of 30 kV, typically these same conditions are used today. Short analysis times (10-30 min.) and high efficiencies (400,000 theoretical plates) were demonstrated for separations of amino acids, dipeptides, and amines. In addition, the theoretical aspects of CE were outlined [20,21].

Within a few years, research in academia, government, and industry throughout the world was quickly advancing the CE instrumentation and expanding its use to a wide range of applications [22-24]. One reason for the accelerated rate of development is that the CE technique uses inexpensive instrumentation and readily available capillary columns. Although automated commercial instruments are currently available from several manufacturers, a large portion of research occurs on instrumentation that has been assembled "in-house". Additionally, when compared to its major competitor HPLC, CE uses minute volumes of solvents and it generates considerably less waste. The inherent advantages of CE listed below continue to make it an attractive separation technique:

- Capable of high separation voltages

- high efficiency separations ($N > 10^5$ to 10^6)
- fast separations
- small sample volumes (1 to 50-nL injected) and waste generation
- numerous modes that can be optimized to separate positively? neutral, and negatively charged inorganic ions, organic molecules, and large biomolecules
- operates in aqueous or mixed aqueous-organic media

Separation Theory

The majority of the following discussion was adapted from two excellent monographs on CE, the *Handbook of Capillary Electrophoresis and High Performance Capillary Electrophoresis-An Introduction* [25,26]. A typical CE system is shown in Figure (1.1); the main components consist of a high voltage power supply (0 to 30 kV), a polyimide-coated fused-silica capillary with an internal diameter less than or equal to 100 μm , two buffer reservoirs that can accommodate both the capillary and the electrodes, a power supply, and a detector. Under normal operation, the reservoirs and the capillary are filled with an aqueous running buffer. The capillary inlet is placed into the sample vial and the sample is introduced into the capillary column by one of several injection techniques. Subsequently, the capillary inlet is placed back into the buffer reservoir and an electric field is applied. The electric field causes the solutes to

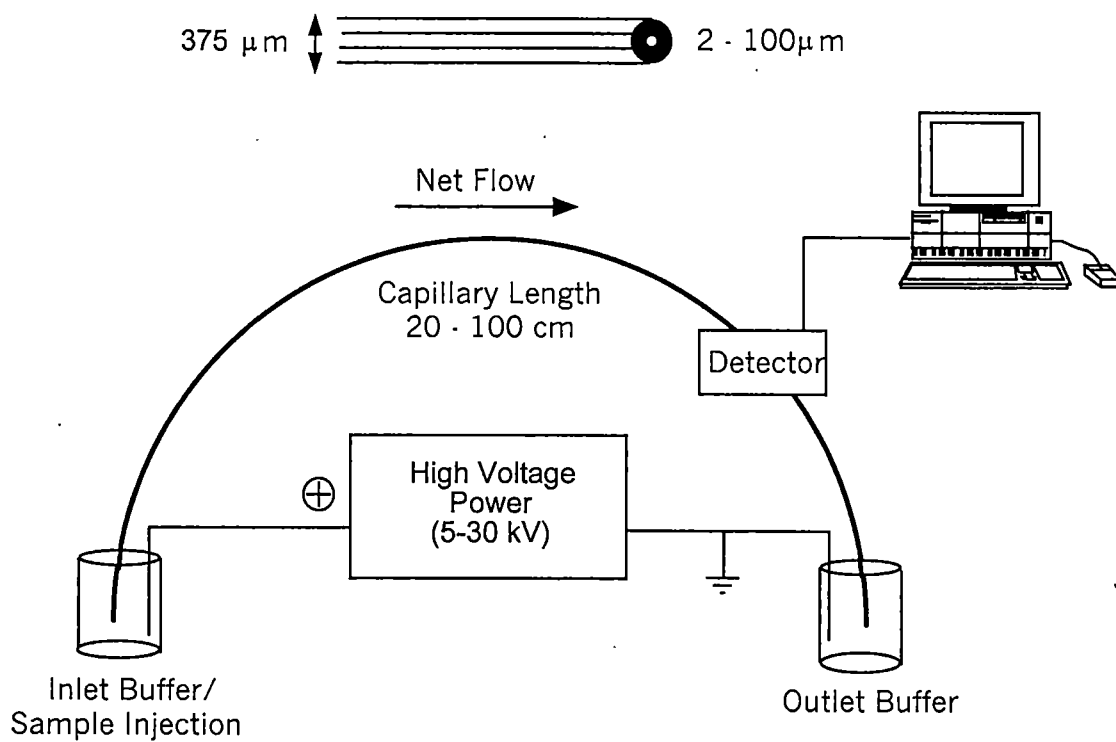


Figure 1.1 General schematic of a CE instrument.

migrate through the capillary; ideally they would migrate at different rates. As the solutes pass by the detector a signal is sent to either an integrator or a computer acquisition system. An electropherogram, which is a plot of detector response versus time, is produced in which the separated compounds appear as peaks with different migration times.

Electrophoresis

Electrophoresis separations are based on the differences in solute velocity in an electric field. The velocity of an ion, v , under the influence of the applied voltage V , is the product of the electrophoretic mobility, μ_e , and the applied field E ($E=V/L$, where L is the length of the column)

$$v = \mu_e E \quad (1.1)$$

The mobility is determined by the electric force that the molecule experiences, balanced by its frictional drag through the medium. The electrical force can be given by

$$F_E = qE \quad (1.2)$$

and the frictional force for a spherical ion is

$$F_F = -6\pi\eta rv \quad (1.3)$$

where, q is the ion charge, η is the solution viscosity, r is the ion radius, and v is the ion velocity. A steady state is attained during electrophoresis, where the two forces are equal, but in opposite directions

$$qE = 6\pi\eta rv \quad (1.4)$$

Solving for velocity and substituting Equation (1.4) into Equation (1.1) results in Equation (1.5), which describes the mobility in terms of physical parameters

$$\mu E = \frac{q}{6\pi\eta r} \quad (1.5)$$

Both the size and charge of the analyte determines the analyte mobility; a small, highly charged analyte will have a high mobility, whereas a large minimally charged species would have a low mobility.

Electroosmotic Flow

The electroosmotic flow (EOF) is one of the most important and unique features of CE. The EOF essentially acts as an “electric field”-driven pump that may be considered analogous to the mechanical pump used in HPLC. An EOF pumping system is much simpler than a mechanical pump (i.e., no moving parts to wear out), however it cannot be controlled as effectively as a mechanical pump. In the late 1800s, Helmholtz first introduced EOF through experiments involving the application of an electrical field to a horizontal glass tube containing an aqueous salt solution [27].

Under aqueous conditions, most solid surfaces possess an excess of negative charges. For fused silica, the numerous silanol groups (SiOH) mostly control the charge on the inner wall that can exist in anionic form (SiO⁻). As shown in Figure (1.2a), the ionized silanol groups will attract cationic species from the buffer. An ionic layer is formed that has a positive charge density, which decreases exponentially as the distance from the wall increases. The

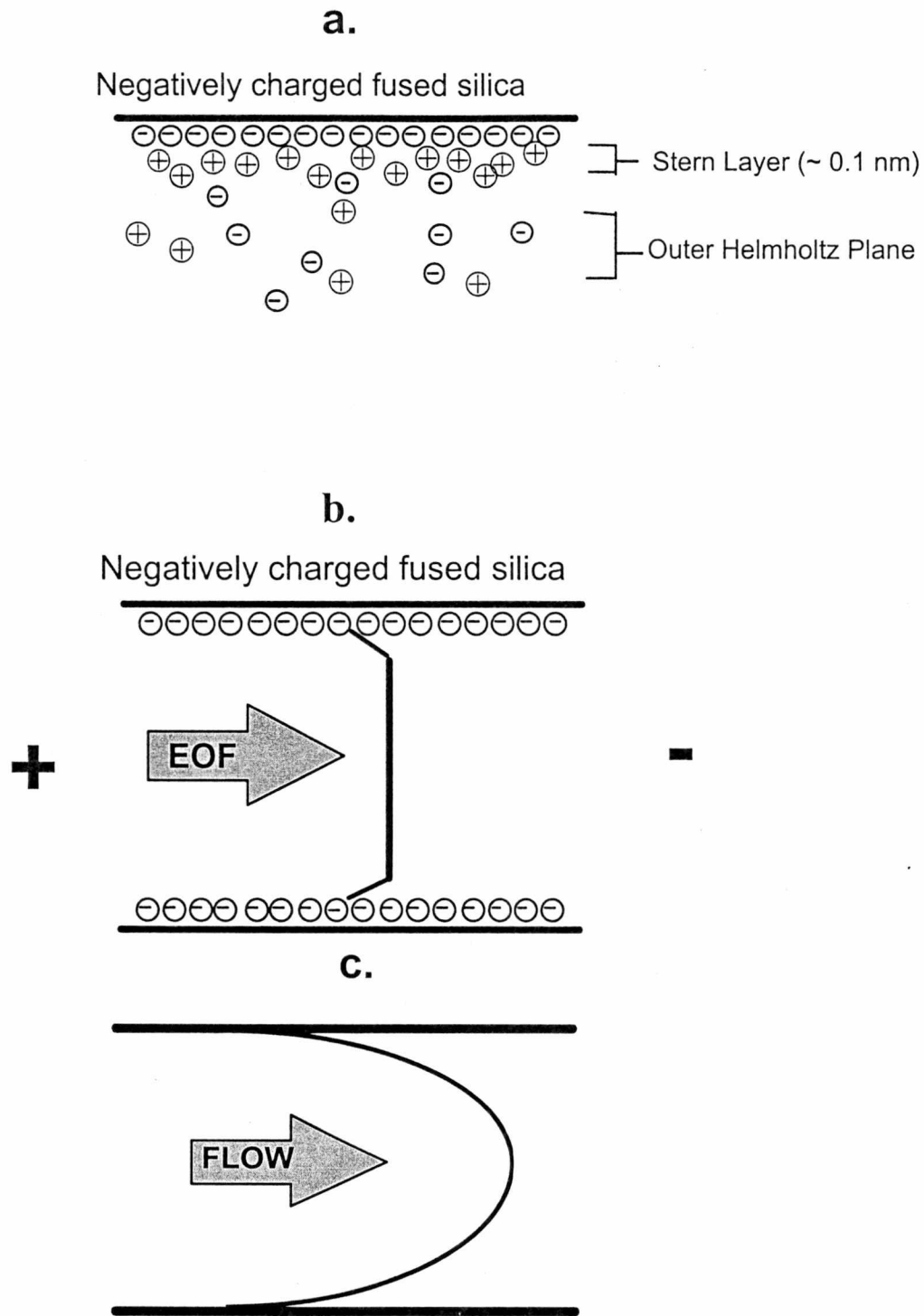


Figure 1.2 Schematics describing electroosmotic and laminar flow: a.) the hydrated cations accumulating near the surface of the fused-silica capillary column, b.) the bulk flow towards the cathode upon application of the electric field, and c.) laminar flow due to the shear force at the wall.

double layer formed closest to the surface is termed the “inner Helmholtz or Stern Layer” and is essentially static. A more diffuse layer formed in the process is termed the “Outer Helmholtz plane” (OHP). Under an applied field, cations in the OHP migrate in the direction of the cathode carrying waters of hydration with them, thus creating a bulk flow of the running buffers.

The magnitude of the EOF can be expressed in terms of velocity, v_{eof} , or mobility, μ_{eof} , by the following equations:

$$v_{EOF} = (\varepsilon \zeta / \eta) E \quad (1.6)$$

or

$$\mu_{EOF} = (\varepsilon \zeta / \eta) \quad (1.7)$$

where ζ is the zeta potential, which is the electric potential across the interface of a solid and a liquid, and ε is the dielectric constant.

An advantageous feature of the EOF is the flat profile of the flow, as illustrated in Figure (1.2b). The driving force of the flow is uniformly distributed along the capillary. No pressure drop in the capillary is observed, which results in the flow being approximately uniform throughout. This flat profile is beneficial for obtaining the high efficiency separations observed in CE, because it does not directly contribute to the dispersion of solute zones. In contrast, the mechanical pump used in HPLC yields a laminar flow due to the shear force of the wall (shown in Figure 1.2c). In a pressure driven system, the flow profile is parabolic,

with the flow velocity being zero at the wall and twice the mean velocity at the center. With the EOF the flow only drops off short distances into the solution, hence it is relatively unimportant to the overall separation process (i.e. other dispersive processes dominate).

The EOF affects the amount of time a solute resides in the capillary, thus affecting both the separation efficiency and resolution of the solutes. As depicted in Figure (1.3), the EOF causes movement of nearly all species in the same direction. Under normal conditions (i.e., when the wall is negatively charged), the flow is from the anode to the cathode (cathodic flow). In a CE run, cations migrate the fastest, neutrals are all carried at the velocity of the EOF but are not separated from each other, and anions migrate slowest since they are attracted to the anode but are still carried by the greater EOF toward the cathode. Additionally, the EOF results in better resolution of anionic solutes that migrate against the flow, whereas the cationic solutes will be more poorly resolved (see below). A disadvantage of the EOF is that its magnitude depends on the ionic state of the capillary wall, which is difficult to control. Consequently, the inconsistencies in EOF result in poor retention time reproducibility.

Analytical Parameters

Migration Time

The migration time is defined as the time required for a solute to migrate to the point of detection. The migration time and other experimental parameters



ELECTROOSMOTIC VELOCITY



ELECTROPHORETIC VELOCITY



ELUTION ORDER

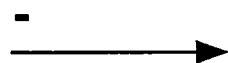


Figure 1.3 Schematic depicts the affect of EOF on separation. Velocity (v) and the elution order for cations (+), neutrals (0), and anions (-) based upon the effects of electrophoresis (ep) of the ionic sample in the presence of a strong electroosmotic flow (eo) towards the cathode.

can be used to calculate the apparent solute mobility

$$\mu_a = \frac{V}{tE} = \frac{lL}{tV} \quad (1.8)$$

and

$$\mu_a = \mu_e + \mu_{EOF} \quad (1.9)$$

where, V is the applied voltage, l is the effective capillary length (to the detector), L is the total capillary length, t is the migration time, and E is the electric field. In the presence of EOF, the measured mobility is called the apparent mobility (μ_a). The effective mobility, (μ_e), can be obtained by measuring the EOF with a neutral marker that moves at a velocity equal to the EOF.

Resolution

In any separation technique, the ultimate goal is resolution, which in electrophoresis is based on the difference in solute mobility. The simplest way to characterize resolution is to divide the difference in migration distance by the average peak width,

$$R_S = \frac{2(x_{12} - x_{11})}{(w_1 + w_2)} \quad (1.10)$$

Where x_i is the migration distance of the analyte i , and the subscript 2 denotes the slower moving component, and w is the width of the peak at the baseline.

In CE the solute zones are usually very sharp (i.e., very efficient), therefore small differences in solute mobility (< 0.05 % in some cases) are often

sufficient for complete resolution. The resolution of two zones in the presence of EOF can be written as

$$Rs = 0.177(\mu_{e(1)} - \mu_{e(2)}) \left\{ \frac{V}{D(\mu_{e,avg} + \mu_{eof})} \right\}^{1/2} \quad (1.11)$$

where, μ_e are the electrophoretic mobilities of the two solutes, V is applied voltage, D is solute's diffusion coefficient, and μ_{eof} is the EOF mobility. When the EOF balances the electrophoretic migration excellent separation is obtained, however at the expense of analysis time.

Efficiency

In CE, efficiency is the most important parameter to consider for separations, whereas in chromatography usually selectivity is the most important parameter. For a Gaussian peak, the baseline peak width (w_b) defines dispersion, which is a result of different solute velocities within the band zones

$$w_b = 4\sigma \quad (1.12)$$

where, σ is the standard deviation of the peak. The efficiency is commonly related to the number of theoretical plates (N) that can be obtained

$$N = \left(\frac{L}{\sigma} \right)^2 \quad (1.13)$$

which, can be related to the height equivalent to a theoretical plate (H) by

$$H = \left(\frac{L}{N} \right) \quad (1.14)$$

where, L is the capillary effective length.

Under ideal conditions in CE (i.e., small injection, no solute-wall interaction, no Joule heating etc.), the dominant contribution to the decrease in efficiency is longitudinal diffusion (along the length of the capillary). The radial diffusion (across the capillary) is unimportant due to the plug-flow profile that is characteristic of EOF (see Figure 1.3). The efficiency can be related to the molecular diffusion term in chromatography

$$\sigma^2 = 2Dt = 2DIL/\mu_e V \quad (1.15)$$

where D is the diffusion coefficient of the solute. Substituting Equation (1.15) into (1.13) yields a fundamental electrophoretic expression for plate number

$$N = \frac{\mu_e V l}{2DL} = \frac{\mu_e E l}{2D} \quad (1.16)$$

As can be seen from Equation (1.16), higher fields yield higher efficiency; this higher efficiency is because the solute spends less time in the capillary.

Additionally, large molecules such as DNA, which have low diffusion coefficients, will exhibit less dispersion than small molecules.

Although longitudinal diffusion ultimately defines the limit of efficiency, under non-ideal experimental conditions, several sources can contribute to zone broadening. Both Joule heating and unlevelled running-buffer reservoirs can lead to laminar flow, which increases radial diffusion that is irrelevant under plug flow conditions. Injection lengths that are longer than the diffusion-controlled zone length can lead to an additional zone broadening. Interaction of the solute with the capillary walls often results in severe peak tailing, which is a major problem

when analyzing cations, such as proteins. Often the conductivity of the sample and the running buffer do not match, which results in either fronted or tailed peaks. Finally, the detector cell size should be small relative to the peak widths.

Experimentally, N can be calculated by using the width at half-height of a Gaussian peak

$$N = 5.54 \left(\frac{t_r}{w_{1/2}} \right)^2 \quad (1.17)$$

where t_r is the retention time and $w_{1/2}$ is the width at half-height.

Select Modes of CE

A family of specialized modes of operation has evolved that collectively constitute "capillary electrophoresis." The most frequently used modes of capillary electrophoresis are capillary zone electrophoresis (CZE), micellar electrokinetic chromatography (MEKC), capillary gel electrophoresis (CGE), capillary isoelectric focusing (CIEF), and capillary isotachopheresis (CITP). One of the advantages of CE is the availability of different modes that expands its versatility. Changing modes often requires only changing the running buffer, since the same fused-silica capillary can be used for more than one mode. An extensive amount of work has been reported on each of the above modes, consequently only the modes that have been utilized for the work reported herein will be discussed further.

Capillary Zone Electrophoresis

Capillary zone electrophoresis (CZE) or free-solution electrophoresis is the most widely used mode due to its simplicity of operation and its versatility. The name CZE is somewhat misleading because it infers that it is the only mode where “zonal” electrophoresis occurs; however other modes like micellar electrokinetic chromatography are also “zonal” electrophoresis modes. In CZE, the capillary and the inlet and exit reservoirs are filled with an electrolyte-running buffer of constant composition. Separation occurs because the solutes migrate in discrete zones at different velocities. As can be seen from Figure (1.4), both cationic and anionic solutes can be separated in CZE, because of the EOF. However, neutral solutes do not migrate and will co-elute with the EOF. Electrophoretic mobility and thus the separations are mainly dependent on the charge-to-size ratio of an ion and, to some extent, on its shape. CZE can be used to separate almost any ionic compounds that are soluble in the running buffer, such as small inorganic anions, large biomolecules. Using non-aqueous buffers, water-insoluble compounds can also be separated [28].

Micellar Electrokinetic Chromatography

As mentioned above, CZE cannot be used for the separation of neutral compounds because they have no electrophoretic mobility. However, additives can be incorporated into the running buffer to aid in the separation of neutral compounds. In this approach, a charged species acting as a pseudo-stationary phase is added to the running buffer. Separation of neutral analytes occurs as a

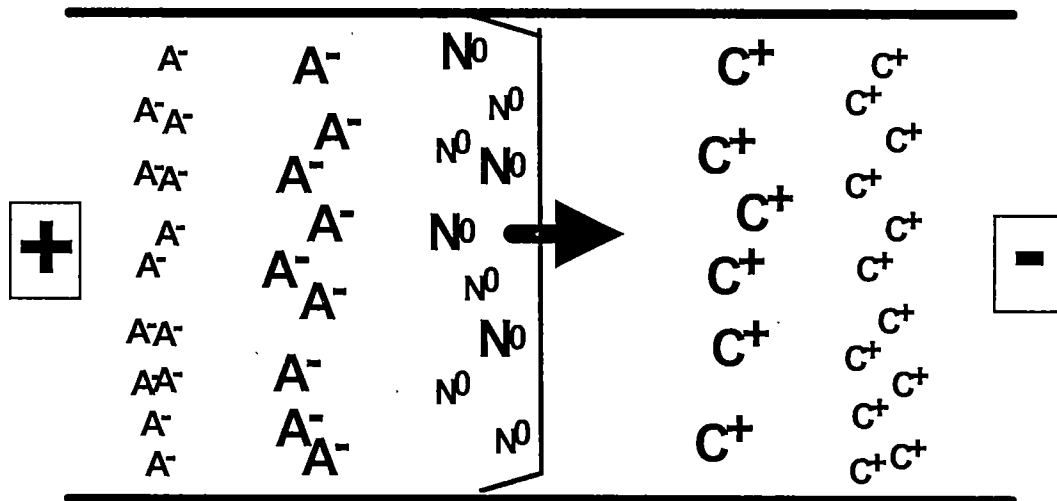


Figure 1.4 Differential-solute migration in CZE: anions (A^-), neutrals (N^0), and cations (C^+) superimposed on electroosmotic flow.

result of partitioning with the additive, which has a mobility different than the electroosmotic mobility. Terabe was the first to use micelles as additives for separations in CE [29]. This technique is known either as micellar electrokinetic chromatography (MEKC) or micellar electrokinetic capillary chromatography (MECC) [30]. MEKC has become one of the most widely used modes of CE. Terabe and Quinino have recently provided an excellent review of electrokinetic chromatography [31].

In MEKC, separation is accomplished by the use of surfactants in the running buffer. Most often, sodium dodecyl sulfate (SDS) is added to the running buffer at a concentration above its critical micelle concentration (CMC). SDS is comprised of a hydrophobic tail and a negatively charged, hydrophilic head. As the concentration of SDS is increased to 8 mM in water (the CMC in water), individual surfactant molecules begin to interact with each other to form micelles. The hydrophobic tails line up and exclude water, while the charged head groups orient toward the surface of the aggregates (Figure 1.5a). The resulting micelles are hydrophilic on the surface but hydrophobic on the interior.

The MEKC process is depicted in Figure (1.5b). The micelles formed, which have an anionic character, have an electrophoretic mobility that is directed toward the anode. Analytes partition between the aqueous phase and the micellar phase, which is analogous to a stationary phase in HPLC. Commonly, MEKC is performed with an EOF that is faster than the migration velocity of the micelles, therefore the electrophoretic mobility of the SDS micelles is less than the EOF mobility and they move slowly toward the cathode. An elution window

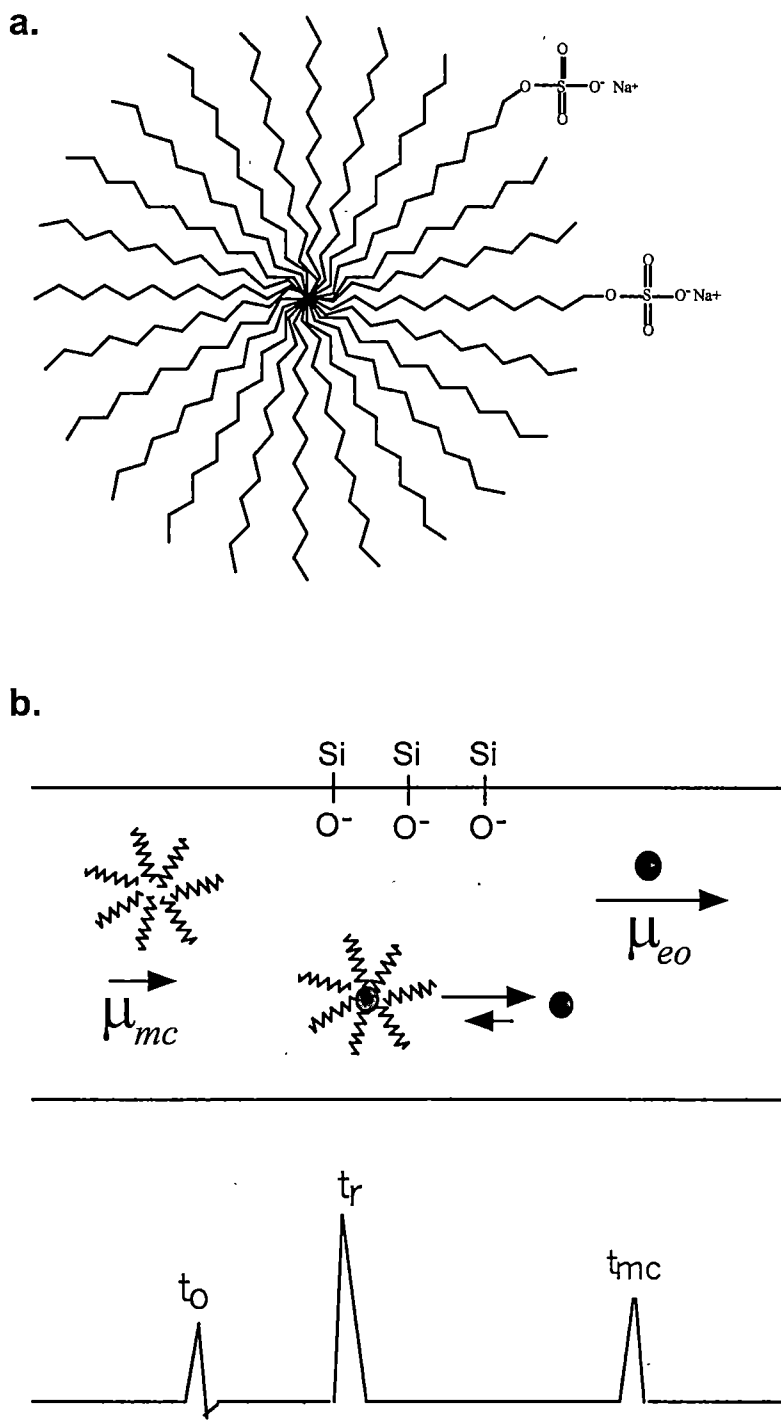


Figure 1.5 Illustrations of MEKC: a.) structure of sodium dodecyl sulfate micelle and b.) schematic of the MEKC process.

is generated because the micelles are actually moving during the separation process. Often organic modifiers, such as methanol or acetonitrile, can be added to the micellar-running buffer to influence solute partitioning with the micellar phase and also to increase the elution window by slowing EOF. For neutral analytes, the elution window is defined as the time between the EOF time, t_o , and the micelle migration time, t_{mc} . Neutral analytes that partition between the two phases will migrate at an intermediate time.

During the migration, the micelles can interact with the solutes through both hydrophobic and electrostatic interactions. Although originally developed for the separation of neutral compounds, MEKC has been used for separation of charged compounds that have similar electrophoretic mobilities. Depending on the nature of the additive, partitioning can be based on a combination of hydrophobicity, ionic attraction, and hydrogen bonding.

Cyclodextrin Capillary Electrophoresis

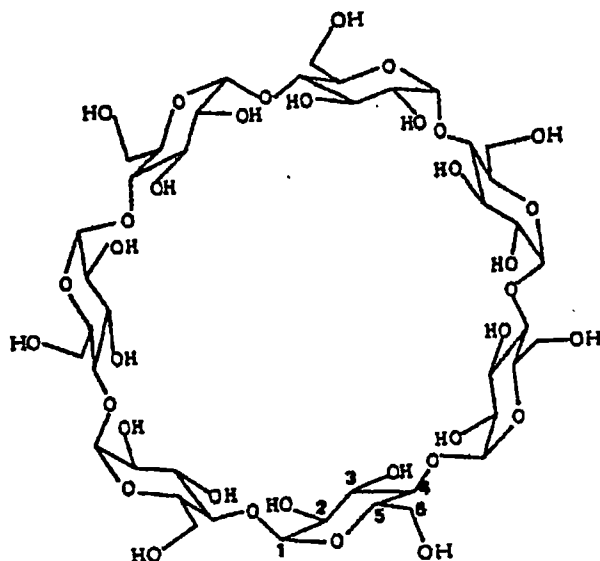
Chirality is very important in pharmaceutical, biotechnological, chemical, and agricultural activities. The subtle differences in the chiral forms of molecules may result in different pharmacological effects in biological systems by determining the pathways of metabolism, disposition, and physiological effects [32]. The racemic drugs may exhibit quite different activity from the optically pure drugs. Often only one of the enantiomers is pharmacologically active and in some instances the other can be toxic. CE has become an attractive technique

for chiral separations and cyclodextrins (CD) have become one of the most popular electrophoretic chiral selectors [33].

Native CDs, as shown in Figure (1.6a), are neutral cyclic oligosaccharides consisting of 6-13 glucopyranose rings. CDs with 6-8 rings, called α -, β -, and γ -cyclodextrin, respectively, are currently used most often in CE separations. Out of these three, β -CD is usually the most effective agent because of its intermediate size. Additionally, a mixture of the CDs can be used to optimize separations. The shape of the cyclodextrin molecules resembles a truncated cone (Figure 1.6b). The diameter of the cavity increases with the number of glucopyranose units. The increase in the cavity volume with the number of glucopyranose units is reflected in the number of water molecules filling the cavity, which are replaced by the analyte molecules during the partitioning process.

CDs are dissolved in the CE running buffer and offer separation systems with high separation efficiency and reasonable selectivity. CDs do not interfere with absorbance detection because they have minimal UV/Vis absorbance above 200 nm. However, the stability of their aqueous solutions is limited, which requires fresh solutions to be prepared daily. In one-dimension, obtaining optimum separation of enantiomers using CDs can be difficult due to the interactions between the enantio- and general-separation mechanisms, which is demonstrated and discussed in Chapter 3.

a.



b.

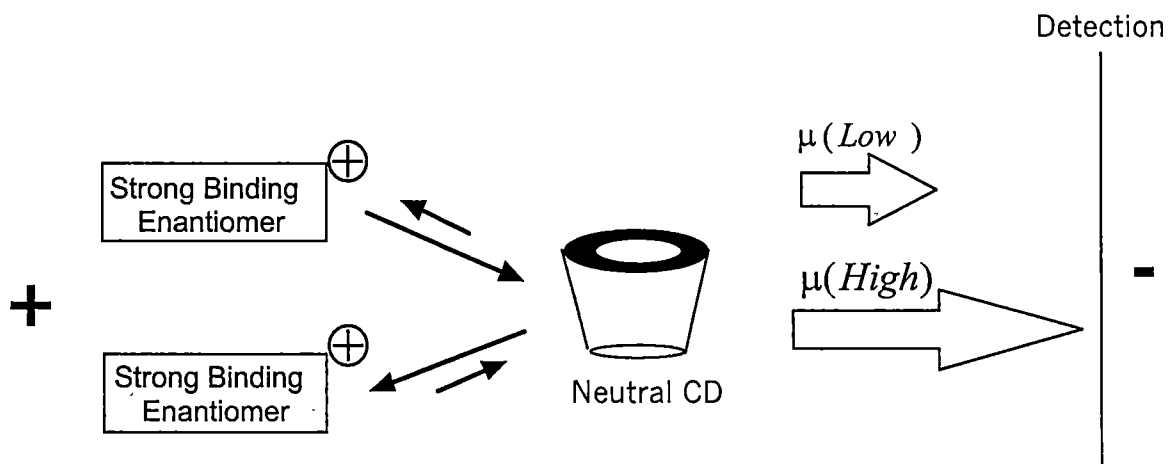


Figure 1.6 Illustrations of cyclodextrin CE: a.) structure of β -CD and schematic of b.) the uncharged CD separation process.

Enantio-selectivity is a result of some combination of interactions between the CD and the chiral compounds. For example, interactions could involve hydrophobicity, size, shape, hydrogen bonding and/or dipole-dipole forces. Factors that can be optimized to improve chiral selectivity are CD concentration, solution pH, and the size of the CD. Additionally, CDs can be chemically modified to alter selectivity (e.g., methyl groups).

In the case of using native or derivatized, non-charged CDs, the migration is illustrated in Figure (1.6b). The analytes can either include completely or include by their hydrophobic parts into the relatively hydrophobic cavity of the CD. Because of the two openings in the CD, the guest compound can penetrate into the cavity from either side. The versatility of the separations can be extended by incorporating CDs into other modes of CE, such as MEKC.

Injection Techniques

The basic instrumental design was discussed previously and is shown schematically in Figure (1.1). The simplicity of the instrumentation is one of the advantages of CE and much of it does not require further explanation. However, due to the uniqueness of the injection techniques, they will be briefly described below.

In CE, minute volumes of sample are loaded onto the capillaries to maintain the high efficiency. The sample plug length is a more critical parameter than the volume. Commonly, the sample plug length is less than 1 to 2 % of the total length of the capillary, which corresponds to an injection length of a few

millimeters (1 to 50 nL depending on the capillary diameter). The small volumes injected are an advantage when a limited sample volume is available, however the small volumes put constraints on detector designs that may limit the sensitivity that can be obtained by conventional detection techniques.

Alternative injection techniques have been developed that allow up to 80 % of the capillary to be filled; subsequently, the analytes are concentrated on-column [34, 35]. However, many of these techniques can not be universally applied and they are almost always more difficult to use. The two commonly used quantitative injection techniques are hydrodynamic and electrokinetic injection.

Hydrodynamic Injection

Hydrodynamic injection is the easiest and the most widely used injection technique, as well as the technique that is used exclusively for the work reported in this dissertation. Typically for siphoning injections, the sample reservoir is raised 5 to 10 cm relative to the exit reservoir. The capillary inlet is placed into the raised sample reservoir for 10 to 30 seconds; subsequently, it is placed back into the inlet buffer reservoir prior to application of the CE running voltage.

The volume of sample loaded will be a function of the capillary dimensions, the viscosity of the buffer in the capillary, the applied pressure, and the time. The volume can be calculated using the Hagen-Poiseuille equation

$$Volume = \frac{\Delta P d^4 \pi t}{128 \eta L} \quad (1.18)$$

where ΔP is the pressure difference across the capillary, d is the capillary inside diameter, t is injection time, η is the buffer viscosity, and L is the total capillary length. For the commonly used siphoning injection the volume injected can be calculated from

$$Volume = 2.84 \times 10^{-8} \frac{H t d^4}{L} \quad (1.19)$$

where H is the height to which the sample is raised in millimeters relative to the exit reservoir. Up to a point efficiency improves with decreasing injection lengths, however injection reproducibility is usually diminished with short injection lengths. For commercial instruments, injection reproducibility can be better than 2 % relative standard deviation (RSD).

Electrokinetic Injection

In electrokinetic injections, an electric field is applied between the sample vial and the exit reservoir, which causes the sample components to migrate into the capillary. Usually a field strength is applied, which is 3 to 5 times lower than that used for the separation. Neutral molecules are pulled into the capillary by the EOF, whereas charged solutes move into the capillary because of both EOF and electrophoretic migration. Discrimination occurs for ionic species since the more mobile ions are loaded to a greater extent than those of lesser mobility.

The quantity injected, Q , is given by

$$Q = V \pi c t r^2 \frac{\mu_{EP} + \mu_{EOF}}{L} \quad (1.20)$$

where V is the injection voltage, c is the sample concentration, t is the time the voltage is applied, r is the capillary radius, μ_{EP} is the electrophoretic mobility of the solute, and μ_{EOF} is the electroosmotic mobility. Sample loading is dependent on the EOF, sample concentration, and sample mobility. Generally, electrokinetic injections are not as reproducible as hydrodynamic injections.

Detection Techniques

The design and development of sensitive and selective detectors has been a major challenge in CE research [36,37]. The same characteristics that make CE an attractive separation technique, likewise make detection difficult. The high separation speeds result in a reduced residence time for the analytes in the detection zone. Commonly, to preserve the high efficiencies, detection is performed on-column where the small capillaries hinder detector interfacing, and result in reduced sensitivities for pathlength-dependent techniques. While an enormous amount of research has gone into detector development for CE, improvements are needed for CE to reach its full potential as an analytical technique.

A variety of detection techniques have been applied to CE; the limits of detection (LOD) of several are compared in Table (1.1). The following discussion will be limited to three optical detection techniques: UV/Vis absorbance, laser-induced fluorescence (LIF), and Raman-based detection.

Table 1.1 LODs for different CE detection techniques

Detection Technique	Typical LOD (M)	References
Direct absorbance	10^{-6}	38
Indirect absorbance	10^{-6}	39
Photothermal Refraction	10^{-8}	40
On-column LIF	10^{-13}	38, 41, 42
Post-column LIF	10^{-16}	43
Indirect LIF	10^{-7}	44
Potentiometry	10^{-8}	45
Conductivity	10^{-8}	46
Amperometry	10^{-8}	47
Refractive index	10^{-6}	48
Raman	10^{-6}	49
Surface-enhanced Raman	10^{-9}	50
Nuclear-Magnetic Resonance	10^{-3}	51
Radioisotope	10^{-10}	52
Laser-induced capillary vibration	10^{-8}	53
Electrospray MS	10^{-9}	54
Matrix-assisted laser desorption MS	10^{-9}	55

Out of these three techniques, UV/Vis absorbance is the most common, LIF is the most sensitive, and Raman provides the most information-rich spectra.

The absorbance and fluorescence processes are nicely illustrated in the Jablonski diagram in Figure (1.7). Absorption results in an electronic transition from the ground singlet state (S_0) to a different vibrational level in the first or higher excited electronic state (S_1 or S_2 , respectively). Molecules in the excited states rapidly dissipate their excess energy. This can occur through a non-radiational process such as vibrational relaxation. Alternatively, the molecules can dissipate this energy through a radiational process such as fluorescence.

In the Raman process, illustrated in figure (1.8), a beam of intense monochromatic light passes through a sample that contains molecules. Most interactions of the incident photons with the sample molecules are elastic (Rayleigh scattering); the scattered light is of the same energy as the incident radiation. A small portion of the excited molecules may undergo a change in polarizability during one of the normal vibrational modes, which provides the basis for the Raman effect. In Raman scattering, the scattered radiation is of a different energy than the incident radiation. The incident radiation raises the molecule in the ground state or thermally-populated excited vibrational state to an intermediate level called a virtual level, which does not correspond to a real energy level of the atom or molecule. If the molecule emits by returning not to the original vibrational state, but to a different vibrational level of the ground electronic state the emitted radiation is of lower energy (Stokes) or higher

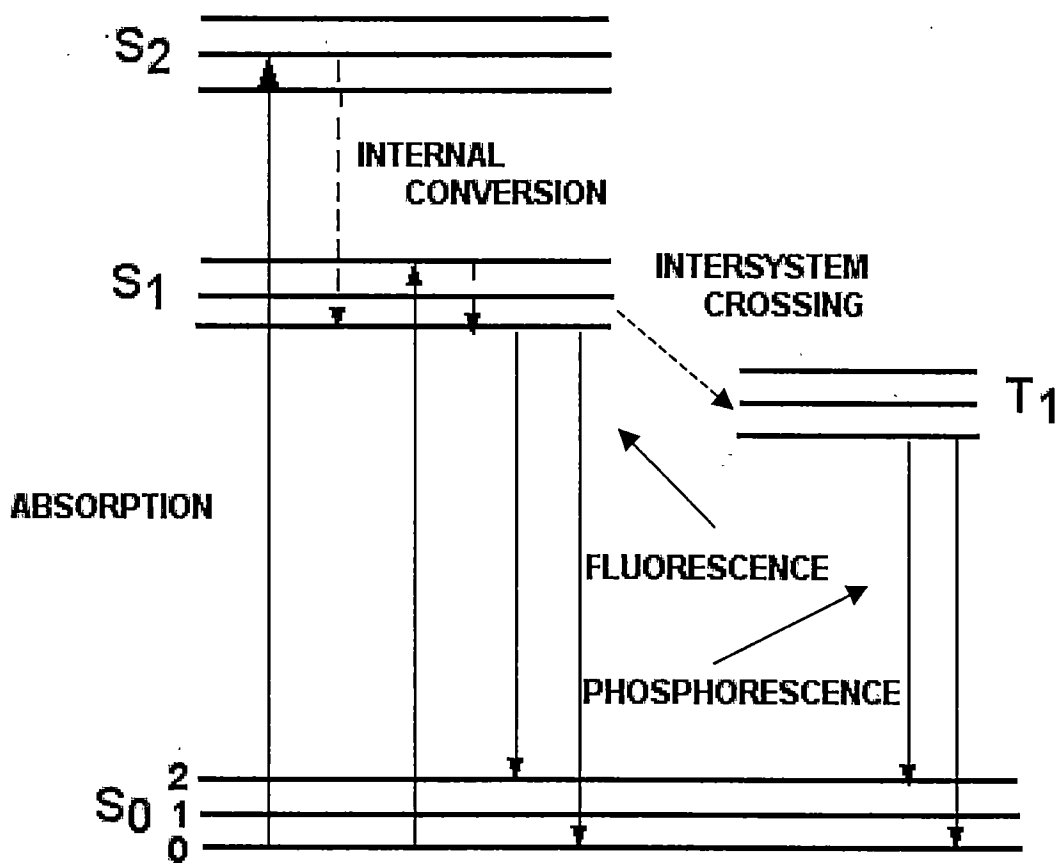


Figure 1.7 Jablonski diagram.

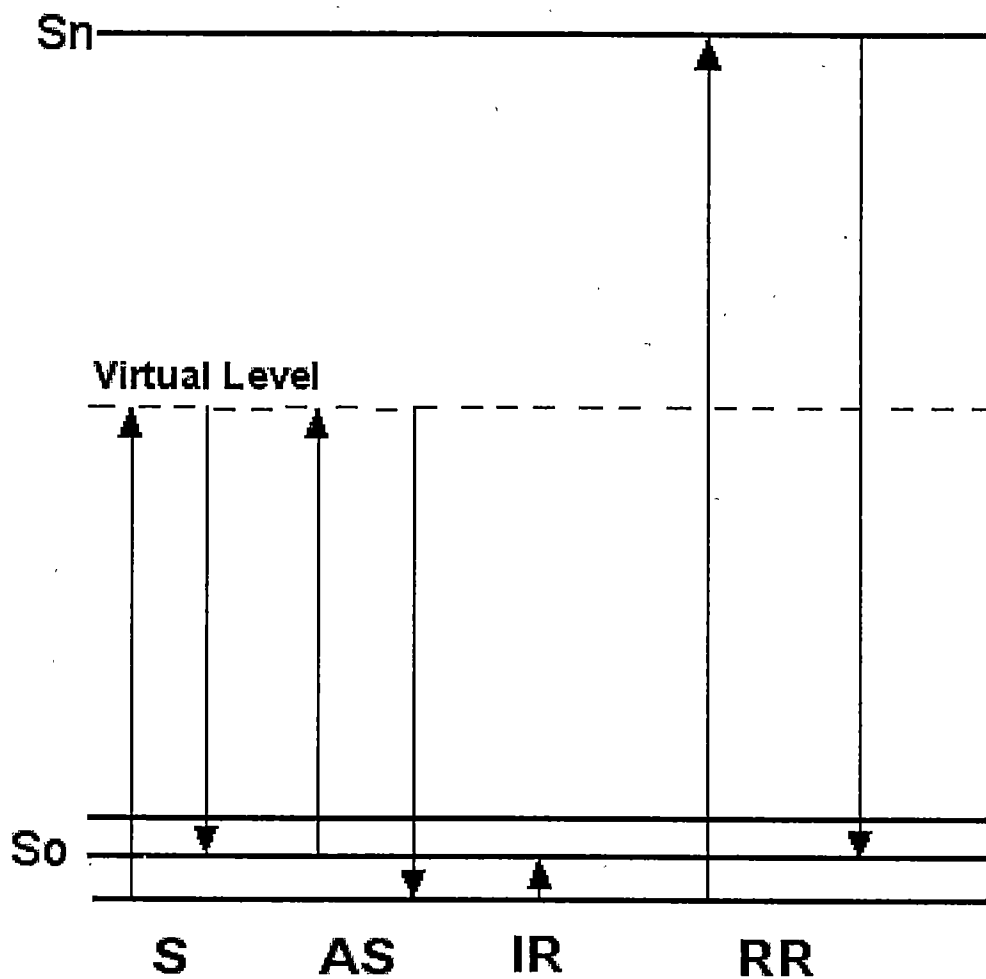


Figure 1.8 Energy-level diagram: stokes-Raman scattering (S), anti-stokes Raman scattering (AS), infrared absorption (IR), and resonance Raman scattering (RR).

energy (anti-Stokes) than the incident radiation. This provides a richly detailed vibrational spectrum of a molecule. Resonance Raman, as shown in Figure (1.8), occurs when the frequency of the exciting radiation coincides with or is in the region of an electronic absorption band. Resonance Raman lines can be 10^2 to 10^4 times more intense than in ordinary Raman [56].

Ultraviolet and Visible Absorption

Absorbance detectors are by far the most commonly used on-column detectors for microseparations. Their popularity is a result of the wide availability of commercial instruments. With only a slight modification, HPLC detectors can be used for CE experiments. Additionally, a large number of compounds absorb in the UV/Vis region of the electromagnetic spectrum. Basically all organic molecules have some absorption in the deep UV (160 to 180 nm), however access to this region is problematic due to absorbance by the optics and by ambient air. Fortunately, a large number of organic compounds can be detected in the 195 to 254-nm region, which is readily accessible. Unfortunately, in this region the molar absorptivity of many compounds is relatively low, resulting in poor S/N ratios for compounds that do not include pi bonds.

The accessible UV/Vis region from 200 to 800 nm, corresponds to energies of about 150 to 36 kcal mole⁻¹ [57]. Energy of this magnitude corresponds to the energy difference between electronic states of molecules. For example, the common electronic transitions are from pi bonding orbitals to pi antibonding orbitals ($\pi \rightarrow \pi^*$) and from nonbonding electrons to pi antibonding

orbitals ($n \rightarrow \pi^*$). Wide ranges of compounds containing the following functional groups exhibit these transitions: carbonyls, carboxylates, and esters to mention a few.

In a CE UV/Vis instrument, the lamp output is directed through an aperture and onto the detection region of a fused-silica capillary, which has had the polyimide coating removed. Wavelength selection is achieved by use of either optical filters or a diffraction grating. The transmitted radiation is directed onto a detector, usually a photomultiplier or a diode-array detector (DAD). When light passes through the absorbing molecules in the detection region, the extent of absorption depends upon the number of photon-absorbers present. A decrease in the intensity of the transmitted light reaching the photo detector is observed, when an absorbing molecule absorbs a photon and is promoted to an excited electronic state. The signal is processed and either sent to an integrator or a PC based data collection system, which is used to create an electropherogram.

In absorbance detection, the absorbance of a solute is dependent on path length, b , concentration C , and molar absorptivity, ϵ , as defined by the Lambert-Beer law

$$\text{Log } I_0/I = A = \epsilon bC \quad (1.21)$$

where I_0 is the intensity of radiation incident upon the sample, I is the intensity of radiation emergent from the sample, and A is the measured sample absorbance.

The major limitation of absorbance detection in CE is poor limits of detection (LOD), generally in the 10^{-4} - 10^{-6} M range. A fundamental limitation of

absorbance measurements is the fact that one is looking for a small difference between two relatively large signals. Additionally, the short on-column pathlength in CE exacerbates the limitations of the technique making solutes with poor absorptivity even more difficult to analyze. There have been several approaches to improve detector performance, one of which is to extend the absorbance pathlengths through bubble or Z-shaped detection cells. These techniques can improve the S/N by factors ranging from 3 to 10. Reproducibility for UV/Vis detection can be better than 2 % RSD [38].

Many times migration time or mobility measurements are insufficient to confirm peak identity. Therefore, ideally the detection technique would provide spectral information for analyte identification. As a general rule, the UV/Vis region of the electromagnetic spectrum is a poor region for compound identification, due to the lack of structural information and to the broad absorption spectra typically encountered in the liquid phase. Because rotational and vibrational modes will be found combined with electronic transitions, the UV/Vis spectrum is a function of the entire compound rather than specific bonds. However as mentioned previously, a diode-array detector can be employed in CE analyses to obtain a UV/Vis spectrum. In certain instances the UV/Vis spectra can be helpful in analyte identification when related to migration times. For example, in the analysis of dyes for forensic samples, the UV/Vis spectra help discriminate between dye components and background peaks by comparing the sample spectrum to a library spectrum [58].

Laser Induced Fluorescence

Laser induced fluorescence (LIF) methods have some of the best performance characteristics of any CE detection mode in terms of linearity, sensitivity, and limits of detection. The LODs for the best CE/laser-based systems are below 10^{-13} M or mass LODs of less than 10 molecules [38,41,42]. Moreover, single molecule detection has been demonstrated for CE using LIF [43].

Typically, LIF has been limited to research laboratories because of the lack of commercial instruments, and the fact that fluorescence is less universal than UV-Vis absorption. A fluorescence system typically consists of an excitation source, optics to focus the excitation source onto the capillary or other sample cell, collection optics, and the detection system. Much of the work published deals with methods to convert samples into fluorescent forms (i.e, derivatization, either pre-, on-, or post-column) [59]. Nevertheless, some compounds do exhibit native fluorescence under the correct conditions. Swaile and Sepaniak were the first to demonstrate native fluorescence with on-column detection using a UV excitation (frequency doubled Ar-ion laser-257 nm) [41]. Unfortunately, when native fluorescence is used the signal is often weak and the background signal can be high, leading to poorer signal-to-noise ratios than those produced by fluorophore-tagged analytes. Additionally, the UV lasers needed to produce native fluorescence in many compounds are expensive and not readily available.

The quantitative relationship between fluorescence intensity and concentration may be derived from Beer's law [60]. The fundamental equation for fluorescence intensity at low absorption (i.e. at low ϵbC) is

$$F = 2.3I_o\phi_F f(\theta)g(\lambda)\epsilon bC \quad (1.22)$$

where I_o is the incident radiation, ϕ_F is the fluorescence efficiency, $f(\theta)$ represents the geometrical factor as determined by the solid angle of the fluorescing radiation subtended by the detector, $g(\lambda)$ defines the sensitivity of the detector as a function of the fluorescent wavelength incident on it, and ϵbC is the molar absorptivity, path length, and concentration, respectively.

Unlike when UV/Vis absorption is used for detection, the limitations of the short pathlength in CE can be compensated by increasing the source irradiance. As detailed in Equation (1.22), a linear dependence exists between the intensity of fluorescence and the excitation intensity. Thus, the signal-to-noise can be increased by working at high excitation intensities (the "fluorescence advantage"). In LIF-CE measurements, lasers are used as the excitation source because they increase the sensitivity of the technique and they allow the systems to be miniaturized to the smallest diameter capillaries.

Typically when LIF is used for detection in CE, most attention is focused on detection limits and not obtaining spectral information. This is due to the fact that fluorescence from samples in the liquid-state solutions (as with UV/Vis absorption spectra) is rather featureless, and provides little structural information. Nevertheless, as with UV/Vis absorption, wavelength resolved emission could be

used in some cases for analyte identification in CE analyses [61]. Additionally, wavelength resolution can be exploited to discriminate between sources of interferences and/or to increase the S/N ratios. Fluorescence line narrowing, which is fluorescence obtained at ultra-low temperatures, has been used in CE to produce spectra that show sufficient structure to enable discrimination of closely related compounds [62].

Raman

The advantage of Raman spectroscopy over LIF and UV/Vis absorption detection is its ability to provide information-rich spectra, which reveal detailed information about the vibrations of the separated molecules. The vibrations are specific to functional groups in a molecule, therefore the Raman spectra are useful for analyte identification, as well as the ability to elucidate the structures of unknown compounds. In many cases combining the migration time with the Raman spectrum would allow for unambiguous identification of the analytes.

Unfortunately, the analytical potential of Raman as a detection technique is poor due to the extremely small cross section for Raman scattering. In Table (1.2) the typical cross-sections for UV/Vis absorption, fluorescence, Rayleigh scattering, and Raman scattering are presented. Very little credence is given for a CE-Raman system if no analyte enrichment or signal enhancement can be achieved. The sample analytes could be either concentrated prior to CE

Table 1.2 Cross-sections for various photophysical processes [68]

Process	σ (cm²)
UV absorption	10^{-18}
Fluorescence	10^{-19}
Rayleigh Scatter	10^{-26}
Raman Scatter	10^{-29}

Reference: Stevenson, C.L.; Vo-Dinh, T. Modern Techniques in Raman Spectroscopy, Laserna, J.J. Ed, John Wiley and Sons, Chichester, 1996, pp 22.

analysis or they could be concentrated in the capillary by a number of analyte enrichment techniques [34,35]. Theoretically, higher laser powers and/or longer acquisition times could also enhance the S/N. In on-column detection, longer acquisition times are not an acceptable option due to the short residence time of the solute zone in the detection region. However, if off-column detection is utilized, longer acquisition times could be used to increase the signal-to-noise. Resonance Raman and surface-enhanced Raman scattering (SERS) are two modes that are commonly employed to enhance the Raman signal [56,63]. Resonance Raman can be used to give enhancements of 10^2 to 10^4 by using an excitation wavelength that is near coincident with the molecular resonance of the analyte of interest. A problem with resonance Raman is that interference from fluorescence can occur in the same wavelength region. Surface-enhanced techniques, which occur when the analytes are in close proximity to certain metal surfaces, commonly give enhancements of 10^6 or higher and for certain instances SERS has been utilized for single molecule detection. Potentially, SERS-based detection is capable of sensitivities that rival those of LIF, with the added benefit of producing detailed spectra.

A brief discussion of the classical theory of light scattering can provide a better understanding of the Raman process and of the SERS process, which will be discussed further in Chapter 4. An incident light beam induces an oscillation dipole, μ , in a particle which scatters light at the frequency of the dipole oscillation. The fundamental frequency component of the dipole moment can be represented by Equation (1.23):

$$\mu(t) = \mu^\circ \cos(2\pi \nu t) \quad (1.23)$$

where ν is the dipole oscillation (i.e., scattering) frequency, and μ° is the maximum induced dipole moment for a given frequency component of μ . The induced dipole moment can be approximated as:

$$\mu(t) = P \bullet E_{inc}(t) \quad (1.24)$$

where, P is the polarizability of the molecule and E_{inc} is the incident electric field intensity. The polarizability is a term that relates the ease with which molecular orbitals are deformed by the presence of an external field. For a vibration to be Raman active there must be a change in polarizability during the vibration.

Due to the complexity of the scattering process, it is difficult to develop a fundamental equation relating the Raman intensity to molecular parameters. The following equation gives important parameters that influence the radiant power of Raman scattering ϕ_R [64]:

$$\phi_R \propto \sigma(\nu_{ex}) \nu_{ex}^4 E_o n_i e^{-E_i/kT} \quad (1.25)$$

where $\sigma(\nu_{ex})$ is the Raman cross section in cm^2 , n_i is the number density in state i , and the exponential term is the Boltzmann factor for state i . The light source used for Raman scattering has been shown to be very important. Because the Raman signal is directly proportional to the source irradiance E_o , lasers are employed almost exclusively in modern Raman spectroscopy. Additionally, the Raman intensity is highly dependent on the frequency of excitation, ν_{ex}^4 .

Therefore, the lower the wavelength of excitation radiation the higher the Raman

intensity, although many times fluorescence at the lower wavelength competes with the Raman scattering.

An advantage of using Raman in CE is that it uses instrumentation similar to LIF; additionally many laboratories are equipped with Raman instrumentation. The instrumentation required to measure Raman scatter includes a monochromatic excitation source, a high-resolution dispersive element, an appropriate single-channel or multichannel detector. Typically, the excitation source is a laser, which is passed through optical filters to reject unwanted plasma lines and directed onto the sample (capillary with polyimide removed, liquid cell, or solid substrate). The scattered light from the sample is collected through the appropriate optics and focused onto entrance slit of a dispersive element. The dispersive element is either scanned and a photomultiplier tube (PMT) detects the Raman scatter or the Raman scatter is dispersed by a spectrograph onto a multichannel detector, such as a charge-coupled device.

There are several examples in the literature of normal Raman being applied to CE and related techniques. Most recently, Walker et al. monitored the separation of herbicides on a glass microchip by employing isotachopheresis techniques to concentrate the sample [65]. Raman isotachopherograms of the pesticides at concentrations as low as 2.3×10^{-7} M were obtained. Morris et al. used normal Raman spectroscopy as an on-line detector for CE [66]. Sub-ppm mixtures of nitrate and perchlorate samples were separated and detected after performing sample stacking to concentrate the sample. Additionally, Raman has

been used as a diagnostic tool to measure steady state and transient intracapillary temperature gradients during CZE [67].

CE Research and Development Needs

For the past 20 years, researchers have been establishing capillary electrophoresis as the foremost technique for performing high-efficiency liquid separations. However, throughout those years, a prevailing limitation of CE has been poor retention time reproducibility, which is exacerbated when analyzing complex samples that are present in minute volumes. The poor reproducibility can be linked to inconsistencies in the EOF. In CE, the separated peaks must be identified by their migration times and/or from a characteristic-detector response. As previously noted, the conventional detection techniques, absorbance and fluorescence, routinely do not provide detailed spectra from which the separated compounds can be identified. Therefore, the design and development of a more selective spectroscopic detection technique for CE would be beneficial when analyzing complex samples. Several detection techniques that are excellent for analyte identification are not easily amenable to the on-column format. For example, matrix-assisted laser desorption/ mass spectrometry and surface-enhanced Raman scattering are detection techniques that have been used extensively to provide information-rich spectra, however typically these techniques are used to detect compounds on planar substrates. Consequently, a CE technique is needed that will preserve the high-efficiency

separation on a planar substrate, subsequently allowing a variety of powerful detection techniques to be employed.

Chapter 2. DESIGN AND OPTIMIZATION OF ELECTROFILAMENT DEPOSITION

Introduction

In conventional CE, the injected sample is separated and detected on-column, after which the effluent is discarded in the exit-buffer reservoir. Consequently, the opportunity for additional analyses of the separated compounds is essentially lost. The technique reported in this chapter will effectively preserve the separation by depositing the effluent onto a planar substrate. As a result additional analysis, such as two-dimensional separations or surface-enhanced Raman scattering-based detection, can be performed.

Off-column methods of detection can be tedious and compromise separation efficiency. There are, however, numerous advantages to the off-column approach. These include long time constants or signal averaging to improve detectability or acquire spectra, the possibility of using detection and separation conditions that are not compatible, and the possibility of using slow and/or multiple step post-separation derivatization chemistries to facilitate detection. In addition to traditional detection techniques such as absorbance and fluorescence, detection on planar substrates has been performed using a variety of information-rich techniques [69]. Matrix assisted laser desorption mass spectrometry (MALDI/MS) [70], Fourier transform infrared spectroscopy (FTIR) [71], and surface-enhanced Raman scattering (SERS) [56] can provide detailed spectra and specific structural information that could be used for analyte

identification and structural elucidation. Additionally, such techniques as post-column radionuclide detection [72], chemiluminescence [73], fluorescence line-narrowing [74], photoacoustic spectroscopy [75], and secondary ion mass spectrometry (SIMS) have been used for detection on planar substrates [76].

Deposition Techniques for Column Chromatography

When depositing effluent from a chromatography column, the foremost concern is the preservation of the on-column separation. There are several parameters that can contribute to band broadening during deposition. For example, the diameter of the deposited track must be minimized to maintain the separation efficiency. When spray techniques are employed to deposit chromatographic effluent, the width of the deposited track adds to the overall size of the deposited band. The track width is expected to be at least as wide as the diameter of the spray. For a given set of conditions as the diameter of the track increases, the efficiency and resolution are decreased. For example, if the spray had a diameter of 50 μm and the deposited band was 50 μm x 150 μm , the deposition technique would contribute 33 % to the length of the deposited band. This increases to 67 % for a 200- μm diameter spray for the same band.

Essentially, two different approaches can be used to collect the on-column effluent for further analyses: fractions can be collected as they elute from the column or the entire effluent can be comprehensively deposited so as to preserve the separation in time and space [77]. The following discussion will be limited to comprehensive deposition techniques. A variety of deposition

techniques have been employed for high-performance liquid chromatography (HPLC) and for CE. These techniques can be separated into two categories, either direct-deposition techniques (also known as blotting) or spray techniques. The majority of the work involving CE has been with direct-deposition techniques.

As early as 1990, Zare et al. used a grounded on-column frit to close the CE circuit, which allowed the capillary outlet to be coupled to a moving piece of filter paper [78]. Using this method, they were able to deposit the effluent along a track on the filter paper, which became a record of the separation. Since Zare's initial work, commonly the end of the CE capillary has been coated with a conductive metal to complete the electrical connections to close the CE circuit [79, 80]. In regard to maintaining separation performance, the most impressive work was performed by Sweedler et al [81]. By continuously translating a membrane underneath a metal-coated capillary, 350- μm wide tracks were created, which demonstrated off-column separation efficiencies of 170,000 plates.

Spray techniques use either ultrasonic-based nebulization, gas-based nebulization or electrically driven spray to deposit the effluent. Currently, the only commercially available instrument is a HPLC-FTIR (Bourne Scientific, Inc.), which operates under a vacuum and uses an ultrasonic nebulizer to spray the HPLC stream onto a moving substrate [82]. The majority of the spray techniques described in the literature use a spray jet assembly, which is based on a conventional gas nebulizer that uses heated nitrogen to nebulize the effluent onto a planar substrate. Typically, these spray assemblies are well suited to the

high flow rates of HPLC. Due to the inherent width of the spray jet, these techniques are not adequate for maintaining the high-efficiencies that are characteristic of CE separations.

Conversely, electrosprays are more suited to the low flow rates of CE. However, under conventional electrospray conditions, the width of the electrospray is also too wide to preserve the on-column CE efficiency. Two applications of conventional electrospray for continuous deposition have been reported. Beavis et al. used nebulizer-gas-assisted electrospray for the deposition onto a substrate for subsequent SIMS analysis [83]. The nebulizer gas increased the evaporation rate during the spray process and assisted with the spatial focusing of the spray plume. An electrostatic field was used to further focus the spray plume. For these experiments, the deposited spots had a diameter of ~ 1 mm. McLeod et al. also used conventional ES for deposition of analyte solutions [84]. However, their method suffered from poor performance, because the spray had a diameter of ~ 1 cm.

Description of the Electrofilament Process

In the work reported herein, a non-conventional form of ES has been developed to deposit spatially focused CE effluent. In conventional ES, used for introducing liquids into a mass spectrometer, an electric field is applied to a metal capillary [85]. Subsequently, charge accumulates at the liquid surface and is drawn toward the counter electrode such that a liquid cone forms (Taylor cone). At a sufficiently high voltage (~ 2 kV for CH₃OH solution), a liquid filament is

emitted from the Taylor cone and small droplets form. At higher voltages (~ 3 – 5 kV), the liquid filament shortens and at a point that is 0 to 2 mm from the Taylor cone, the Rayleigh limit is reached wherein the droplet charge overcomes surface tension and the liquid filament rapidly expands (Rayleigh explosion). Under these conditions a very fine mist (Figure 2.1a) is produced, which is more optimal for sampling into a mass spectrometer and for production of gas phase ions. In the work presented in this paper, an uncommonly used mode of ES is employed to deposit spatially focused analyte bands from a CE capillary. I have termed this the electrofilament (EF) mode of electrospray. In contrast to the conventional ES mode, a lower voltage (1.5 kV to 2.0 kV) is used, which produces a narrow (~20 μm) liquid filament (Figure 2.1b) that extends from the capillary to a non-conductive planar substrate (placed under a grounding mask) without the occurrence of a Rayleigh explosion. Results of the evaluation of the EF for depositing spatially focused effluent from a CE column are presented in this Chapter.

Experimental

Chemicals and Materials

Unless otherwise noted, the chemicals used to perform the experiments described in this chapter were purchased from Sigma Chemical Co. (St. Louis, MO). The CE running-buffer solution was composed of 4-mM dibasic sodium phosphate and 2.4-mM sodium tetraborate (pH ~ 9). For experiments involving

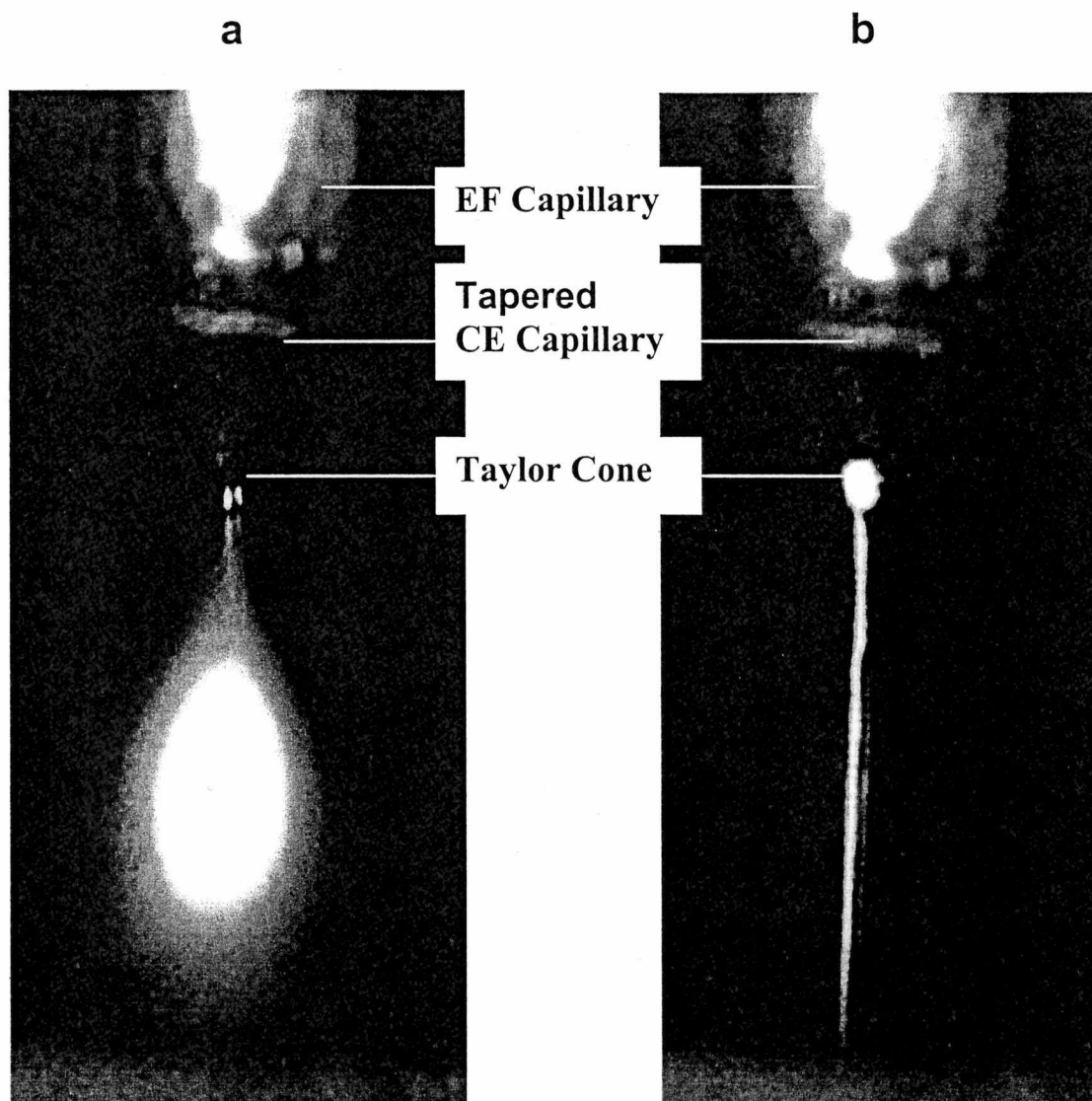


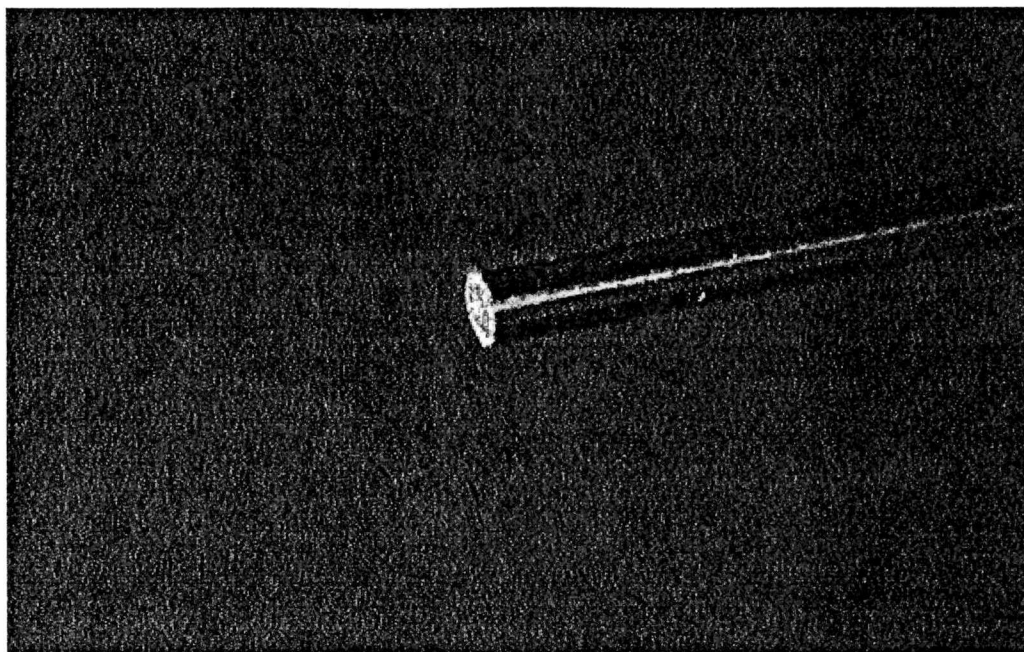
Figure 2.1 Images of the electrospay operating (a) under normal and (b) EF conditions: an ES voltage of 4 kV was used in (a) and in (b) conditions were optimized for EF deposition with a voltage of 2 kV. Experimental conditions are described in the Experimental Section.

injections of anthracene, 20% (v/v) acetonitrile (Fisher Scientific) was added to the CE running buffer. In the micellar electrokinetic capillary chromatography (MEKC) experiments, 50-mM of sodium dodecyl sulfate (SDS) was added to the CE running buffer. The EF liquid sheath solution was composed of 90% methanol (Fisher Scientific, Pittsburgh, PA) /10% (v/v)CE buffer at pH ~7. Fluorescein, eosin Y, and kiton red (Exciton, Dayton, OH) were diluted to the specified concentration in water and/or methanol. Anthracene was diluted in acetonitrile. The substrate used for collecting the deposited bands was adsorbosil octadecyl modified RP-TLC plates (Fisher Scientific).

CE Separations

The CE apparatus was constructed in-house using a 30-kV high voltage power supply (Gamma High Voltage Research, Ormond Beach, FL) operated in constant voltage mode. Under normal CE conditions a running voltage of 15 kV was used, this was increased to 17 kV when an EF voltage of 2 kV was applied. Fused silica capillaries (Polymicro Technologies, Phoenix, AZ), 50 μm i.d., 360 μm o.d., and 40-50 cm in length were tapered to reduce the volume of the Taylor cone, which subsequently reduces the mixing volume. The tapering procedure consisted of placing one cleanly cut end of the fused silica capillary (see Figure 2.2a) into the chuck of a high-speed rotary tool (Dremel, Racine, WI), to rapidly rotate the capillary. The opposite end of the capillary was then drawn across a piece of fiber optic polishing paper at a $\sim 45^\circ$ angle until the tip of the capillary was tapered adequately (see Figure 2.2b).

a.



b.



Figure 2.2 Images of fused-silica capillary used for EF deposition: (a) cleanly-cut end and (b) tapered end.

Hydrodynamic injections were made at a height of 10 cm for 10 sec. An in-house fiber optic LIF cell was used for the on-column detection [86]. The cell is placed immediately before the EF tee (~ 5 cm from the end of the CE capillary) used in the EF apparatus. An argon ion laser (Uniphase, San Jose, CA) operating at 488 nm (10 mW) was focused onto the excitation fiber optic with a biconvex, 25-mm diameter, $f/2$ lens. For the anthracene experiments, a helium-cadmium laser (Omnichrome, Chino, CA) was used to supply the 325-nm laser line. The fluorescence was collected by the emission fiber optic. The end of the emission fiber was placed against a colored glass cut-on filter (518 or 428 nm), which was directly in front of the photo-cathode of a photo-multiplier tube (PMT) (HC-120, Hamamatsu Corp., Bridgewater, NJ). The signal from the PMT was directed to a strip-chart recorder (model 302, Yokogawa Corp. of America, Newnan, GA) and/or a data acquisition board (NI SC-2071, National Instruments, Austin, TX). For on-column experiments, the retention times (t_r) were obtained from the maximum of the peak profile. The theoretical plate numbers were calculated by the tangent method ($N = 16(t_r/W_b)^2$) where: t_r is retention time and W_b is the width at baseline.

EF Deposition

The CE deposition system described in this chapter uses an interface with a coaxial liquid sheath arrangement to deposit the effluent from a capillary column (see Figure 2.3). The liquid sheath (10% CE buffer/ 90% methanol, v/v) provides electrical contact between the EF capillary and the CE buffer, closing

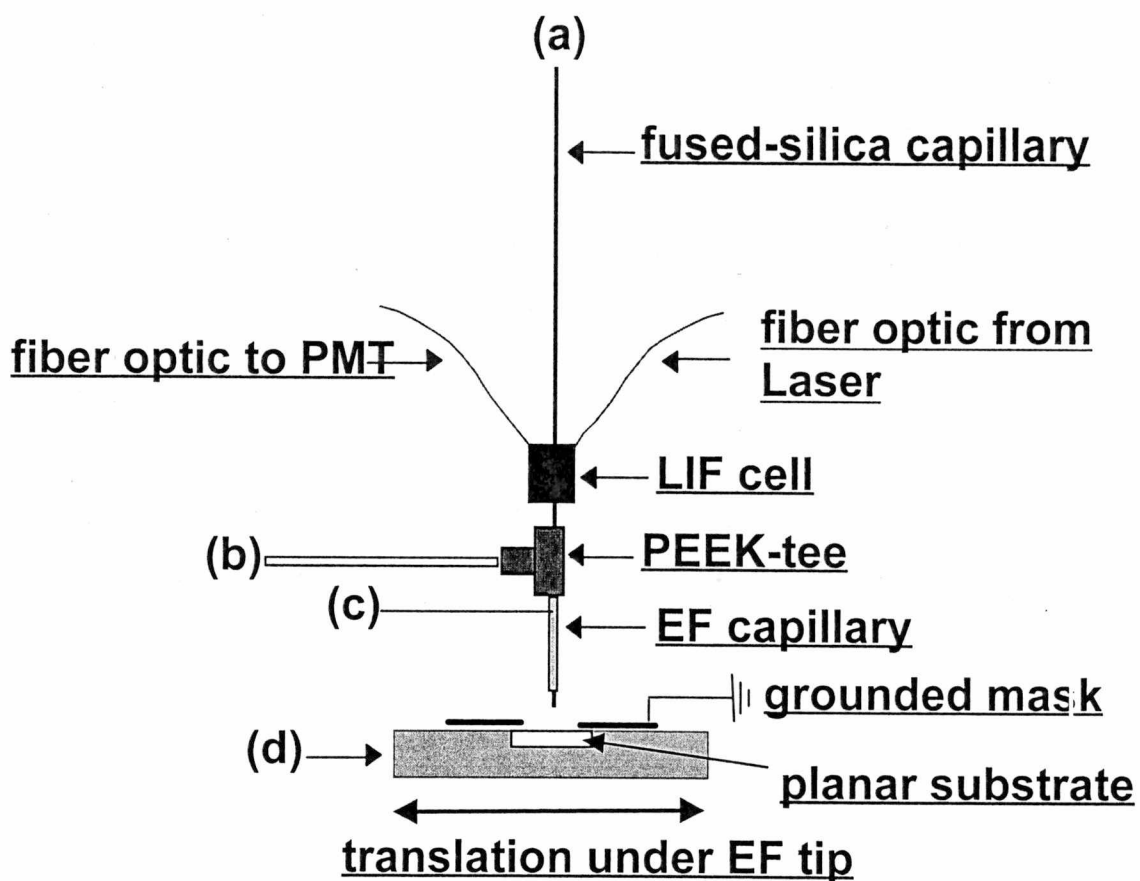


Figure 2.3 Schematic diagram of the EF deposition apparatus. (a) CE high voltage power supply; (b) syringe pump to supply liquid-sheath solution; (c) EF high voltage power supply; (d) heated aluminum block with substrate that is translated under the EF.

the CE circuit. The liquid sheath flow (0.5 – 1.0 $\mu\text{l}/\text{min}$) is supplied by a syringe pump (Fisher Scientific, Pittsburgh, PA). The fluid is pumped through PEEKTM-tubing that is connected to a PEEKTM-tee (Upchurch Scientific, Oak Harbor, WA). The tapered fused silica capillary was passed through the on-column fiber optic LIF cell, the tee, and an $\sim 2\text{-cm}$ section of narrow bore (400 μm i.d. X 700 μm o.d.) stainless steel (SS) tube (EF capillary) that was fixed to the tee. The tapered-end of the CE capillary extended $\sim 500 \mu\text{m}$ beyond the end of the SS capillary. The tip of the capillary was mounted vertically ($\sim 1\text{-}2 \text{ mm}$) above the substrate.

A stainless steel grounding mask (250 μm thick) with a 2-mm x 2-cm machined slit was placed directly over the TLC plate substrate. The TLC plate was mounted in an aluminum block that could be heated with a cartridge heater. The aluminum block was mounted on a programmable translation stage (Klinger Scientific, Richmond Hill, NY) that was electrically insulated from the block. The TLC plate was translated under the EF tip at various rates. The EF voltage (1.5 – 2.0 kV) was supplied by a high voltage power supply (Tennelec, TC 950). A helium-neon laser (Edmund Scientific, Barrington, NJ) was directed onto the liquid filament to enhance visualization by a Panasonic KR222 video microscope (Edmund Scientific, Barrington, NJ). This allowed us to observe and document the physical characteristics of the EF. For the CE/EF deposition experiments, t_r was estimated from the on-column t_r , taking into account the extra 5-cm of column.

Off-Column LIF Detection Instrumentation

Two off-column LIF systems were employed; a scanning PMT system and a charge-coupled device (CCD) imaging system, which are illustrated in Figure (2.4). An argon ion laser was used with a laser line filter to give a primary line of 488 nm (10 mW). The laser light was passed through a mirror (M3) with a 2-mm diameter hole and focused onto the substrate with a biconvex, 25-mm-diameter, $f/1$ lens. The programmable stepper motor was used to translate the substrate under the focused laser beam. The substrate was attached to the stepper motor by an XY stage, which allowed the deposited bands to be optimized relative to the focused laser beam for maximum signal. The fluorescence and the scattered laser light from the TLC plate was collected and collimated by the same $f/1$ lens and directed through a cut-on filter (518 nm) and a holographic 488-nm notch filter (Kaiser Optical, Ann Arbor, MI). A second $f/1$ lens focused the light onto a PMT as described previously. A pen recorder and/or a data-acquisition board were used to obtain hardcopies of the electropherograms.

The CCD imaging system is depicted in Figure 2.4b. An argon ion laser (Coherent Innova 300, Santa Clara, CA) was used to supply the 488-nm light (10-50 mW). The laser beam was expanded to a diameter of 2 cm using a 25-mm, $f/4$ double concave lens. A cut-on filter was placed over a Navitar 7000 close focus zoom lens (Edmond Scientific, Barrington, NJ) attached to a model ST-6 CCD imaging camera (Santa Barbara Instrument Group, Santa Barbara,

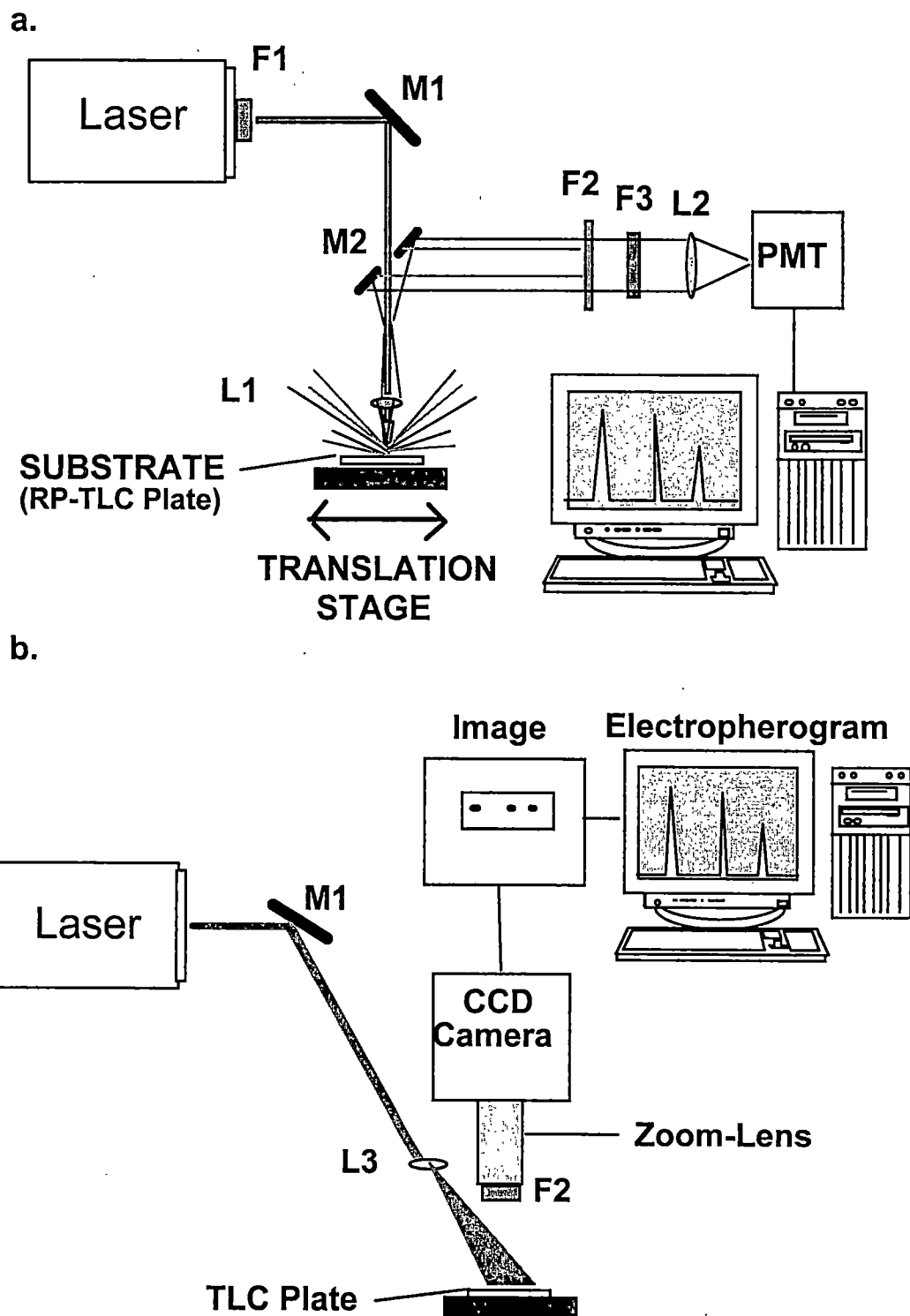


Figure 2.4 Schematic diagrams of the (a) PMT and of the (b) CCD LIF off-column instrumentation used to detect the deposited analytes. Figure labels: mirrors M1 and M2 direct the laser, mirror M2 has a 5-mm hole in the center, L1 and L2 are 25 mm f/1 biconvex lenses, L3 is a double concave lens, F1 is a laser line filter, F2 is a cut-on filter, and F3 is a holographic notch filter.

CA), which had a 375 x 241 pixel array with a size of 23 x 27 μm . Once the CCD image of the deposited bands was saved, the data was converted into ASCII format and loaded into a spreadsheet or GRAMS 386 software (Galactic Industries Corp., Salem, NH) for reconstruction of the electropherogram.

Results and Discussion

Evaluation of the Electrofilament

As previously discussed, when spray techniques are employed to deposit chromatographic effluent, the width of the deposited track adds to the overall size of the deposited band. For a given set of conditions, as the diameter of the track increases the efficiency and resolution are decreased. The newly developed EF technique deposits tracks that are $\sim 100 \mu\text{m}$ in width. Since the liquid filament is considerably narrower ($\sim 20 \mu\text{m}$), there is some broadening occurring on the substrate. It may be possible to deposit narrower bands by employing a more selective substrate than the TLC plate, which would effectively reduce the on-substrate band broadening. By diluting the CE buffer with kiton red and EF depositing onto a RP-TLC plate, a band size of $100 \mu\text{m} \times 800 \mu\text{m}$ is commonly obtained at a translation rate of 1.2 cm/min. Under these conditions, the EF deposition technique is only contributing 13% to the total length of the deposited band.

Electrofilament Effects on the On-Column Separation Performance

Ideally, the deposition technique would not interfere with the on-column separation. Interfacing CE with an ES ionization source for mass spectrometry, under normal (Rayleigh explosion) conditions, has been well documented [87, 88]. The effects of the ES source on the CE separation have largely been ignored until recently [89-93]. Migration irreproducibility and reduced separation efficiency have been observed when ES is interfaced with CE. Reported reasons for the reduced separation performance are moving ionic boundaries [89], penetration of the liquid sheath by diffusion into the CE capillary, electrode reaction at the ES capillary resulting in pH modification [90], and the effects of the ES electric field that penetrates across the CE capillary [93].

When the LIF cell was used for on-column detection (~ 5.0 cm before the EF tip) and the EF voltage (~1.5 kV) was applied, the following on-column results were obtained: an increase in retention times, an extreme amount of peak tailing, and a loss of peak height. One explanation for this behavior is that electrolysis at the ES electrode results in changing conditions inside the CE capillary during a run. To further investigate the temporal characteristics of this phenomenon, four consecutive injections of fluorescein were made with 17-kV CE voltage applied for 1.0 minute between each injection. After the fourth injection the CE voltage and an EF voltage of 2.0-kV was applied for the remainder of the run. The results of this experiment are shown in Figure (2.5). When compared to the same experiment without the EF voltage, increased retention times, peak tailing, and a loss in signal are observed with longer elution times. As expected the first

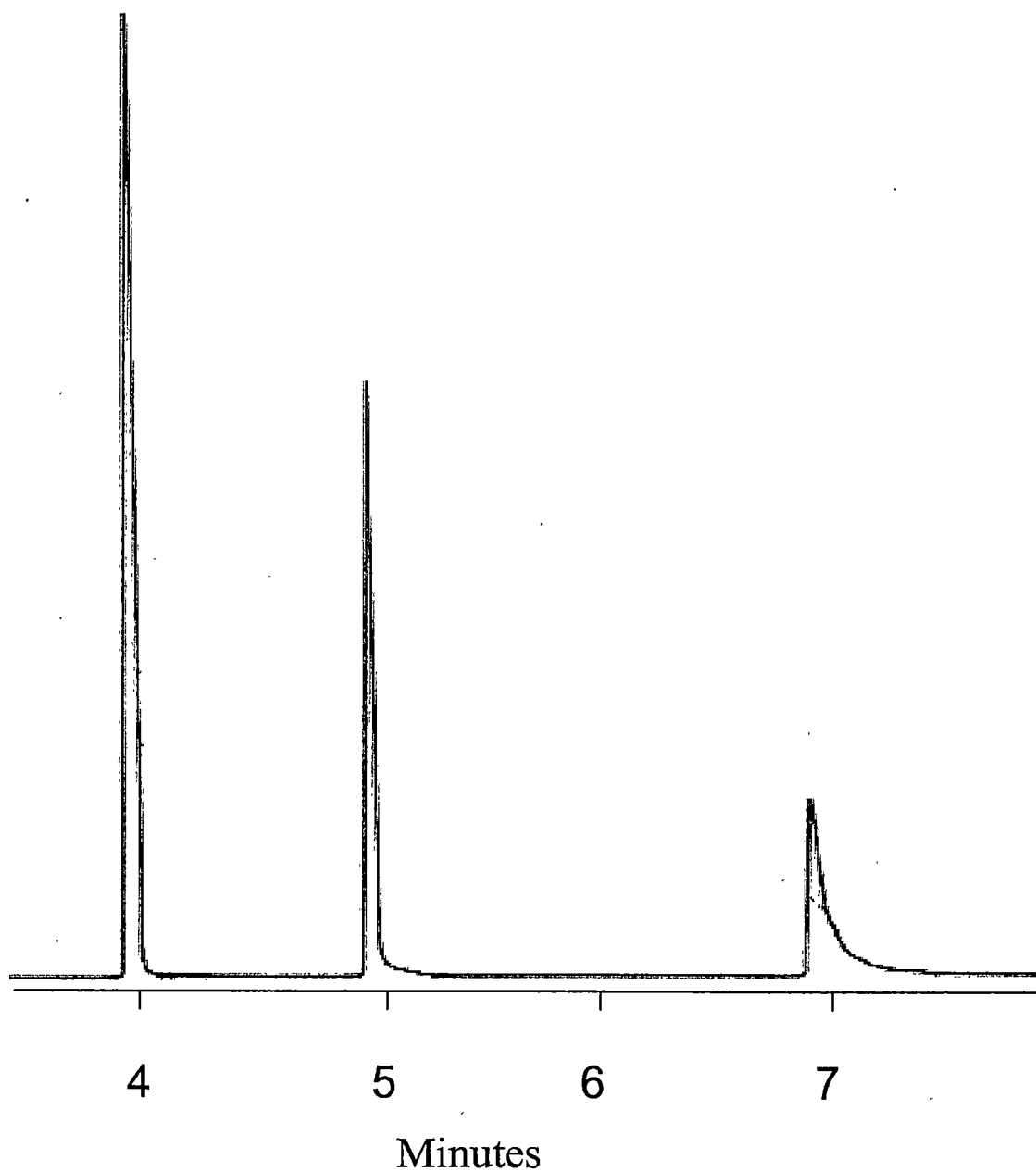
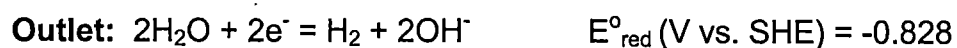


Figure 2.5 Electropherogram showing the effect of the EF voltage on the LIF on-column performance. Four consecutive injections, the fourth was not detected, of 10^{-5} M fluorescein were made with the CE voltage applied for 1 min. between each injection. After the fourth injection, the CE voltage and the EF voltage were applied

two peaks are separated by 1.0 minute, however the second and third peaks are separated by approximately 2.0 minutes. The peak height decreased substantially and the efficiency decreased by 55% between the first and third injections, which represents ~ 6.0 minutes into the run. No signal from the fourth injection was detected. Repetitions of the experiment shown in Figure (2.5) resulted in the same general pattern of fluorescein peaks although migration times varied somewhat. Differences are ascribed to manual timing of the injections and the point at which the EF voltage is applied.

The results, presented in Figure (2.5), demonstrate a dynamic situation where the EF process is affecting the on-column separation. An important consequence of the electrochemistry in ES and in CE is an alteration of the buffer pH. As demonstrated by Moini et al., when CE is interfaced with ES, the electrochemical reactions at the CE outlet/ES capillary can be more complicated than the individual processes of CE and/or ES [94]. Depending on the polarity of the voltages, the pH at the capillary outlet could be increased or decreased, which could have disastrous affects on the on-column separation performance. In conventional CE, the electrolysis of water can change the pH in the buffer reservoirs and inside the CE column [95]. Under cathodic-flow, the CE inlet forms the anode and the grounded-outlet forms the cathode. Water reacts according to:



Normally, large buffer reservoirs (≥ 1 ml) are used in CE to substantially reduce any pH changes. Under the conditions used herein, the effective outlet reservoir volume (i.e. the Taylor cone) was observed with the video microscope to be < 100 nL. Therefore, any electrolysis occurring at the EF electrode will be concentrated in a very small volume at the tip of the CE capillary.

Van Berkel and colleagues have reported changes as great as 4 pH units in bulk solution caused by the ES voltage [96]. The following ES reactions might occur in positive ion mode:



Cook and coworkers have monitored a decrease in the pH of electrosprayed solutions by using LIF [97].

Over time, the electrolysis due to the voltages results in non-equilibrium conditions (e.g. pH gradient), which affect the on-column separation. For example, lowering of the pH could affect the ionization state of the analytes, which in turn can affect the retention times (by changing the electrophoretic velocity), the efficiency (by increasing analyte interactions with the fused-silica wall), and the signal intensities (by lowering the fluorescence quantum efficiency). In addition to influencing the analyte, lowering of the pH will decrease the EOF.

The deterioration in the on-column separation performance, which occurs when an EF voltage is applied, could be a specific problem affecting the dyes analyzed or it could be a more general problem. Under the conditions used, fluorescein is negatively charged and kiton red is positively charged. However, anthracene is a neutral compound that does not contain acidic and basic functional groups. The on-column LIF signal from anthracene was monitored with and without the EF voltage. A small decrease in intensity was observed for the anthracene peak with an EF voltage of 2 kV, which was within a standard deviation of the measurement reproducibility. However, no extreme peak tailing was observed, indicating that the on-column conditions resulting from the EF voltage may affect certain analytes to a greater extent than others. CE uses a variety of running-buffers to separate acidic, basic, and neutral compounds. Therefore it is desirable to develop a robust deposition technique that can be used for a wide range of conditions.

Several experiments were performed in an attempt to reduce the effects caused by the EF voltage. If the problems are due to a change in pH at the CE outlet, then a possible solution is to increase the buffer capacity of either the CE buffer or the liquid sheath solution. Initially, various CE buffers, such as phosphate/borate, ammonia, CHES, CAPS, and TRIS at different concentrations and at different pH values were investigated. Additionally, different combinations of liquid sheath solutions, at different concentrations, and at different pH values were studied. Mixed results were obtained for these experiments. For example, the buffer concentration was increased two- and four-fold in the liquid sheath

solution. Initially, this reduced the problems; however, the results of these experiments were not reproducible. In each of these experiments, the on-column tailing was a major limitation.

A hydrodynamic flow was provided by raising the inlet reservoir to improve the on-column separation performance when the EF voltage was applied. The hydrodynamic flow effectively increases the buffer flow at the CE outlet and it counters the migration of electrolysis products into the CE capillary, thus reducing the non-equilibrium conditions. One advantage of this method is it does not change the separation chemistry of the CE system developed. Additionally, the results obtained with this method were reproducible. The effect of the inlet reservoir height on peak height and asymmetry for kiton red when an EF voltage of 2-kV was applied is illustrated in Figure (2.6). For these studies, asymmetry is a direct reflection of the amount of peak tailing that was observed. As the inlet height was increased, the peak tailing was reduced, and the peak height was increased. At an inlet height of 10 cm a maximum was reached for peak height and a minimum was reached for the asymmetry factor (reflecting the most symmetrical peak). The asymmetry factor is defined as the ratio of peak half-widths at 10% of peak height. The flow rate equivalent of raising the CE inlet 10 cm was calculated using Equation (1.18) to be ~ 0.4 nl/s.

Under normal CE conditions, raising the inlet to induce hydrodynamic flow will result in reduced separation efficiencies [98]. However, the conditions created by the EF interface are not normally accounted for by conventional theory. Datta and Kotamarhi [99] developed a model for dispersion when both

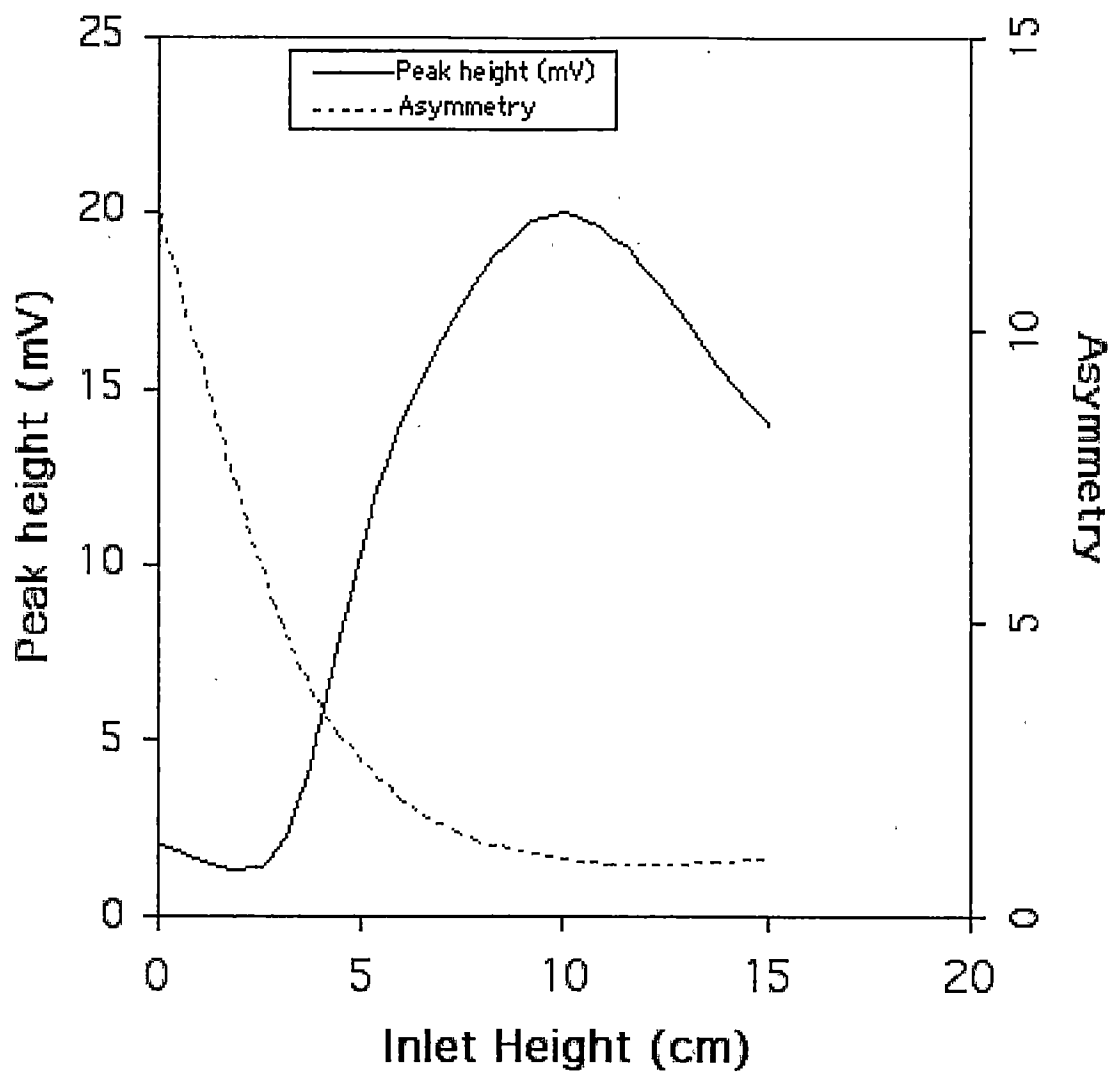


Figure 2.6 Effect of inlet reservoir height on peak height and asymmetry factor of kiton red when an EF voltage of 2 kV is applied.

electroosmotic flow and hydrodynamic flow exists, using the electroosmotic velocity profile developed by Rice and Whitehead [100]. Under these conditions, the plate height (H) expression is given by

$$H = \frac{2D}{v_{tot}} + \frac{r^2}{24Dv_{tot}} v_p^2 + \beta \quad (2.1)$$

where, D is the diffusion coefficient, v_{tot} is the total average velocity, r is the capillary inside radius, and v_p is the hydrodynamic flow velocity component. To account for the loss of separation efficiency associated with conditions not accounted for by conventional theory a third variable, β , has been introduced to Equation (2.1). β represents contributions to H resulting from non-equilibrium conditions, adsorption, pH changes, etc.; effects that are exacerbated by the EF process. When there are no hydrodynamic flow and EF effects present, Equation (2.1) reduces to the diffusion limited dispersion case. The theoretical plate count (N), which is a measure of efficiency, is inversely proportional to the plate height (see Equation 1.14).

In Table 2.1, Equation (2.1) is solved as a function of inlet height for kiton red. H is experimentally obtained for different conditions. The H calculated using Equation (2.1) may not agree with the H experimentally determined, due to an assumption of a diffusion coefficient of 2×10^{-5} cm²/s. Moreover, there are considerable errors in estimating both retention times and efficiency from electropherograms under peak tailing conditions. The existence of a β -term

Table 2.1 Equation (2.1) solved as a function of inlet reservoir height over the outlet reservoir for kiton red.

Inlet height ^a (cm)	H ^b (cm)	$\frac{2D}{v_{tot}}$ c (cm)	$\frac{r^2}{24Dv_{tot}} v_p$ (cm)	β (cm)
0 (no ES)	1.1E-03	2.1E-04	0	8.9E-04
0	7.2E-02	2.2E-04	0	7.2E-02
10	1.2E-03	1.9E-04	8.1E-04	-
15	1.6E-03	1.8E-04	1.3E-03	-

- a.) Height of inlet reservoir above the outlet reservoir.
- b.) Experimentally determined plate height.
- c.) Diffusion coefficient is assumed to be 2.0×10^{-5} cm²/sec.

without EF voltage is likely due to capillary wall adsorption by the positively charged analyte. When the inlet and outlet are approximately equal height and the EF voltage is applied, a dramatic eighty-fold increase in β is observed. When the β -term dominates an extreme amount of on-column peak tailing is observed (Figure 2.7a). Raising the inlet to 10-cm causes the β -term to be reduced dramatically. Under these conditions, we obtain a minimum for H when the EF voltage is applied, despite the presence of a hydrodynamic flow contribution to H. The value of β at 10-cm inlet height is listed as less than the no EF case. This probably reflects the errors discussed above. By providing hydrodynamic flow, we have minimized the on-column effects caused by the EF voltage, as indicated by the symmetrical peak observed (Figure 2.7b). As the inlet height is raised further to 15-cm, the hydrodynamic flow term increases and symmetrical band broadening occurs as predicted by Equation (2.1).

Optimization of Deposition Conditions

There are several variables, such as EF voltage, sheath liquid composition and flow rate, distance between EF tip and collection substrate, and type of substrate, which could affect the performance of the deposition system. There is a complex interrelationship that exists for many of these variables, thus preventing them from being optimized independently. For example, the distance between the EF tip and the collection substrate can be optimized between ~1-5 mm. However, when this distance is varied the EF voltage has to be changed to

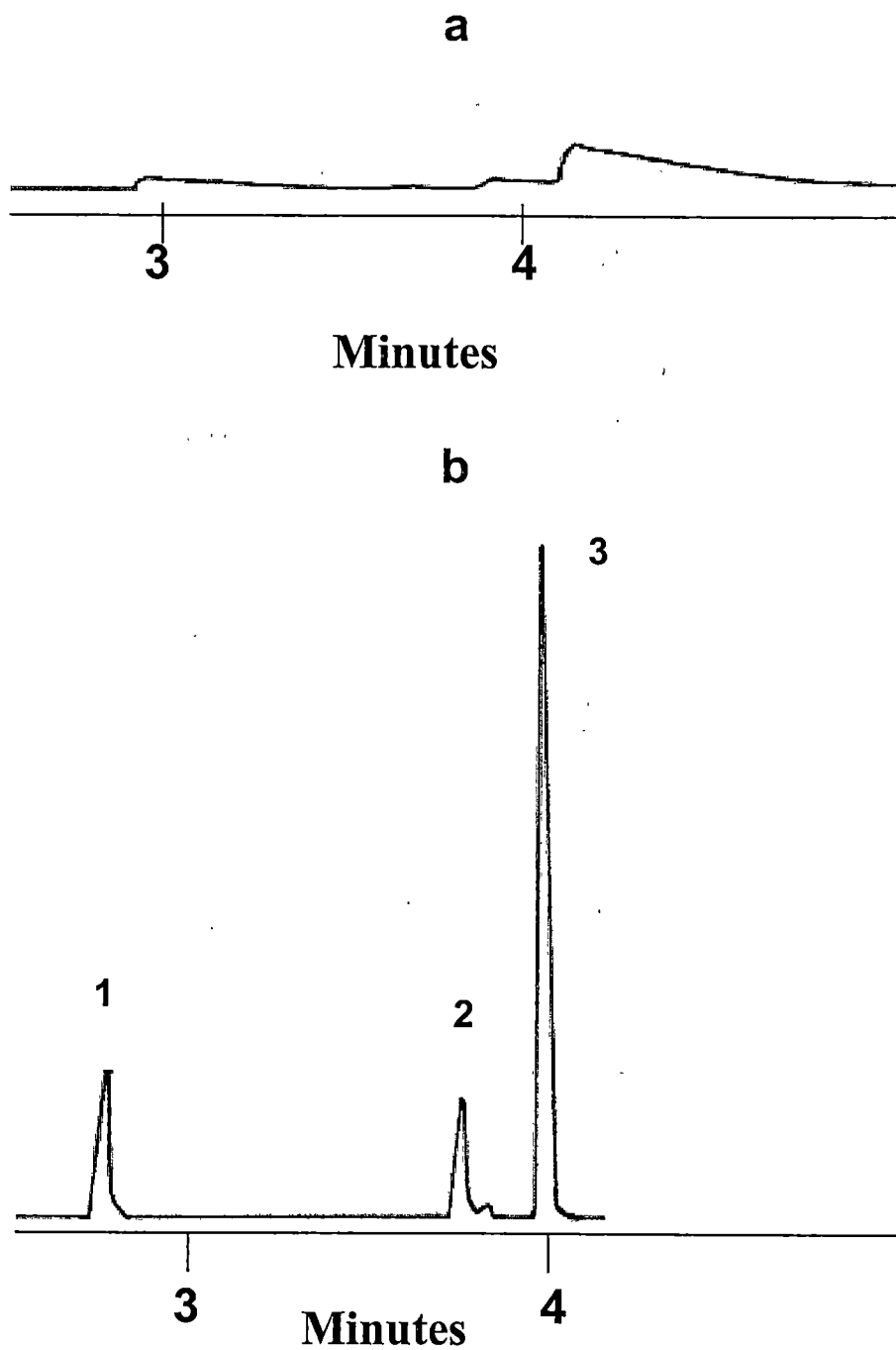


Figure 2.7 On-column electropherograms during EF deposition (a) with the inlet-buffer reservoir level with outlet and (b) with it 10-cm above the outlet. Analytes used for the experiments: (1) kiton red, (2) eosin Y, and (3) fluorescein. Conditions as described in the Experimental.

maintain the liquid filament. The critical variables that are optimized in this work are temperature of the substrate (RP-TLC plate) and substrate translation rate.

As is the case for any chromatography, the distribution of the solute between the mobile phase (in our case the liquid sheath solution and the CE buffer) and the solid phase (RP-TLC plate) results from the balance of forces between the solute and the two phases. The total flow of the CE/EF does not exceed 2 $\mu\text{l}/\text{min}$. This flow is directed in a small area on the TLC plate, which results in a considerable amount of wetting when the substrate is at room temperature. The majority of the wetting is due to the sheath liquid (90% CH_3OH). Methanol is used because its low surface tension renders it one of the easiest solutions to stretch out into a Taylor cone and obtain a liquid filament [85]. The analytes, kiton red and fluorescein, are very soluble in CH_3OH . An advantage may be realized by using a sheath liquid in which the solutes of interest are not so soluble. Increasing the substrate temperature during depositions can result in the reduction of on-substrate broadening, by forcing the solute molecules into the solid phase by changing the phase ratio via rapid evaporation. A dramatic improvement is obtained for fluorescein by increasing the temperature, while kiton red exhibits considerably less improvement, presumably because it partitions more efficiently into the stationary phase of the TLC plates reducing the on-substrate band broadening. Excessive temperatures could cause thermal degradation of deposited analytes or damage to stationary

phase. The results of increasing substrate temperature are shown in Table (2.2). For these optimization experiments, standard deviations were not tabulated.

The translation rate of the substrate under the EF tip was varied to determine its affect on separation efficiency and resolution. The results for these experiments are shown in Table (2.3). As the translation rate increases, the resolution and efficiency increase. The efficiency increases because broadening due to the width of the track has less of a contribution to the total band length. In theory, an improvement in the LOD should be realized by translating at slower rates, which would concentrate the bands onto smaller spots on the substrates. Based on a conventional TLC, a LOD of 5 pg for LIF is typical for a 10-mm² spot size [101]. Therefore, a 200 μm x 300 μm band (0.06 mm²) is expected to produce an LIF LOD of 30 fg, whereas, a 50 μm x 150 μm band (.0075 mm²) would have a LIF LOD of 4 fg. Experimentally, as the translation rate was reduced from 1.2 cm/min. to 0.5 cm/min., we did observe a modest increase in peak height. However, we would expect an ~ 2.4 fold increase in peak height. At the slowest translation rate, there is more on-substrate broadening that occurs, which reduces the expected concentration effect. Additionally, when analyte bands are concentrated into a small spot there could be self-absorption of the fluorescence, which would reduce the signal obtained.

Table 2.2 Effects of substrate temperature, during analyte deposition, on detection and separation parameters.^a

°C ^b	Peak Height ^c		Efficiency (N/m)	
	Kiton Red	Fluorescein	Kiton Red	Fluorescein
25	36000	1320	55000	22000
70	32000	4720	60000	75000

- a.) Experiments performed at a translation rate of 1.2 cm/min.
- b.) Temperature of the substrate during deposition.
- c.) Peak height obtained from the CCD camera in counts / sec with a laser power of 10-mW.

Table 2.3 Effects of substrate translation rate on detection and separation parameters.

Translation ^a (cm / min.)	Rs	Peak Height ^b		Efficiency (N/m)	
		Kiton Red	Fluorescein	Kiton Red	Fluorescein
0.24	2.7	149000	10300	3300	2900
0.50	6.8	162000	27100	20000	17000
1.20	15.	138000	19000	55000	68000

- a.) The rate at which the substrate was translated under the electrospray.
- b.) Peak height obtained on the CCD camera in counts/ sec with a laser power of 50-mW.

Comparison of On- and Off-Column Electropherograms

In Figure (2.8), the on-column separation is directly compared to the off-column separation, at a substrate temperature of 65 °C and a translation rate of 1.2 cm/min. On-column theoretical plate counts per meter of 46,000 and 60,000 were obtained for kiton red and fluorescein, respectively. These compare to 48,000 and 65,000 plates per meter obtained for those same separated bands deposited onto a RP-TLC plate. The on-column peak resolution was 13, which compared to 14 for the off-column detection. Admittedly, the on-column efficiencies are not as great as one often observes for CE. However, these results illustrate that the EF process does not drastically reduce the separation performance obtained on-column. A measurement error of ~ 10% accounts for the increase in plate count observed for the off-column detection. The relative signal intensities of kiton red and fluorescein do not agree for the on- and off-column detection in Figure (2.8). Several differences between fluorescence of an analyte in solution (on-column) and on a TLC plate have been reported [101]. Poor reproducibility due to an inability to inject constant volumes and consistently control electroosmotic flow (EOF) is an inherent problem of CE. The problems with reproducibility may be magnified when the EF technique is involved. Table (2.4) gives % RSD values for several separation and detection parameters as they relate to off- and on-column detection. The reproducibility of the off-column LIF detection is comparable with that of the on-column LIF detection. The detection parameters (peak height and area) are probably limited by the precision of the manual injection process, which is the case for normal CE.

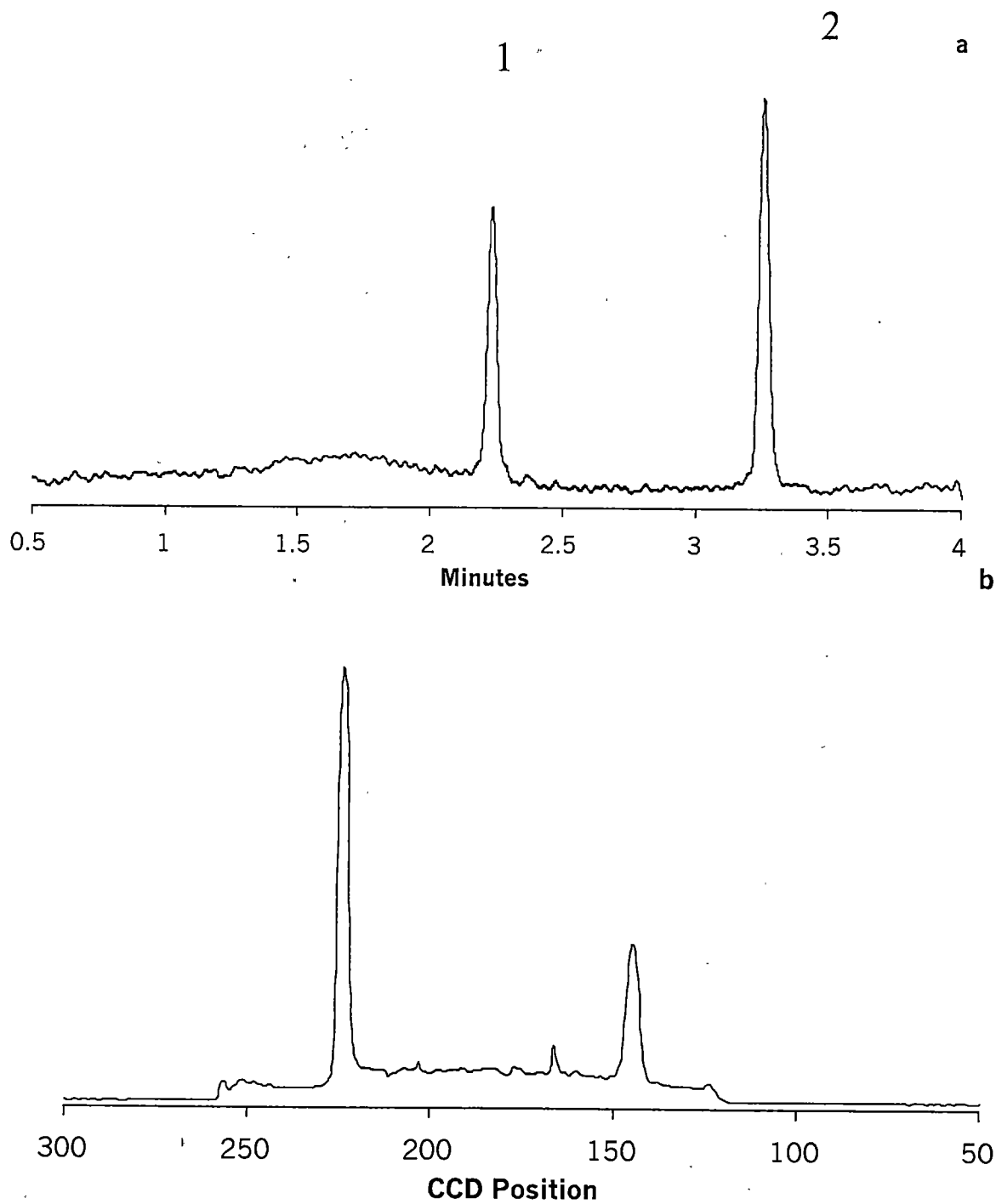


Figure 2.8 Electropherograms of kiton red (1) and fluorescein (2) comparing (a) the on-column LIF detection and (b) the off-column LIF detection. A substrate temperature of 65°C and a translation rate of 1.2 cm/min were used. All other conditions are described in the Experimental.

Table 2.4 Comparison of reproducibility for on- and off-column detection of kiton red.

	On-column (PMT) %RSD	Off-column (CCD) % RSD	Off-column (PMT) % RSD
Retention time (Rt)	4	4	4
Peak width (Wb)	10	7	17
Peak area	13	10	13
Peak height	17	14	11
Efficiency (N)	17	15	14

Additionally, the electrochemistry effects resulting from the EF voltage could affect retention time reproducibility.

The real advantages of preserving a CE separation onto a substrate will be realized when more information rich techniques, such as MALDI-MS or SERS are employed. However, we wanted to characterize the quantitative nature of the LIF detection. Figure (2.9) shows the calibration curve obtained for kiton red deposited by EF-CE onto RP-TLC plates and detected with the PMT LIF system. This curve illustrates a linear dynamic range of 10^3 and a LOD 10^{-8} M for kiton red. Surface features on the TLC plates, with approximately the same dimensions as the deposited bands, limit the LOD that is obtainable. With more uniform substrates the advantage of off-line LIF detection should be more fully realized.

The versatility of CE is partially due to its ability to separate negatively charged, positively charged, or neutral compounds. For the neutral solutes, a pseudo stationary phase (e.g., SDS or cyclodextrin) is added to the buffer to achieve separations. These additives are not normally used with CE-ESI mass spectrometry [102]. However, they should not present a problem when using an EF to deposit onto substrates. Under MEKC conditions, a stable liquid filament was obtained with 50-mM of SDS added to the CE buffer. The retention times of kiton red and Fluorescein increased and the elution order reversed when the SDS is added to the CE buffer, but separation performance was not appreciably altered. The EF mode of electrospray offers an alternative technique for spatially depositing the effluent from a CE capillary.

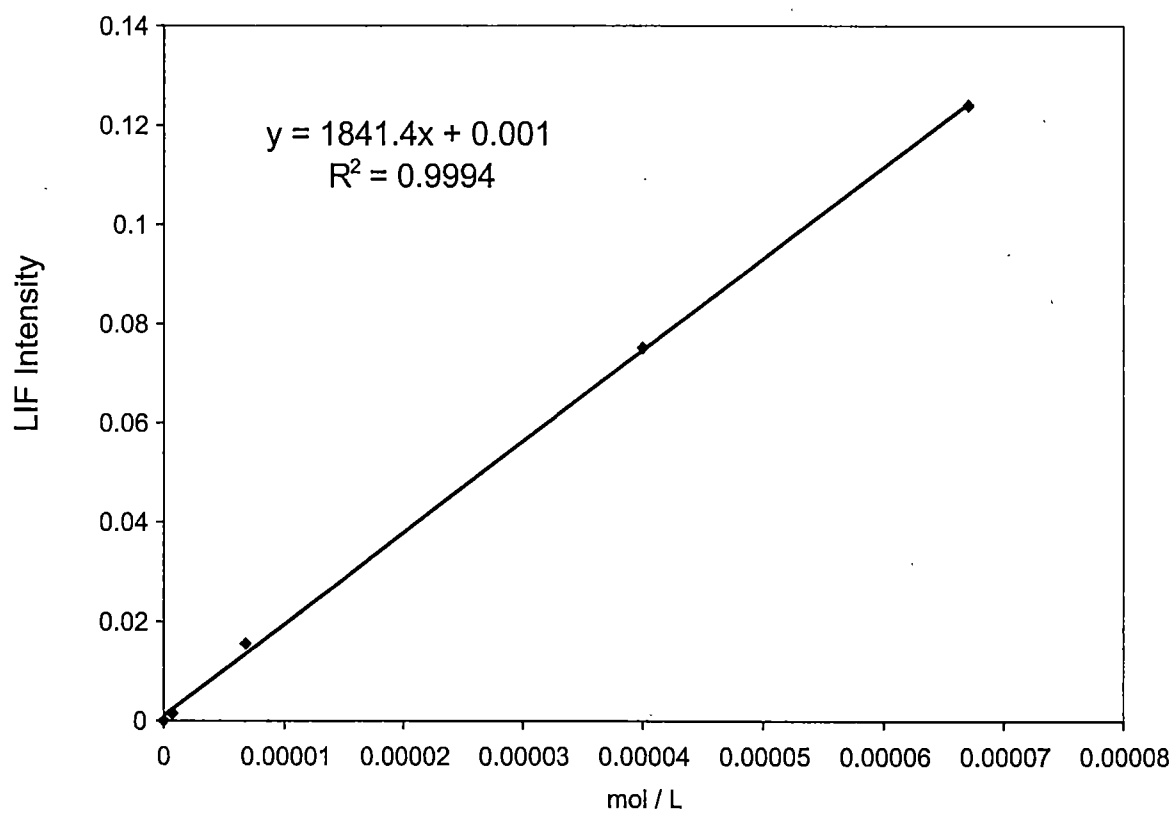


Figure 2.9 Calibration curve for kiton red deposited on a RP-TLC plate and detected using the PMT scanning instrument.

Chapter 3. TWO-DIMENSIONAL CAPILLARY ELECTROPHORESIS/THIN-LAYER CHROMATOGRAPHY

Introduction

Capillary electrophoresis (CE) has been used to separate complex mixtures in one dimension, however the peak capacity (n_c) is limited in one-dimensional separations. Peak capacity is defined as the maximum number of Gaussian peaks that can be placed side-by-side within the available separation space and is calculated as follows [103]:

$$n_c = 1 + \frac{N^{1/2} \ln t_{\max}/t_{\min}}{4R_s} \quad (3.1)$$

where, N is the number of theoretical plates and R_s is the resolution. The workable elution range is represented by the ratio t_{\max}/t_{\min} , the ratio of the latest and earliest eluting peaks, respectively. Commonly, increasing the efficiency (N), for example by increasing the column length, will increase the peak capacity of a system.

The peak capacity is an ideal approximation of the resolving power of a chromatographic system. In reality, component peaks usually distribute themselves somewhat randomly. Davis and Giddings estimated that due to disordered distributions of component peaks no more than 18% of the full peak capacity of a system can be used to generate adequate resolution [104].

Considering this low estimate and the demands being placed on separation techniques by complex sample matrices, research into the development and optimization of two-dimensional (2D) separations is needed and on-going.

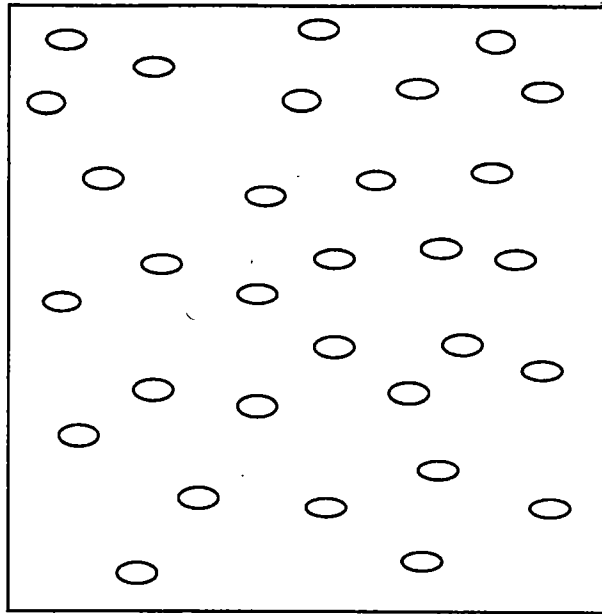
In multidimensional separation systems, a component peak separated in the primary dimension undergoes subsequent separation in at least one additional dimension. While n_c is limited in the 1st-dimension, by using a 2nd-dimension it can be significantly enhanced. Giddings reported 2D separations have peak capacities that are equal to the product of the peak capacities of the one-dimensional methods [105]. The 2D n_c is calculated below:

$$n_c = n_1 * n_2 \quad (3.2)$$

where, the 1st and 2nd dimension peak capacities are n_1 and n_2 , respectively.

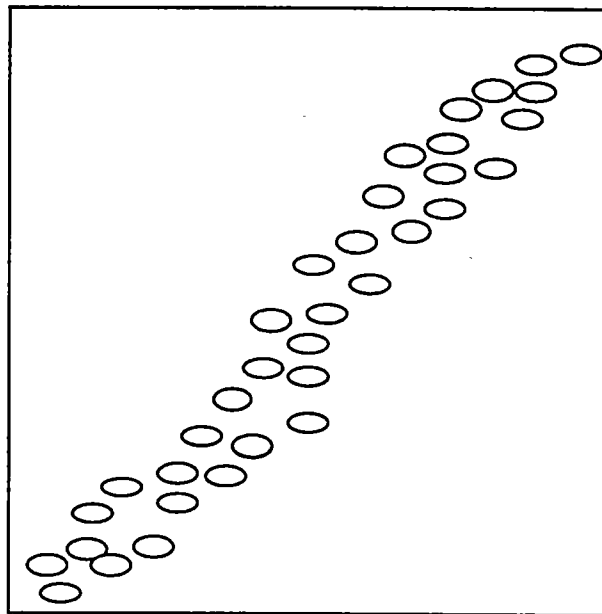
In 2D separations, two distinctly different separation mechanisms are coupled together. The information gained from the 1st separation should not be duplicated in the 2nd separation. As shown in Figure (3.1), peaks appear as spots in the theoretical 2D separations. The separation is considered to be orthogonal if the spots are distributed randomly across the separation space, as in Figure (3.1a). However, if there is a correlation between the separation spots, as in Figure (3.1b), the separation mechanisms are similar in nature (i.e. some of the information gained in the 1st dimension was reproduced in the 2nd dimension). When the separation mechanisms are not orthogonal, the optimum multi-dimensional peak capacity will not be realized. For CE and TLC, analytes are separated by two different displacement techniques represented by

a.



DIMENSION 2

b.



DIMENSION 2

Figure 3.1 Theoretical 2D separations: (a) has a high degree of orthogonality and (b) has separation mechanisms that are similar (non-orthogonal).

electrophoretic and chromatographic mechanisms, respectively. Consequently, a high degree of orthogonality is possible with this approach.

Admittedly, the coupling of CE to thin-layer chromatography (TLC) reported in this chapter could be tedious and compromise separation efficiency. However, many advantages can be realized by this coupling. In addition to the potential for high n_c , as outlined by Poole [106], many advantages can be derived from exploiting the inherent attributes of TLC: separation of samples in parallel, disposable stationary phases, and a convenient storage device for archiving separations, to mention a few. Several advantages that were discussed in Chapter 2 can be attributed to the off-column nature of the CE-TLC experiment. For example, long time constants or signal averaging can be used to improve detectability or acquire spectra.

In the work presented in this chapter, the electrofilament (EF) mode of electrospray, as described in Chapter 2, is used to deposit the effluent from the CE column onto the TLC plate. In the CE-TLC experiment, the TLC plate first stores the on-column CE separation (1st dimension) and then serves as the stationary phase for subsequent TLC separations (2nd dimension). Consequently, the two separation dimensions are separated in time and space, allowing them to be optimized completely independently of one another.

CE Two-Dimensional 2D-Separations

Planar chromatography and slab-gel electrophoresis are established methods for 2D separations [107, 108]. Jorgenson et al. demonstrated

comprehensive 2D liquid chromatography-capillary electrophoresis (LC-CE) methods in the early 1990's. Reverse-phased HPLC was interfaced with CZE to create a coupled column system. The HPLC column was frequently sampled by the CZE portion of the system, which was coupled to a data acquisition system that could be used to view separations in both dimensions. This technique clearly demonstrated the advantages of 2D methods by obtaining peak capacities in the range of 2000 to 20,000 [109-112]. Jorgenson and Moore have also demonstrated comprehensive three-dimensional separation of peptides using size exclusion chromatography, reversed phase HPLC, and CZE [113]. In this work, separation occurred through differences in size, hydrophobicity, and electrophoretic mobility. More recently, Ramsey et al. employed microfabricated fluidic devices that combine micellar electrokinetic chromatography and high-speed open-channel electrophoresis on a single "lab-on-a-chip" structure for rapid two-dimensional separation of peptides [114]. In this work, peak capacities for the 2D methods were estimated to be in the 500 to 1000 range.

The majority of the 2D separations coupling column chromatography to planar chromatography have coupled liquid chromatography to TLC. Poole and Somsen have recently provided excellent reviews of the LC-TLC techniques [106, 115]. Deposition techniques for column chromatography were extensively covered in Chapter 2. For these methods the most common interface is a spray jet (nebulizer-based spray), which allows the whole column effluent to be applied to the TLC plates [54, 71]. Spray jets are useful when the flow rate is in the

range of 5 to 100 $\mu\text{l}/\text{min}$, however when higher flow rates are utilized the effluent has to be split.

Sweedler et al. has published the only example of CE being coupled to a form of planar chromatography, channel-gel electrophoresis [116]. By moving the outlet end of capillary along the entrance of a channel, both separations were preserved. Mixtures of peptides were well resolved in 15 min., with theoretical plate numbers in the 20,000 to 50,000 range. Until the work reported herein, the coupling of CE to TLC for the purpose of 2D separations had not been investigated.

Thin-Layer Chromatography

TLC belongs to a family of planar chromatography techniques, which includes slab-gel electrophoresis that was discussed in Chapter 1. TLC has been used to separate a wide variety of compounds (organic, inorganic, biologicals, polymers, chirals) for assorted applications including environmental, pharmaceutical and food analysis [106]. Although TLC is limited to peak capacities of 10 to 50, Shi and Davis showed that only a small n_c is needed in the second dimension to produce adequate separation of components in complex mixtures [117]. Although TLC has experienced a downturn in its industrial use, as discussed in the review by Poole, there is still much interest in it as a technique complementary to HPLC [106].

Although more sophisticated TLC methods involving forced flow and electroosmotic flow exists [110], the simple experimental set-up used in the work

described herein is shown in Figure (3.2a). In the conventional TLC experiment, a sample is applied to the separation layer as a spot or band near the bottom edge of the plate. The separation is carried out in an enclosed chamber by contacting the bottom edge of the plate (just below the sample spots) with the mobile phase, which advances through the sorbent layer by capillary forces. A sample is separated by different rates of migration in the direction traveled by the mobile phase. After the mobile phase has evaporated, the component spots can be evaluated using various detection techniques.

The retardation factor value (R_f) is the fundamental parameter used to characterize the position of the spots (see Figure 3.2b) and is given by Equation (3.3)

$$R_f = \frac{Z_x}{(Z_f - Z_o)} \quad (3.3)$$

where, Z_x is the distance traveled by the sample from its origin, $(Z_f - Z_o)$ is the distance traveled by the mobile phase from the sample origin, Z_f the distance traveled by the mobile phase measured from the highest position on the plate at the start of the separation, and z_o the distance from the sample origin to the position used as the origin for the mobile phase.

R_f is related to the more common chromatographic retention parameter, capacity factor (k), by

$$k = \frac{(1 - R_f)}{R_f} \quad (3.4)$$

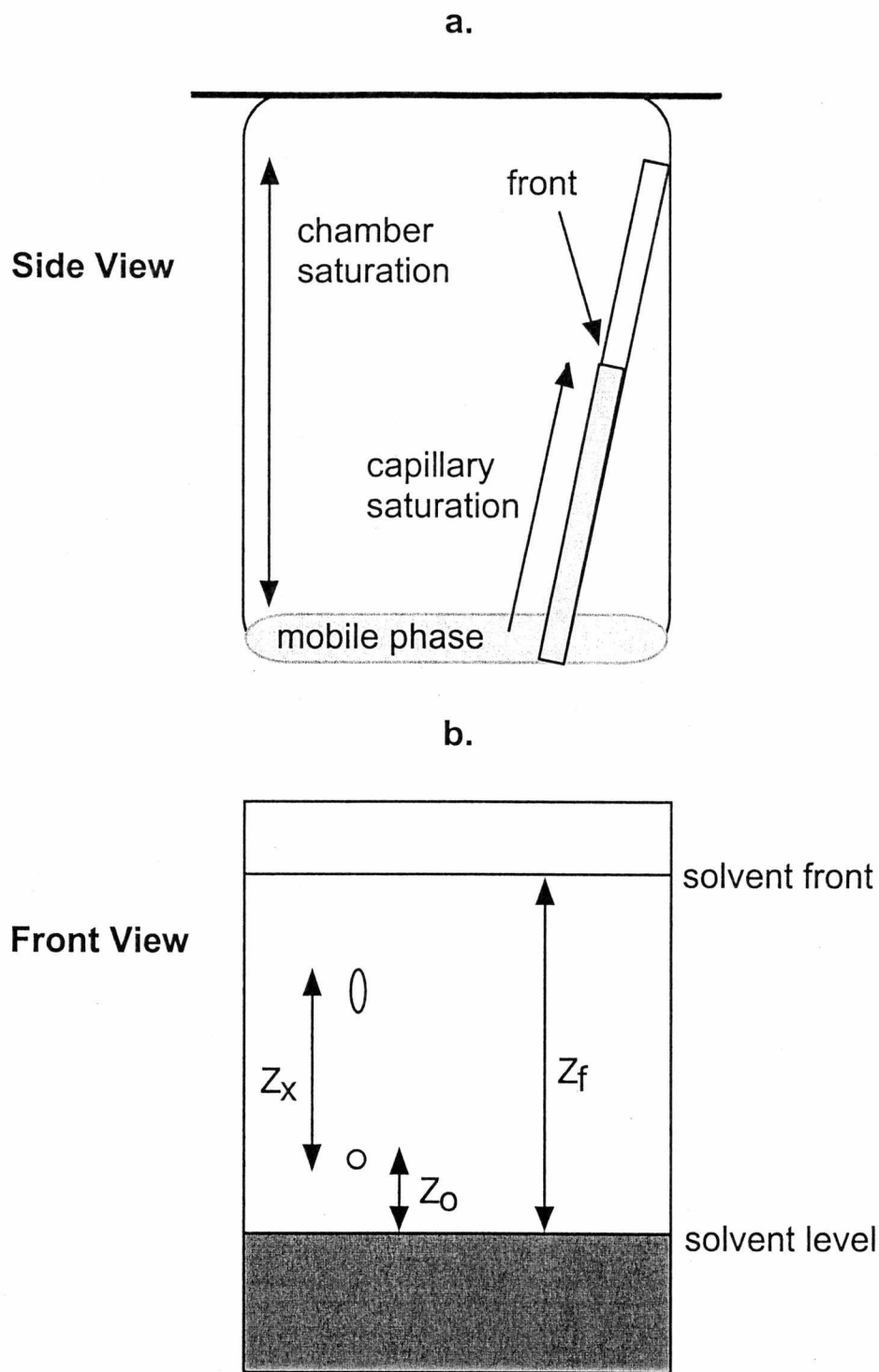


Figure 3.2 Illustrations depicting (a) the TLC experimental set-up and (b) the nomenclature used to define the R_f value in Equation (3.3).

The capacity factor of a sample zone is defined as the ratio of the time spent by the solute in the stationary phase compared to the time it spends in the mobile phase.

Chiral Amino Acid Separations

The capability of the 2D CE/TLC technique developed in this work is demonstrated by separating dansylated (DNS)-amino acids and their enantiomers. The separation of chiral compounds is of key importance for many different fields of applications, e.g. pharmaceutical, industrial, forensic, biological, and clinical [30]. CE has proven useful in the analysis of chiral compounds and particularly in the analysis of amino acid enantiomers [118, 119]. Commonly, cyclodextrins (CD) are added to CE for chiral separations, as discussed in Chapter 1. In CD mediated MEKC, inclusion complex formation modifies retention by reducing the electrophoretic mobility of charged solutes in CE and by inhibiting the association of neutral solutes with the micellar phase [120]. As illustrated by Sepaniak et al., the optimization of on-column CD-CE chiral separations can be difficult, because both the general and enantio-selective elution behaviors must be considered in one-dimension [121]. In CD-CE and in CD-mediated MEKC the optimization of these two elution mechanisms will not be independent. In contrast, by de-coupling the general and enantiomeric separations in the CE-TLC technique, the two separations can be more effectively optimized.

The separation of the enantiomers is carried out on TLC chiral precoated plates or on plates impregnated with chiral substances [122]. The chiral TLC separation technique used in the work presented in this Chapter was first introduced by Armstrong et al. and was extended by Lepri et al. and LeFevre [123-125]. The method involves the use of reversed-phase (RP) TLC with a high concentration of β -CD in the mobile phase. Similar to CE, inclusion complexes with the chiral CDs modify retention, thus permitting enantio-selectivity. The β -CD has a limited solubility in hydro-organic solvents, approximately 0.017 M, which proves to be insufficient for the TLC separation of enantiomers. Resolution of enantiomers is achieved by increasing the concentration of β -CD above its solubility in pure water by the addition of urea [123]. This planar method has separated all but two (proline and tryptophan) of the dansyl derivatives of the nineteen common optically active amino acids found in proteins.

Experimental

Chemicals and Materials

Unless otherwise noted, the chemicals used to perform the experiments described in this chapter were purchased from Sigma Chemical Co. (St. Louis, MO). The CE buffer solution was composed of 10-mM sodium tetraborate (pH ~ 9.5) and in the MEKC experiments 40-mM sodium dodecyl sulfate was added. In the on-column CD-mediated MEKC experiments, either β - or γ -CD at various

concentrations were added to the MEKC buffer. For on-column experiments, when the concentration of β -CD is above 0.017 M a 5-M solution of urea was added to increase the solubility. In the TLC experiments, a high concentration of β -CD (0.2 M) was dissolved in a saturated urea solution. The TLC mobile phase consisted of acetonitrile-0.2M β -CD solution (20:80 v/v). In addition, sodium chloride (0.6 M) was added to the TLC mobile phase to stabilize the binder of the reversed-phase plates. Without this salt, mobile phases containing more than 50% water can dissolve the binder of reverse-phase plates. The EF liquid sheath solution was composed of 90% methanol (Fisher Scientific, Pittsburgh, PA) and 10% CE buffer at a pH \sim 7. The TLC plates were adsorbosil octadecyl modified RP-TLC plates (Fisher Scientific, Pittsburgh, PA). The 5-dimethylaminonaphthalene-1-sulfonyl (DNS)-DL-amino acids, leucine (Leu), valine (Val), norvaline (Norv), and norleucine (Norl), were dissolved in water at a concentration of 10^{-3} M for the two-dimensional experiments and at 10^{-4} M for the on-column experiments.

CE Separations and EF Deposition

The CE and EF deposition systems are described in Chapter 2. Fused silica capillaries (Polymicro Technologies, Phoenix, AZ), 50 μ m i.d., 360 μ m o.d., 62 cm length (57 cm to the LIF window) were tapered to reduce the mixing volume at the end of the CE capillary. Hydrodynamic injections were made at a height of 10 cm for 10 sec. Losses in efficiency (as described in Chapter 2) due

to the less than ideal conditions of our EF interface can be mitigated to large degree by introducing a hydrodynamic flow toward the detection side of the capillary. Thus, we have found it advantageous to raise the inlet of the 50 μm i.d. capillary approximately 10 cm (see Chapter 2). An in-house fiber optic LIF cell was used for the on-column detection experiments (~ 5 cm from the end of the capillary) [86]. A helium-cadmium laser (Omnichrome, Chino, CA) was used to excite the fluorescence at 325 nm. The TLC plate temperature was maintained at 45 $^{\circ}\text{C}$. For the on-column experiments, the migration times (t_r) were obtained from the maximum of the peak profiles. The theoretical plate numbers were calculated by the half-height method ($N = 5.54 (t_r/w_{1/2})^2$) where: t_r is the migration time and $w_{1/2}$ is the width at half-height. For the off-column experiments, t_r was estimated from the on-column t_r , taking into account the extra 5-cm of column.

TLC Separations

After the MEKC separated DNS-amino acids were EF deposited onto a TLC plate, the chiral separations were performed as follows. All developments were carried out in a sealed TLC chamber at room temperature, with a piece of filter paper enclosed to help saturate the chamber with solvent vapor. The plates were developed for approximately 40 minutes. After the plates had fully developed, the solvent was allowed to evaporate before imaging the plates. All plates were stored at 0 $^{\circ}\text{C}$ after development.

CCD LIF Imaging Instrumentation

The detection instrumentation is shown in Figure (3.3). A helium-cadmium laser (Omnichrome, Chino, CA) was used to supply the 325-nm light. The laser beam was focused onto the end of a fiber optic 301 core/ 329 clad (Polymicro Technologies, Phoenix, AZ) with a biconvex, 25-mm diameter, f/2 lens, which produced a homogenous expanded beam at its output. The fiber optic was positioned at a distance from the TLC plate, which resulted in the light being expanded to a diameter of approximately 2 cm. A cut-on filter (50% @ 428 nm) was placed over a close focus zoom lens (Edmond Scientific, Barrington, NJ) attached to a model ST-6 CCD imaging camera (Santa Barbara Instrument Group, Santa Barbara, CA). Once the CCD images of the deposited bands or the developed plates were saved in TIFF format, the spectroscopic mode of the CCD camera was used to obtain data in ASCII format. The ASCII formatted data was loaded into a spreadsheet for reconstruction of the electropherogram.

Results and Discussion

One-Dimensional CE Separations of Amino Acid Enantiomers

As previously stated, CE has successfully been applied to chiral separations of amino acids by introducing CDs into the running buffer. When mixtures of amino acids are analyzed, optimization in one-dimension can often be laborious. The effects of separation conditions on general elution behavior must be considered or separated enantiomer pairs will co-elute with the

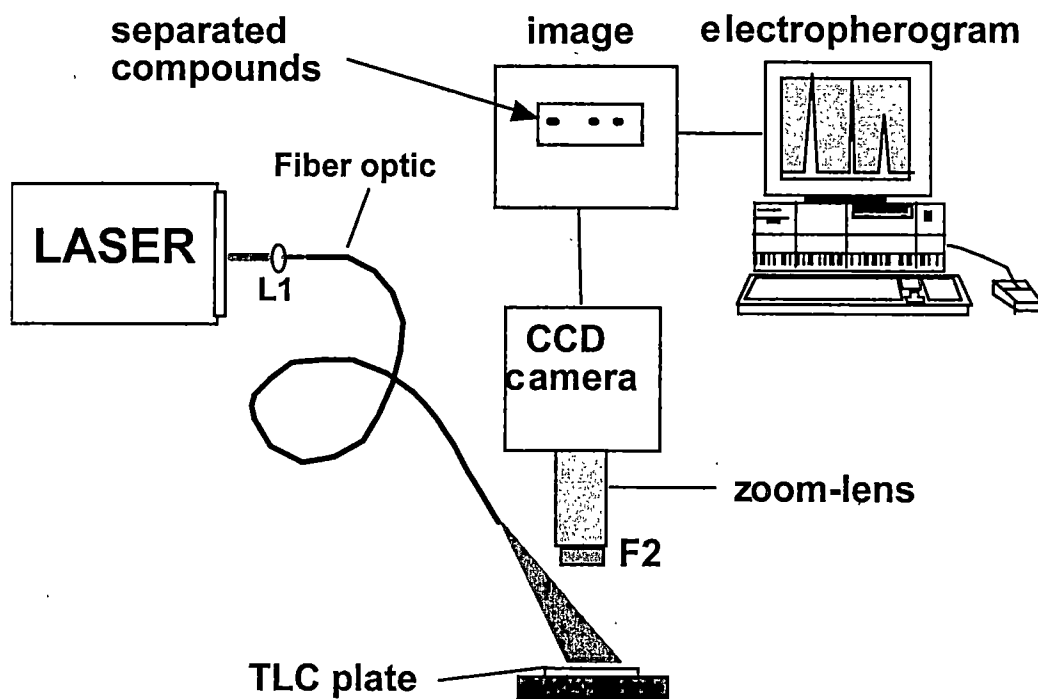


Figure 3.3 Schematic diagram of the fiber-optic LIF off-column instrumentation used to detect the deposited analytes. Figure labels: L1 is a 25 mm f/1 biconvex lenses, and F2 is a cut-on filter.

enantiomers of other DNS-AAs. The ability of one-dimensional CE is demonstrated by separating the enantiomers of four DNS-amino acids: Val, Leu, Norv, and Norl. As seen in Figure (3.4a), these negatively charged (-1) DNS-amino acids could not be separated by differences in electrophoretic mobility. However, when SDS is added to the running buffer adequate resolution is obtained (Figure 3.4b) for the general separation. The mixture could not be separated when only 10-mM of β -CD (no SDS) is added to the running buffer. Furthermore, no separation of the amino acid enantiomers is observed with the addition of 10-mM of β -CD to the SDS running buffer (Figure 3.5a). Presumably, the DNS-DL-amino acids are more favorably partitioned into the SDS than into the cavity of the β -CD. Potentially, increased separation of the enantiomers is possible by increasing the ratio of β -CD to SDS. An increase in enantio-separation is observed for Norv when 75-mM of β -CD is added to the running buffer, however a reduction in efficiency and resolution for the general separation is also observed (Figure 3.5b). In this experiment, a 5-M urea solution is added to solubilize the high concentration of β -CD. Due to the high concentration of urea, micelles may not be present.

In general, it has been reported that γ -CD provides for better resolution of the DNS-amino acid enantiomers [121]. This can be attributed to a more appropriate fit of the DNS label into the larger γ -CD cavity as compared to the β -CD cavity. Again, the mixture could not be separated in one-dimension when

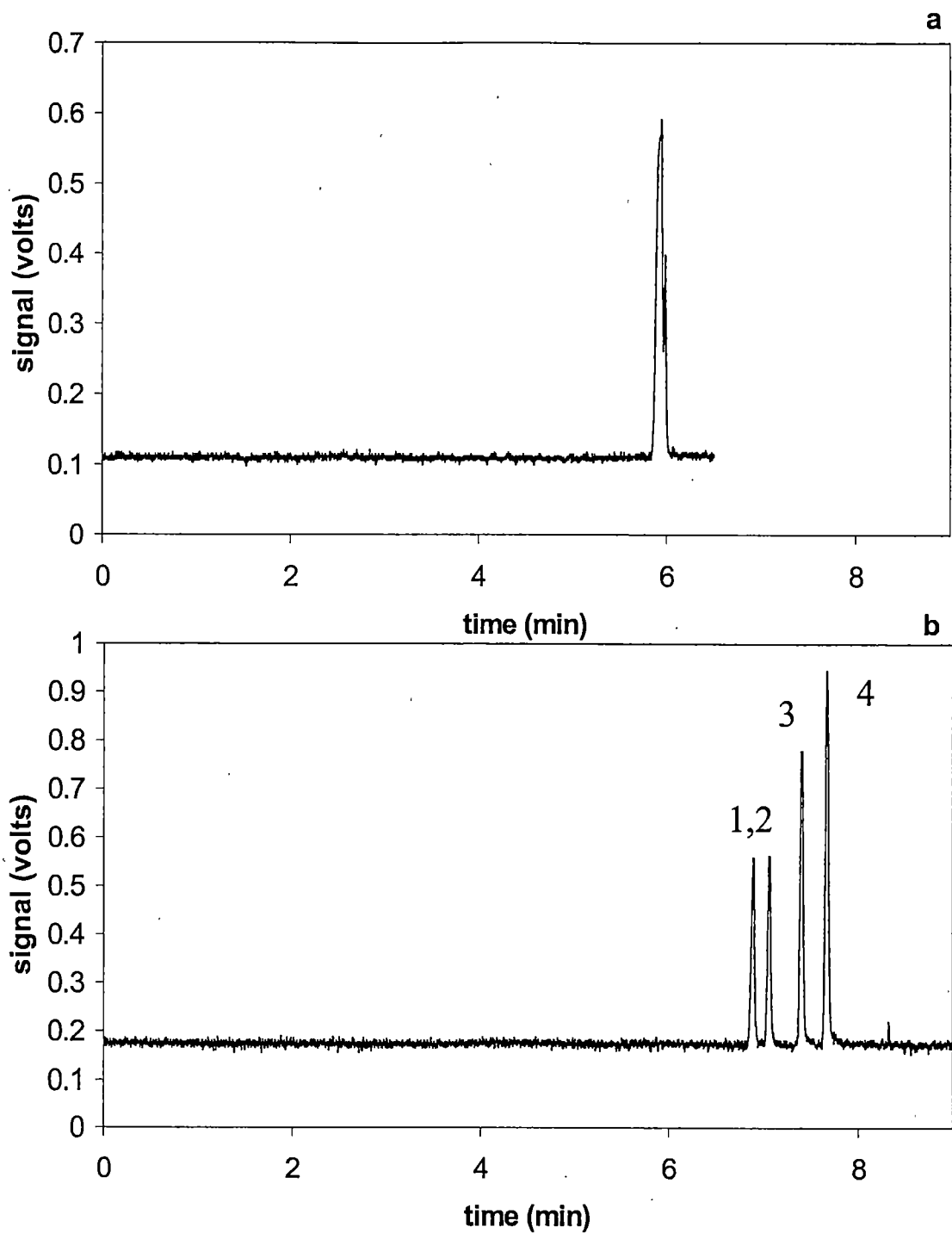


Figure 3.4 Comparison of one-dimensional separations of DNS-AAAs: running buffers composed of (a) 10-mM sodium tetraborate and (b) 40-mM SDS/10-mM sodium tetraborate. Peak identification: Val (1), Norv (2), Leu (3), Norl (4). Conditions are described in the experimental section.

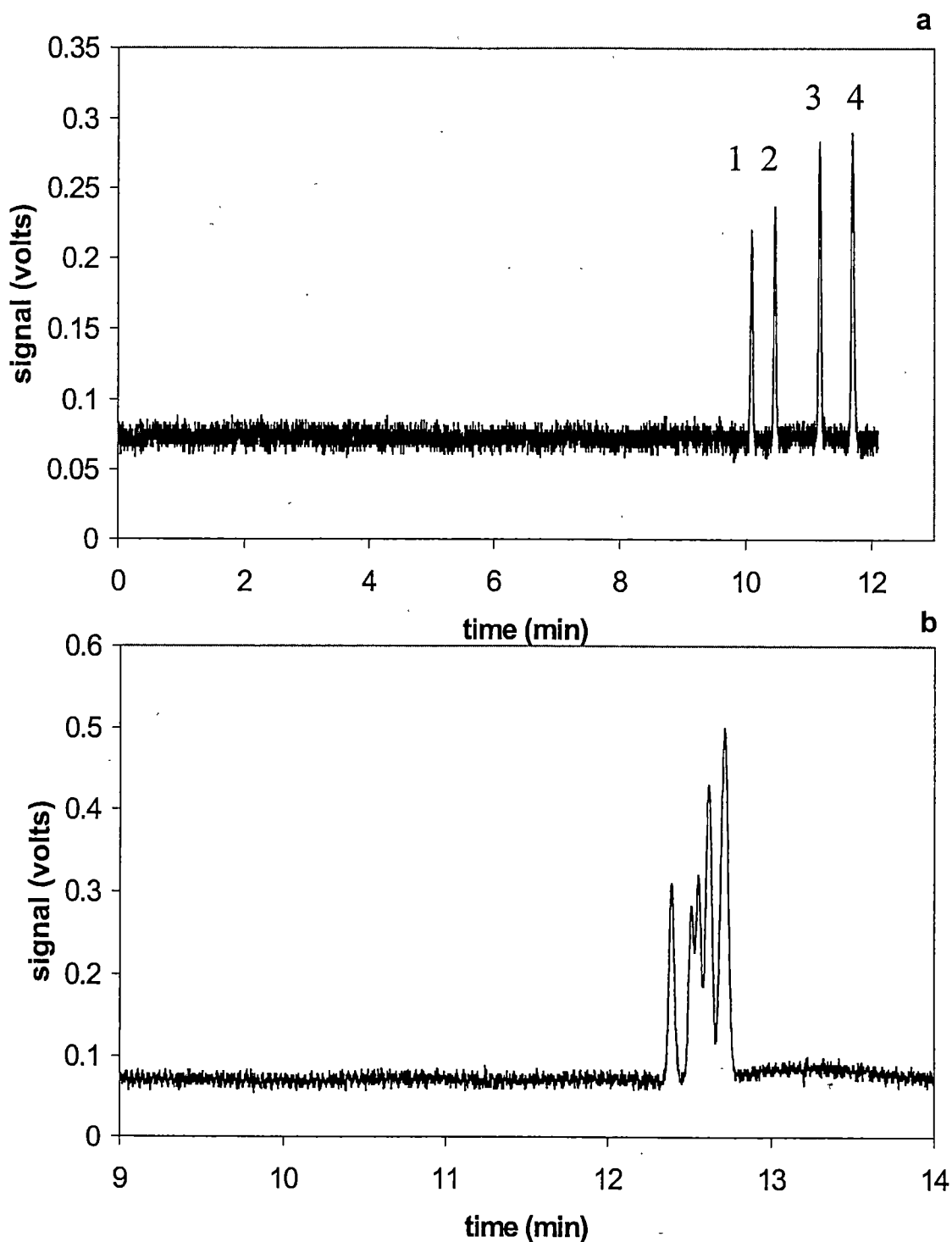


Figure 3.5 Comparison of one-dimensional separations of the enantiomers of DNS-AAs using β -CD: running buffers composed of 40-mM SDS/10-mM sodium tetraborate and either (a) 10-mM β -CD or (b) 75-mM β -CD with 5-mM urea. Peak identification: Val (1), Norv (2), Leu (3), Norl (4). Conditions are described in the experimental section.

only 10-mM γ -CD (no SDS) is added to the running buffer. In Figure (3.6), the DNS-amino acid mixture is separated using low-, mid-, and high-concentrations of γ -CD added to the SDS running buffer. As the concentration of γ -CD is increased, the resolution of the early eluting peaks is increased; concurrently, the resolution of the later eluting peaks is decreased. At a concentration of 15 mM, the L-Leu and D-Norl co-elute. Admittedly, by optimizing buffer concentration, pH, voltages, and etc. baseline separation of many enantiomer mixtures could potentially be obtained in one-dimension. Nevertheless, as the complexity of the sample increase the optimization becomes increasingly difficult. The separation, in Figure (3.6), clearly demonstrates the problems of optimization that can occur when general and enantio-elution mechanisms act concurrently in one-dimension. In the CE-TLC 2D technique, the optimization of the general separation for the DNS-amino acid mixture is completely separate from the optimization of the enantiomer separation.

Comparison of On- and Off-Column Electropherograms

Coupling CE to TLC must meet three criteria to be considered a comprehensive 2D separation [109]: the transfer from the CE capillary must occur with little loss of analyte or degradation of separation efficiency; the separated components should not be allowed to recombine during transfer or in subsequent separation steps; and the separation of analytes must occur by different mechanisms. When these three criteria are met, the CE-TLC separation is truly two-dimensional.

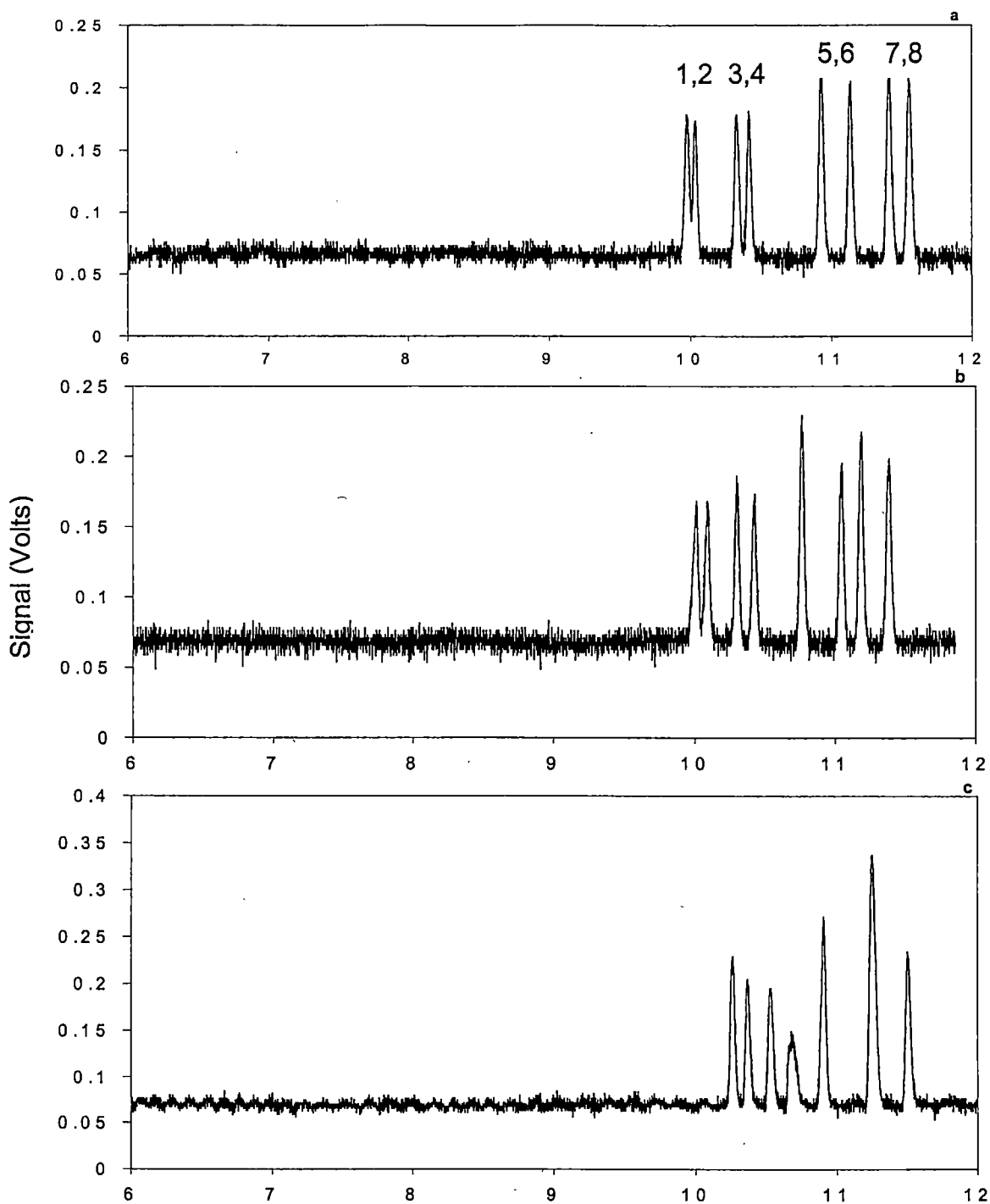


Figure 3.6 Comparison of one-dimensional separations of DNS-amino acids. (a) 5 mM γ -CD, (b) 10 mM γ -CD, and (c) 15 mM γ -CD added to SDS running buffer. Peaks: D-Val (1), L-Val (2), D-Norv (3), L Norv (4), D-Leu (5), L-Leu (6), D-Norl (7), L-Norl (8). Conditions are described in the experimental section.

Under optimum conditions, CE can generate extremely high plate counts and it is crucial for any 2D-CE technique to preserve these high efficiencies. The EF process must contribute as little loss of analyte or degradation of separation efficiency as possible. As explained in Chapter 2, as the diameter of the deposited track increases, efficiency and resolution are decreased, thus emphasizing the need to deposit narrow bands. The dimensions of the deposited bands are on average $200\ \mu\text{m} \times 1.0\ \text{mm}$ for a translation rate of $1.0\ \text{cm/min}$. These were slightly wider tracks than those reported in the work described in Chapter 2. For the 2D-experiments, the temperature of the TLC plate during deposition was limited to $45\ ^\circ\text{C}$ because the fluorescence background of the plate increased with temperature. Additionally, due to the elution range of the DNS-AAs the translation rate was limited to $1.0\ \text{cm/min}$. Nevertheless under the conditions used, the EF deposition technique is contributing 20 % to the total length of the deposited band. Since the liquid filament is considerably narrower, there is obviously some broadening occurring on the substrate. Potentially, increasing the translation rate or temperature could decrease the on-substrate band broadening (see Chapter 2).

In Figure (3.7), the on- and off-column electropherograms are directly compared. Table (3.1) compares the on-column plate counts per meter for the electropherograms shown in Figure (3.7). As shown in Table (3.2), the resolution between the peaks for the same electropherogram decreased between 3 % and 20 %. At a higher translation rate, an increase in resolution and efficiency would be expected. The efficiency increases because broadening due

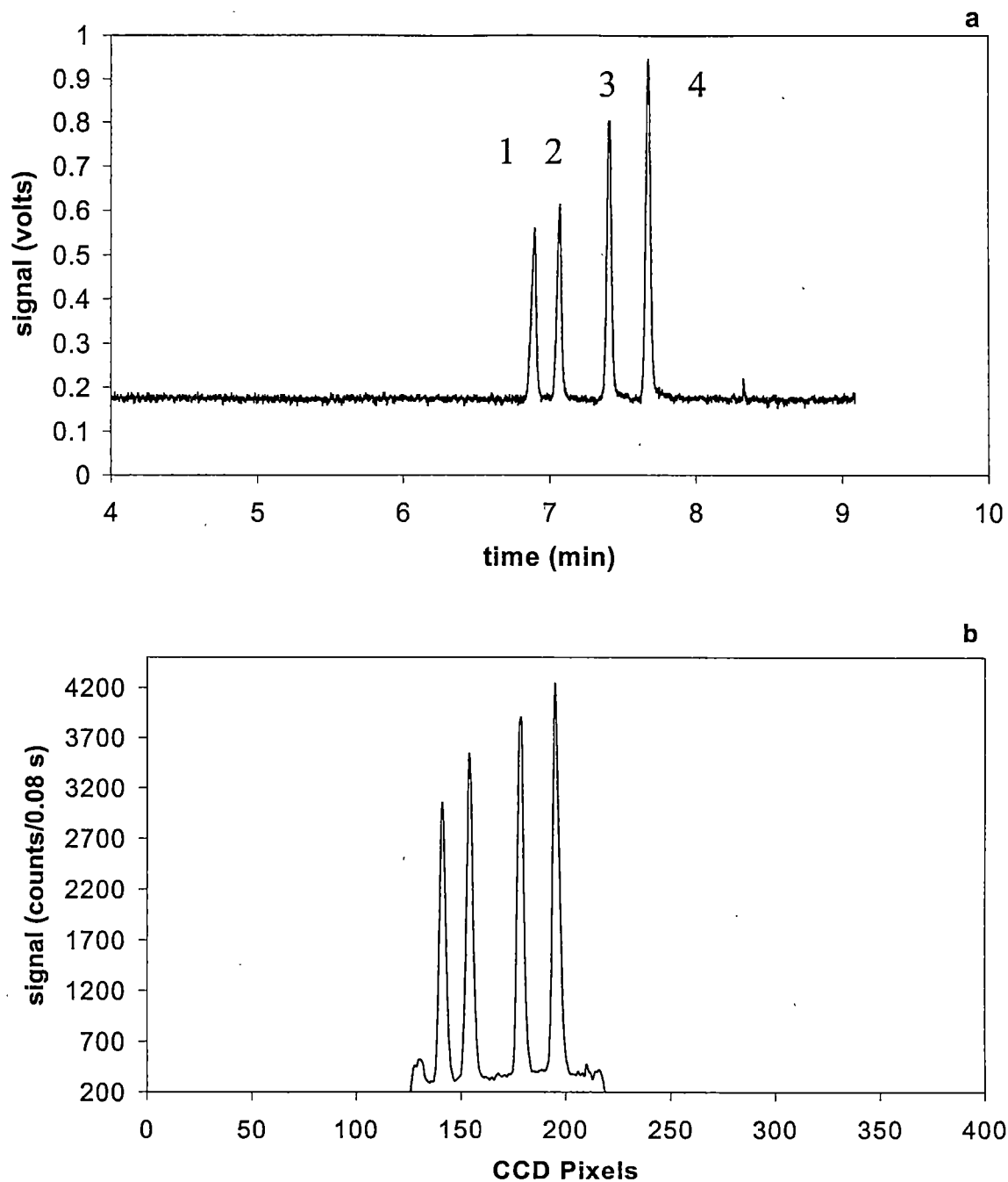


Figure 3.7 Electropherograms of Val (1), Norv (2), Leu (3), and Norl (4) comparing the (a) on- and (b) off-column LIF detection while electrospray depositing. Conditions are described in the experimental.

Table 3.1 Comparison of efficiency for on- and off-column detection using electrofilament deposition

	N_{1/2}/m On-column	N_{1/2}/m Off-column	% Decrease
DNS-DL-Val	300,000	150,000	50
DNS-DL-Norv	320,000	170,000	47
DNS-DL-Leu	210,000	190,000	10
DNS-DL-Norl	170,000	130,000	24

Table 3.2 Comparison of resolution for on- and off-column detection using electrofilament deposition

	Rs On-column	Rs Off-column	% Decrease
DNS-DL-Val			
DNS-DL-Norv	7.0	5.6	20
DNS-DL-Leu	10.0	9.7	3
DNS-DL-Norl	5.7	4.9	14

to the width of the track has less of a contribution to the total band length. In theory an improvement in the limit of detection should be realized by translating at slower rates. The slower translation rates concentrate the bands onto smaller spots on the TLC plate. As mentioned previously, the choice of translation rates was limited in these experiments. As documented in Table (3.1), the EF process contributes to band dispersion to a greater extent for the analyte bands with high efficiencies. Nevertheless, these results illustrate that the EF process preserves the separation obtained on-column for the DNS-amino acids. Thus, the CE-TLC technique meets the first two criteria defined previously for a 2D separation.

In the electropherograms in Figure (3.7), a relatively high concentration (10^{-3} M) of DNS-amino acids is employed. Lower concentrations could not be used, because after developing the TLC plate the fluorescence is too weak to be imaged. Unfortunately, the equipment used had several limitations, such as reduced laser power due to expanding the beam, background fluorescence from the TLC plates, and a non-intensified CCD camera. In Figure (3.8), the electropherogram is shown for a 10^{-6} M mixture of the DNS-amino acids. Surface features on the TLC plates, with approximately the same dimensions as the deposited bands, limit the LOD that is obtainable.

Two-Dimensional Separation of Amino-Acid Enantiomers

In Figure (3.9), a CCD imaged TLC plate shows the four deposited DNS-DL-amino acids from the CE-MEKC separation in the first dimension and the baseline resolution of the DNS-amino acid enantiomers from the TLC separation

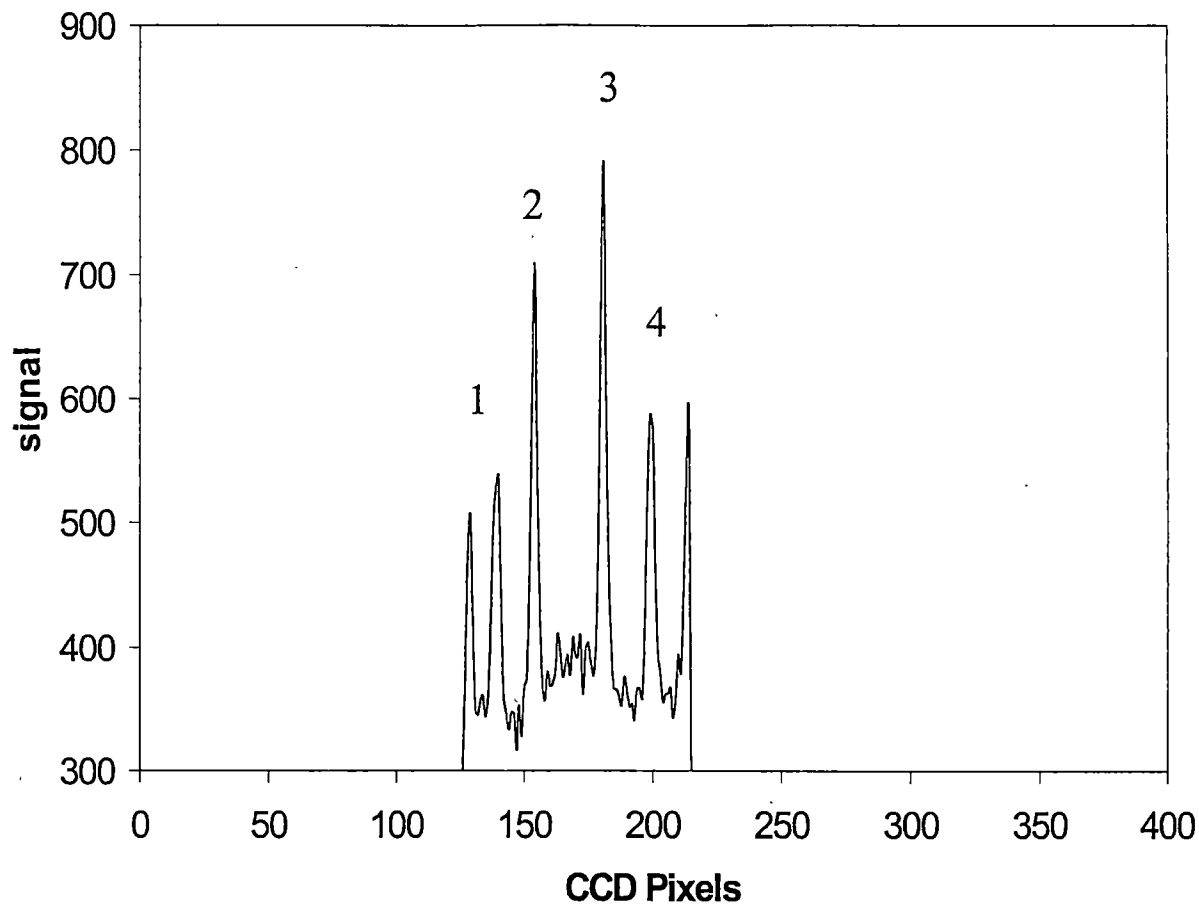


Figure 3.8 Electropherogram demonstrating the off-column LIF detection limit obtained by using the CCD camera to image the RP-TLC plate. The mixture of DNS-amino acids Val (1), Norv (2), Leu (3), and Norl (4) was diluted to a concentration of 1.0 μM . The outer peaks are a result of laser scatter from the edges of the TLC plate. Conditions are described in the experimental.

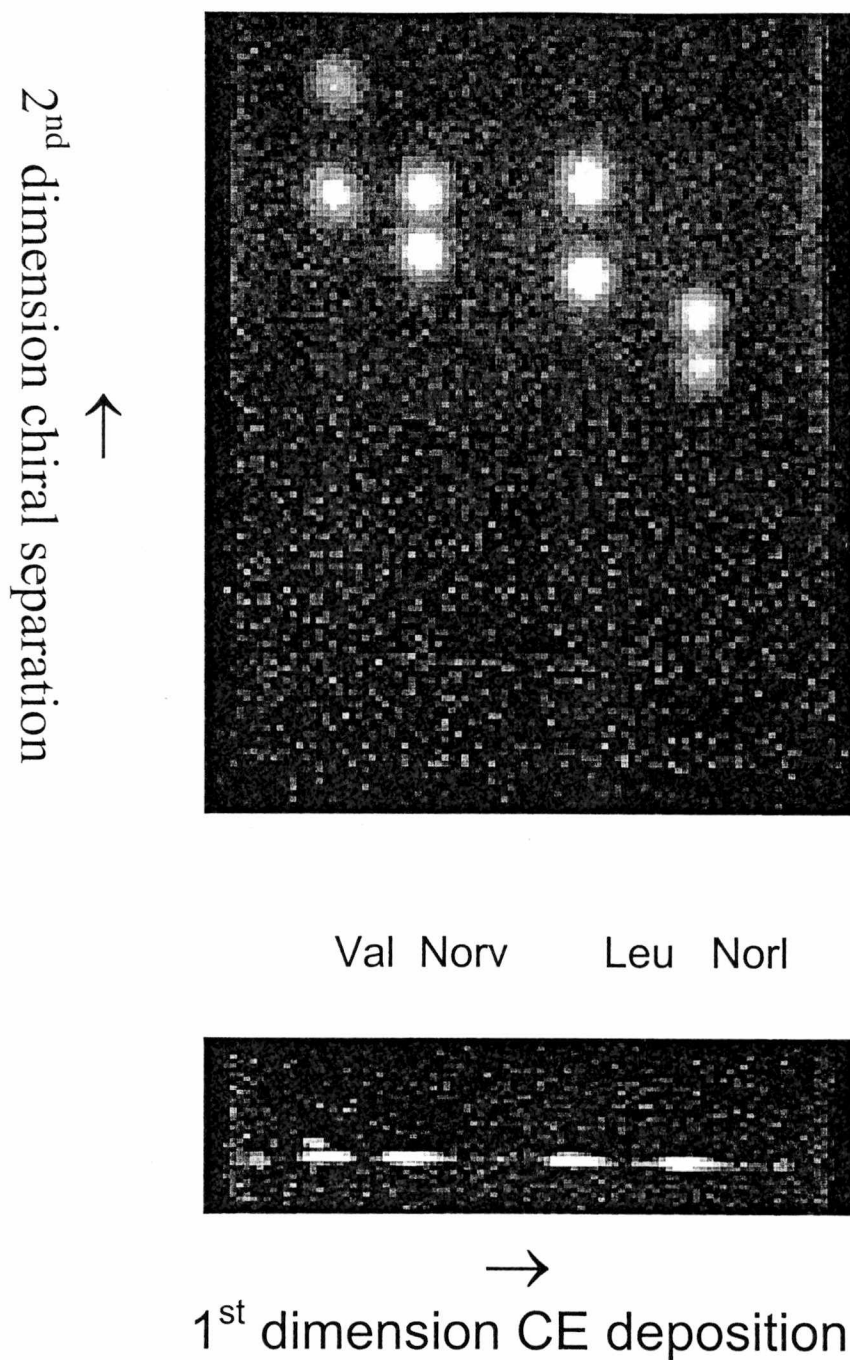


Figure 3.9 CCD images of the two-dimensional CE-TLC separations. The bottom image is the separated DNS-amino acids deposited from the CE capillary. The top image is the deposited DNS-amino acid enantiomers separated by TLC using a β -CD modified mobile phase. Conditions are described in the experimental section.

in the second-dimension. Note that in each case, the D-isomer eluted ahead of the L-isomer, because the D-isomer complexes to a greater extent with the β -CD in the mobile phase. The retention behavior follows that observed for the γ -CD mediated MEKC separation in Figure (3.6). However, it is the opposite of that observed for a β -CD bonded phase [121]. The dimensions of the initial deposited DNS-amino acids are $\sim 200 \mu\text{m} \times 1.0 \text{ mm}$. After developing with the β -CD modified mobile phase, the initial bands broaden to a size $\sim 2\text{-}1.5 \text{ mm} \times 1.5 \text{ mm}$. In Table (3.3), the separation data is given for the four DNS-DL-amino acids.

One advantage of 2D separations is the sample is separated independently by two different mechanisms. However, during the two separations, dispersive displacements (i.e. band broadening) also take place in each dimension. In TLC spreading along the displacement axis is normally greater than lateral spreading [105]. During its migration in the CE capillary, the initial zone largely broadens because of longitudinal diffusion, causing it to assume a Gaussian shape. In TLC, spreading along the flow axis includes all the dispersive contributions to total plate height, whereas lateral spreading includes fewer contributions. The TLC flow axis is at a right angle to the CE deposition. As can be seen in Figure (3.9), the initial deposited band is $200 \mu\text{m}$ wide and broadens to $\sim 2\text{-}1.5 \text{ mm}$ after the TLC separation, whereas the length of the deposited band is 1 mm and broadens too only $\sim 1.5 \text{ mm}$. Commonly, in a high-performance TLC separation efficiencies of $\sim 10,000$ plates are obtainable. Assuming a migration distance of 10 cm , the width of the band at $10,000$ plates

Table 3.3 TLC separation data for DNS-amino acids.

	Zo (cm)	Zx (L)	Zx (D)	Rf(L)	Rf(D)	α
Val	0.40	2.30	3.00	0.28	0.36	1.3
Norv	0.40	1090	2.30	0.23	0.28	1.2
Leu	0.40	1.80	2.40	0.22	0.29	1.3
Norl	0.40	1.20	1.60	0.15	0.19	1.3

would be 2.5 mm. Thus, reduction in resolution due to the width of the EF deposited band (200 μm) is expected to be negligible in these studies.

The last criterion that must be met for the CE-TLC technique to be truly two-dimensional is that the separation mechanisms must be significantly different (i.e., orthogonal). An interrelationship exists between the mechanisms controlling separations in MEKC and in reverse-phase (RP)-TLC. In both MEKC and RP-TLC, separations occur through partitioning mechanisms. In MEKC, partitioning occurs between the solute and the pseudo-stationary phase (e.g. SDS) and in RP-TLC partitioning occurs between the solute and the stationary phase. Fundamentally, MEKC and RP-TLC separate compounds based of the differences in hydrophobicity. In MEKC, electrophoretic mobility, hydrogen bonding, and charge interactions with micelles also affect separations [29]. In many cases the elution order in MEKC will resemble that of reversed-phase chromatography, therefore some information gained from the first separation is duplicated in the second separation. The CCD image in Figure (3.9) of the separated enantiomers appears to have a diagonal pattern, which is similar to the theoretical illustration in Figure (3.1b). The DNS-Norl is retained the longest in the SDS pseudo-stationary phase and in the RP-TLC separation. The separation space in the MEKC-RPTLC technique is not fully utilized, therefore the peak capacity is not fully maximized. The separation space could be more fully put to use if normal phase TLC was used for the chiral separations.

In addition to the above mechanisms, the TLC mobile phase used in this work contains a high concentration of cyclodextrins. The exact mechanism for

enantio-selectivity is not known. In all probability, the carboxyl group and/or the NH group of the D-isomer is/are capable of hydrogen bonding with the 2- or 3-position hydroxyls near the mouth of the β -CD cavity to a greater extent than the L-isomer, thereby contributing to the enantio-selectivity [125]. The preferred inclusion of the D-enantiomer was also predicted in prior work based on computational molecular mechanics modeling [121]. Additionally, when the β -CD is added to the mobile phase, multiple complexations to more than one β -CD molecule is possible [126]. The CDs result in a chiral separation mechanism that is not present in the 1st dimension. Thus, meeting the third criteria of a 2D separation.

The real advantage of 2D separations is in the analyses of samples in complex matrices, due to the capability of obtaining very high peak capacities when compared to the 1D separation. The peak capacity of a separation with unit resolution can be calculated by [127]:

$$N_c = L / 4\sigma \quad (3.4)$$

where the authors have defined L as the distance over which peaks can be distributed, and σ is the average standard deviation of these peaks. In 2D deposition experiments, the peak capacity from the on-column separation is calculated from the deposited bands, because band broadening due to the deposition technique will decrease the peak capacity. For the CE deposited DNS-amino acid separation (Figure 3.9), as measured on the actual TLC plate the available elution distance is ~ 2 cm and the average 4σ width is 0.1 cm;

giving a peak capacity of 20. For the TLC enantiomer separation (Figure 5), the available elution distance is 8.3 cm and the average 4σ is 0.15 cm; giving a peak capacity of 55. Thus, the overall peak capacity for this separation is ~ 1100 . In principle, the 2-cm elution distance could be increased substantially by altering the apparatus and thereby, the peak capacities could be increased. In contrast, for the on-column electropherogram (Figure 2a), the available elution range is 15 min and the average 4σ is 0.05 min, thus giving a peak capacity of 300. As discussed above, a reduced peak capacity could be due to the separation space in the 2D technique not being fully utilized. However, when compared to the one-dimensional technique there is a considerable increase in peak capacity. The CE-TLC technique offers an alternate approach to multidimensional separations for analyzing volume-limited complex samples.

Chapter 4. SURFACE-ENHANCED RAMAN SCATTERING FOR OFF-COLUMN DETECTION IN CAPILLARY ELECTROPHORESIS

Introduction

The two major limitations of CE are poor retention time reproducibility and the lack of highly sensitive and selective detectors. As described in Chapter 1, retention times in CE depend on the wall-generated EOF. The EOF is affected by the integrity of the capillary inner-wall surface, which is in a dynamic state that is difficult to control. The poor retention time reproducibility represents one motivation to couple CE with spectroscopic techniques. Combining the spectral information with the observed migration times would allow for explicit analyte identification. Brinkman et al. provides an excellent review of several spectroscopic techniques that have been used for analyte identification in CE [128].

As discussed in Chapter 1, Raman spectrometry is a technique that has the potential to provide rich information about the structure of a molecule. However, the extremely small cross sections for Raman scattering precludes its use as a sensitive CE detection technique. The inherent inefficiency of normal Raman scattering has been overcome by using surface-enhanced techniques. An enormous Raman enhancement has been observed for molecules that are adsorbed onto certain types of metal surfaces. This enhancement has been

termed the surface-enhanced Raman scattering (SERS) effect, which was first observed in the 1970s by Fleischmann et al [129]. Since that time there has been a substantial amount of research on the theoretical aspects and on potential analytical applications [130-132]. An additional enhancement is obtained when the excitation wavelength is coincident with molecular resonance (surface enhanced resonance Raman scattering) [133-135]. Furthermore, often the fluorescence from molecules positioned near the metal surface is quenched. Consequently, the fluorescence quenching allows interference free SERS spectra to be obtained for a greater number of compounds and at lower concentrations [136-138]. As a detection technique for CE, SERS has the potential to combine the structural information content of Raman with the sensitivity of fluorescence.

Theoretical Aspects of SERS

Although there has been much research into the theory of SERS, to date, there is no single model that can explain all of the experimental observations related to the SERS effect. Previous models predict at best maximum enhancements of 10^6 to 10^8 for the SERS effect. However experiments have indicated SERS enhancement factors in the order of 10^{13} are possible [139,140]. Single-molecule studies have also indicated that enhancement in the order 10^{14} to 10^{15} are possible at specific sites referred to as 'hot spots' [141,142]. Nevertheless, it is regularly agreed that the total enhancement is the result of more than one effect. As can be inferred from the classical theory of light

scattering that was discussed in Chapter 1, the enhancement can result from changes in the molecular polarizability (P) and/or in the electric field the molecule experiences (E). The theoretical models have defined at least two major types of mechanisms that contribute to the SERS effect: electromagnetic and chemical.

Electromagnetic Enhancement

The electromagnetic enhancement arises from the excitation of conduction electrons at characteristic frequencies (surface plasmons), which produce large electromagnetic fields near the metal surface. The plasmon frequency depends on size, shape, and the material of the metallic nanoparticles and their environment. At the plasmon frequency, the metal becomes highly polarizable resulting in large local fields on the metal surface. An additional enhancement is due to the excitation of surface plasmons by the Raman emission radiation of the molecule. The electromagnetic enhancement is the major contributor to the SERS signals. The overall enhancement scales roughly as E^4 , and the electromagnetic field decreases with the third power of the distance between the analyte and the metal surface. Typical characteristics of the electromagnetic effect are the molecule is not required to be in direct contact with the metallic surface and the effects should be independent of the chemical nature of the molecule

Chemical Enhancement

The electromagnetic model explains many characteristics of the SERS effect, however experimentally the chemical nature of the molecule of interest has been shown in many cases to be important. Therefore, a second model involving the chemical characteristics of the molecule of interest has been proposed. The chemical enhancement results from electronic coupling between the molecule and the metal, resulting in a Raman enhancement. This is a charge-transfer process that produces an increase in the apparent value of the molecular polarizability (P). Although there may be several different mechanisms, one charge-transfer process can be described as follows: (1) excitation of an electron in the metal into a hot electron state; (2) transfer of the hot electron into the LUMO (lowest unoccupied molecular orbital) of the molecule; (3) transfer of the hot electron from the LUMO, with changed normal coordinates of some internal molecular vibrations, back to the metal; (4) return of the electron to its initial state and Stokes photon creation [131].

In contrast to the electromagnetic model, the adsorbate molecule must be in contact with the SERS-active surface. The mechanism depends on the adsorption site, the geometry of bonding, and the energy levels of the adsorbate molecule. The chemical enhancement is considered to be the lesser of the two enhancements with factors reaching not more than 10 to 100 [131]. The chemical enhancement can provide useful information on chemisorption interactions between the metal and the adsorbate. However, these interactions

are related to a general mechanism and thus are only applicable to specific adsorbate-metal systems.

SERS Substrates

Inevitably, for SERS to fulfill its potential as an analytical method, a SERS-active substrate is required that has the following characteristics: easy to prepare, reproducible, sensitive, robust, and universally active for a large number of compounds. An extensive amount of research has gone into developing and evaluating different types of SERS-active substrates. The following is a partial list of substrates that have been reported in the literature: nitric-acid etched silver foil, electrochemically prepared electrodes, island films deposited on glass surfaces, films deposited by evaporation or sputtering in a vacuum, and arrays of particles created by sophisticated lithographic technology [143-145].

The type of metal on the surface is an important consideration when developing a SERS substrate. Silver has been found to give the strongest surface enhancements followed by gold and copper. Other materials that have been studied for the SERS effect are Li, Na, Cd, and Al [143]. For roughened silver, the blue and green emission lines of the common Ar-ion laser fall into the excitation range of the surface plasmons [131]. The type of metal alone does not define the SERS activity; additionally, nano-sized features on the metal surface are important to the SERS process. The dependence of the SERS signal on the surface roughness exhibits different excitation profiles for different surface

features. For example, diameter sizes in the 10 to 100-nm range appear to be optimal for spherical silver particles [143].

For the work reported herein, SERS is performed on a planar substrate, prepared using metal colloidal solutions as the enhancing media [146-149]. The colloids used most often in SERS are metal sols, which is a liquid dispersion of nanoparticle silver or gold in the 10 to 150-nm size range [131]. The major advantage of using colloids is the ease of preparation. This technique does not require the use of vacuum evaporation chambers and it involves relatively simple experimental procedures. The disadvantages are a lack of stability that is due to coagulation and a lack of uniform particle sizes. However for the following experiments, the colloids were stabilized on a solid support that reduces affects of coagulation. Additionally, the preparation procedure that is described in this chapter reproducibly prepares ~ 100-nm silver particles. Many successful applications of SERS using colloidal systems have been reported in the literature, including the probing of single molecules [131, 150-154].

Applications of SERS

Although SERS is not considered a universal technique, it is increasingly being applied to a wide range of important compounds. SERS has been used to detect illicit drugs, such as cocaine and heroin [155]. Several pharmaceutical and biotechnological applications have been demonstrated, including detection of anti-tumor drugs, neurotransmitters, hemoglobin, and amino acids [156-159]. Electrochemically-roughened silver surfaces were used to obtain SERS spectra

of 19 L -amino acids [159]. Borjesson et al. used SERS to detect a single hemoglobin protein molecule attached to isolated and immobilized silver nanoparticles. SERS substrates have been used to detect low antitumor drug concentrations at a single cell level [158]. SERS was used in assays to detect bilirubin and salicylate in whole blood at levels below the normal or therapeutic level [160]. The sharp Raman bands were sufficiently resolved to allow the analytes to be detected in the presence of a complex matrix such as whole blood. A very exciting area is the use of SERS to monitor DNA and its interactions [161-163]. For example, two probes specifically designed for SERRS were used to detect a 2×10^{-12} M solution of labeled DNA.

SERS-Based Detection for Chromatography

SERS has been used as the detection method for a variety of separation techniques. For example, in thin-layer chromatography, a silver colloid solution was concentrated on top of developed analyte spots [164-166]. In gas chromatography applications, the effluent was trapped either in liquid colloid or on TLC plates coated with silver [167,168]. A flow-cell was designed to accept a SERS substrate for liquid chromatography experiments [169]. Recently, our group has successfully demonstrated on-column SERS detection in CE, using running buffers that contained suspensions of silver colloid [170]. The on-column technique obtained characteristic SERS spectra of analytes in the 10^{-6} to 10^{-9} M ranges, with very little loss in separation performance. However an off-column SERS technique would have several advantages, such as the ability to

use long exposure times to increase the sensitivity, independent optimization of the separation and detection conditions, and the opportunity to employ a variety of SERS-active substrates. In the work reported herein, the effluent from a CE capillary is EF deposited onto a SERS-active substrate. Subsequently, the electropherogram bands are reconstructed and the characteristic SERS spectra of the deposited analytes obtained. This was the first time that off-column SERS detection had been demonstrated for CE.

Experimental

Chemicals and Materials

Unless otherwise noted, the chemicals used to perform the experiments described in this paper were purchased from Sigma-Aldrich Chemical Co. (St. Louis, MO, USA). Water was purified with the Nanopure, ultrapure water system (Barnstead/thermolyne; Dubuque, IA, USA). Solutions were filtered and degassed before use. Unless otherwise noted, the CE running buffer solution was composed of 2-mM sodium tetraborate (pH ca. 9.5). The EF liquid sheath solution was composed of 90 % methanol (Fisher Scientific; Pittsburgh, PA, USA) and 10 % CE buffer at pH ca. 7. The resorufin, sodium salt was purchased from Molecular Probes (Eugene, OR, USA). Benzyloxyresorufin (BzRes) was purchased from GENTEST Corporation (Woburn, MA, USA). The test compounds were diluted to the appropriate concentrations in CE buffer prior to analysis.

CE Separations and EF Deposition

The CE and EF systems were described in Chapter 2. For the following experiments, a running voltage of 17 kV was used; this was increased to 19 kV when an EF voltage of ~2 kV was applied. Fused-silica capillaries (Polymicro Technologies; Phoenix, AZ, USA), 50 μm i.d., 360 μm o.d., 45 cm in length (40 cm to the laser-induced fluorescence (LIF) window) were tapered to reduce the mixing volume at the end of the CE capillary. Hydrodynamic injections were made at a height of 10 cm for 10 s. A helium-cadmium laser operated at 325 nm and 10 mW (Omnichrome; Chino, CA, USA) was used to excite the on-column fluorescence. The SERS substrate was mounted on an aluminum block that was heated to ~ 100 °C to reduce band broadening. The SERS substrate was translated under the EF tip at a rate of 1.0 cm/min. For the on-column experiments, the retention times (t_r) were obtained from the maximum of the peak profiles. The theoretical plate numbers were calculated by the half-height method ($N = 5.54(t_r/w_{1/2})^2$), where t_r is the retention time and $w_{1/2}$ is the width at half-height. For the off-column experiments, t_r was estimated from the on-column t_r , taking into account the extra 5 cm of column.

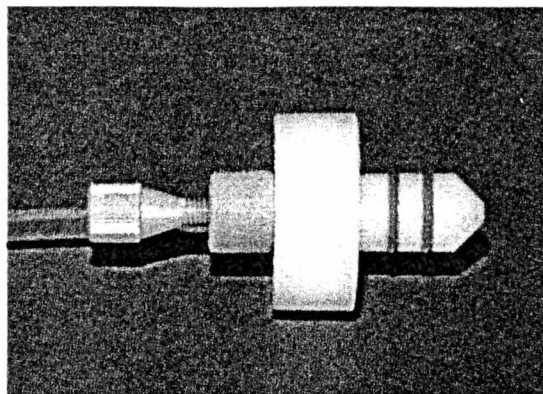
SERS Substrates

The procedure for the silver-colloid preparation was modified from the traditional sodium citrate reduction method [171]. Silver nitrate (180 mg) was dissolved in 500 mL of H_2O and brought to a vigorous boil. While boiling continued, a solution of 2% sodium citrate (10 mL) was added drop wise. The

solution was kept at a boil until the volume was reduced, through evaporation, to approximately 250 mL. Allowing the colloid solution to evaporate to a volume much lower than 250 mL resulted in an excessive amount of silver precipitating out-of-solution. The final solution was stored at room temperature in an amber bottle until use. Solutions stored up to four months have been used to produce quality SERS spectra. The solutions were evaluated using a UV-Vis spectrometer.

SERS-active substrates were prepared by using a MCN-100 high-efficiency nebulizer (CETAC Technologies Inc.; Omaha, NE, USA), shown in Figure (4.1a), to spray the previously prepared silver colloid solutions onto roughened-glass microscope slides (Erie Scientific Co.; Portsmouth, NH, USA). This nebulizer produces a fine mist (see Figure 4.1b), which effectively produces a complete coverage of the silver-colloid solution. Prior to silver deposition, all slides were leached in 3 M nitric acid for ~ 10 min., rinsed with ultra-pure water, and stored in methanol until use. The nebulizer was held at a height of ~ 3 cm above the microscope slide. The microscope slides were placed on a hotplate (Barnstead/thermolyne; Dubuque, IA, USA) at a temperature of ~150 °C during colloidal deposition. A 2-mL volume of the silver-colloid solution was sprayed at a flow rate of ~ 100 $\mu\text{L}/\text{min}$ during the deposition process to create a 0.5 cm by 2 cm band of silver nanoparticles. The nebulizer was translated continuously over the microscope slide at a sufficient speed to facilitate drying of the deposited colloid.

a.



b.

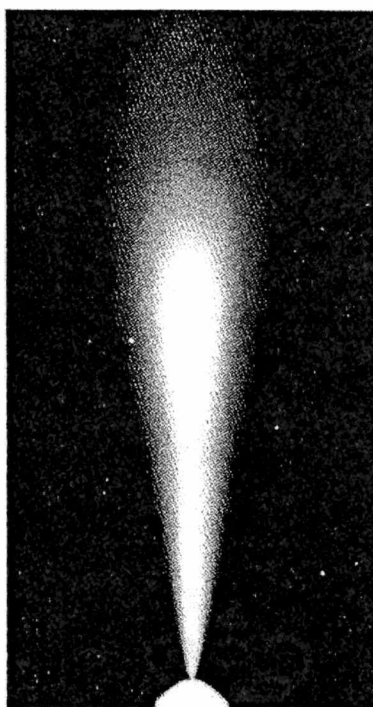


Figure 4.1 Images of the high-efficiency nebulizer used to deposit the silver colloid: (a) side-view of nebulizer and (b) the spray that is produced from the nebulizer.

After preparation, the substrates were stored in the dark and under nitrogen. All substrates were submersed in water for ~ 15 minutes to reduce the background before EF deposition. For the self-assembled monolayer (SAM) experiments, the substrates were submersed in a solution of 4-mM dodecanethiol for ~ 30 min. The SERS substrates were evaluated with a Joel JSM-5300 scanning-electron microscope (Joel; Peabody, MA, USA) and with an X-ray photoelectron spectrometer (Kratos Analytical; Chestnut Ridge, NY, USA).

SERS Detection Instrumentation

A bench-top confocal Raman spectrometer was assembled as shown in Figure (4.2). A Lexel 3500 CW argon ion laser (Lexel Laser, Inc.; Fremont, CA, USA) was tuned to the 514-nm line. The laser was directed onto a 1-inch holographic notch filter (Kaiser Optical Systems, Inc.; Ann Arbor, MI, USA) at an angle so the 514-nm light would be reflected onto a microscope objective (20X, 0.45 NA). The microscope objective focused the laser beam onto the SERS-active substrate. A translation stage was used to translate the substrate under the focused laser beam. The Rayleigh and Raman scatter from the substrate was collected and collimated by the same microscope objective. The collected light was directed onto the previously mentioned notch filter, which was angle tuned to pass the Raman scatter and filter most of the Rayleigh scatter. The scattered light was then focused into a Model 1235 Digital-Triple Spectrograph (EG & G Princeton Applied Research; Princeton, NJ, USA). The 1200 g/mm grating of the spectrograph dispersed the light onto a Model 1455A Intensified

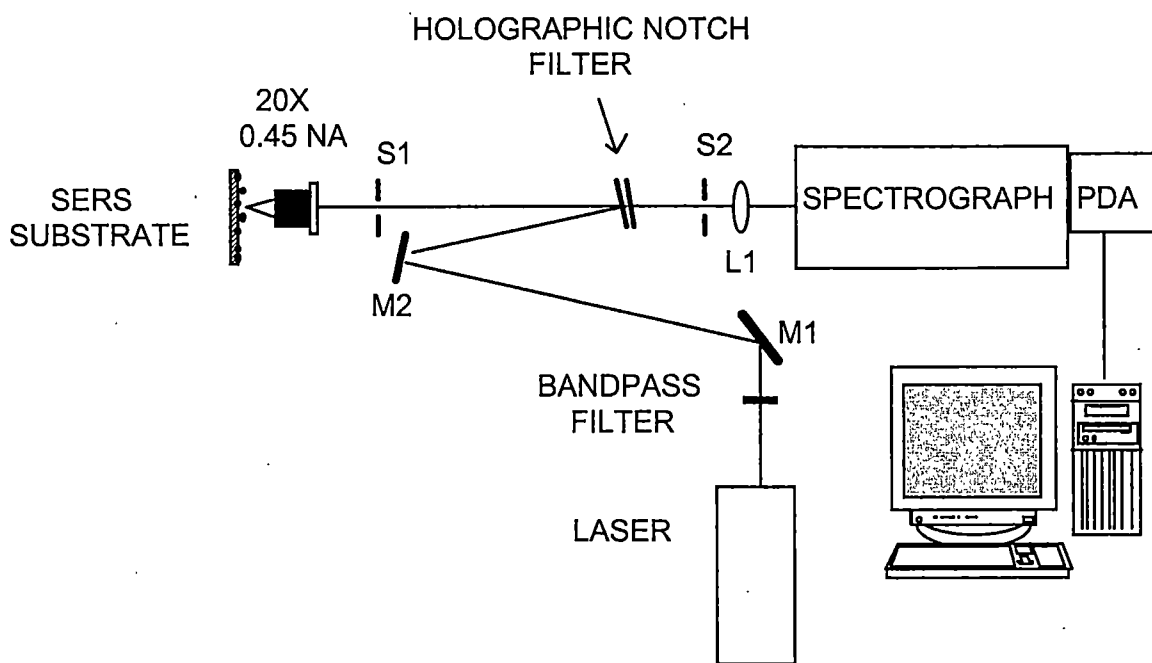


Figure 4.2 Schematic diagram of the confocal-Raman instrument used for obtaining SERS spectra and reconstructing the off-column electropherograms. Figure Labels: S1 and S2 are adjustable iris diaphragms, L1 is a lens, and M1 and M2 are mirrors.

diode array (EG & G Princeton Applied Research; Princeton, NJ, USA). Unless noted otherwise, all experiments were performed with a 1-second exposure time.

Results and Discussion

Development of SERS-Active Substrates

Control of the preparation chemistry is essential to reproducibly preparing SERS substrates from colloidal solutions. The most widely used colloids are prepared by the reduction of silver nitrate with sodium citrate or sodium borohydride; the citrate produces a more uniform nanoparticle-size distribution [147]. Many studies have already been carried out to characterize the citrate colloid preparation [146]. For 514-nm electromagnetic radiation, the optimum silver particle size is ~ 100 nm [172]. In the work reported herein, the colloid preparation was optimized to reproducibly prepare relatively monodispersed 100-nm diameter silver nanoparticles, and at a high concentration so to minimize the volume and time needed to produce a complete silver coverage on the microscope slides using the high-efficiency nebulizer.

The concentrations of silver nitrate and sodium citrate were optimized and evaluated by UV-Vis absorption spectrometry (UV-Vis) and by scanning-electron microscopy (SEM). In the optimization studies, three different concentrations were used: a.) 0.09 g silver nitrate, 1 % citrate, b.) 0.18 g silver nitrate, 2 % citrate, and c.) 0.36 g silver nitrate, 4 % citrate. The colloids were prepared as described in the experimental section, except at the specified reactant

concentrations. The UV-Vis absorption spectrum contains information about the particle concentration (absorbance), particle size (position of λ_{max}), and dispersity of particle size in solution (width of absorbance band). The UV-Vis and SEM analyses indicated that preparation (b) had the largest concentration of nanoparticles with appropriate and most uniform particle size. From the SEM micrographs in Figure (4.3c), it was determined that the silver nanoparticles in preparation (b) were ~ 100 nm in size. Preparation (c) gave similar results, however the higher concentrations of reactants resulted in an excessively large amount of silver precipitating out-of-solution. Based on the above results, preparation (b) was chosen for these studies. Colloid solutions have been prepared a number of times by this method and used over a four-month period without any appreciable change in the observed SERS properties.

The high-efficiency nebulizer used to prepare substrates produces a fine mist, which facilitates drying and creates a complete silver coverage on frosted microscope slides. The frosted-glass adds to the physical robustness of the substrates (i.e., the silver will not easily wipe-off). In Figure (4.3a), a picture is shown of four nanoparticle silver bands that were created by spraying silver colloid solutions onto a microscope slide. Even after colloidal deposition, the underlying μm -sized features of the roughened microscope slides are evident in Figure (4.3b). Illustrated by the SEM micrographs in Figure (4.3c), a 2-mL volume of the colloidal solution resulted in a heterogeneous, loosely packed array of ~ 100 -nm silver particles that forms a relatively complete surface

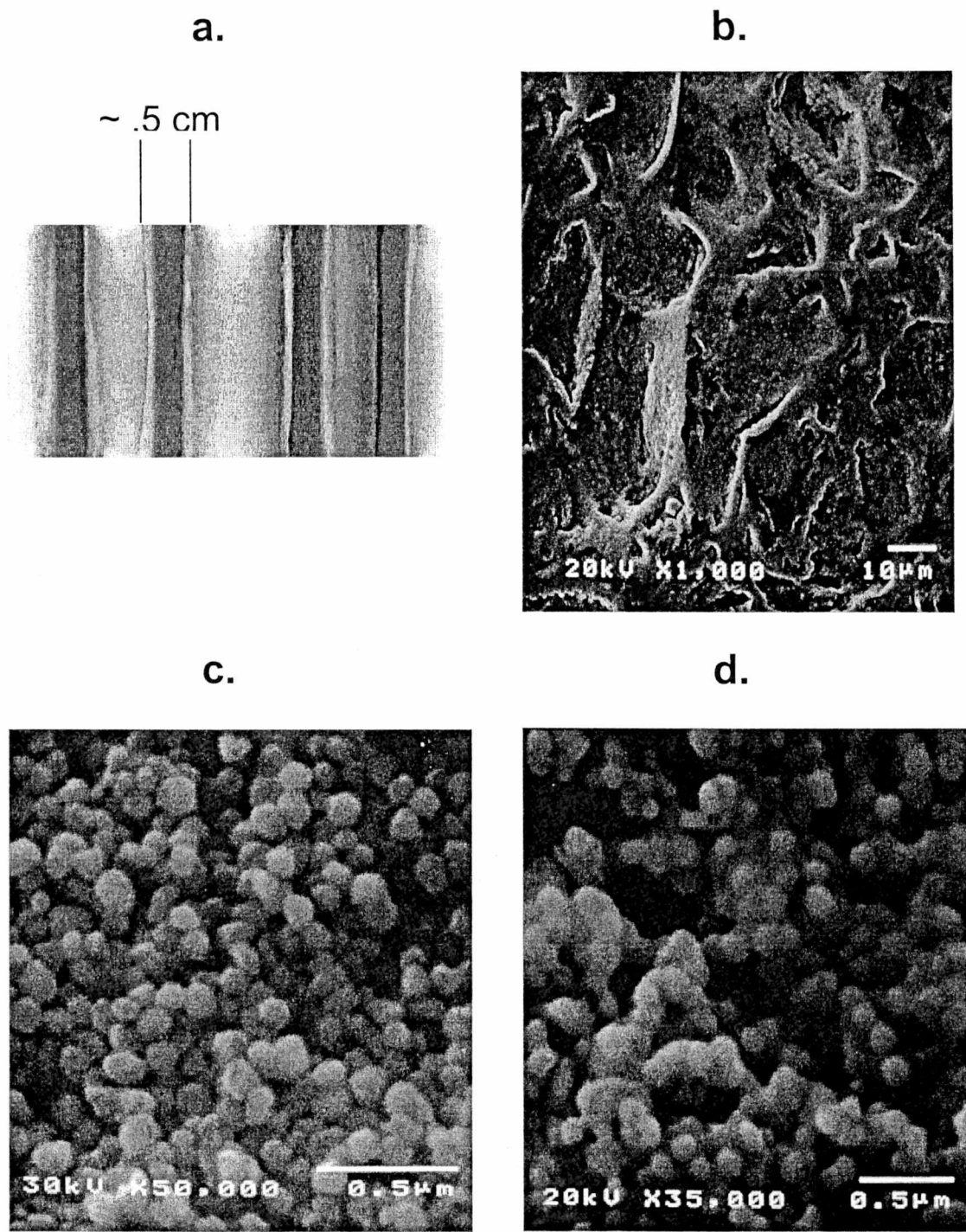
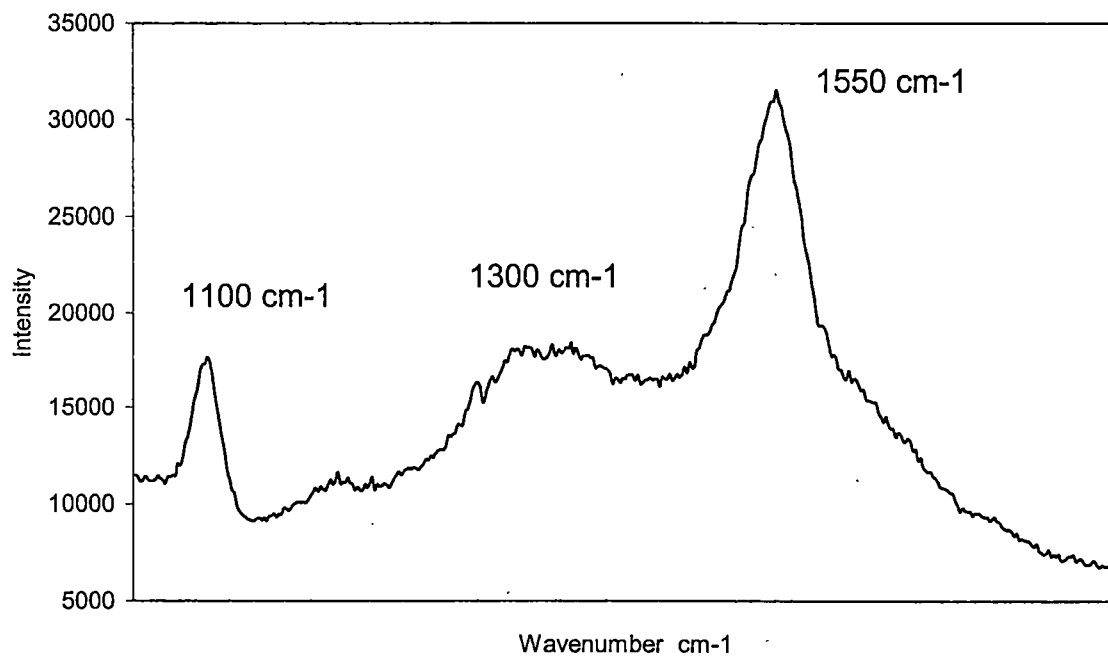


Figure 4.3 Images of the SERS substrate: (a) picture of four bands of deposited silver nanoparticles on a 2-cm wide frosted-glass microscope slide, (b) and (c) SEM micrographs of deposited silver nanoparticles on roughened-glass microscope slides at different magnifications, and (d) SEM micrograph of deposited silver nanoparticles after water was allowed to slowly dry onto the surface.

coverage. The interstitial spacing of the nanoparticles varies from a few to tens of nm throughout the substrate. This spacing could be important in obtaining 'hot spots' that produce an extremely large enhancement [154]. Additionally, substrates used in these studies contained several layers of silver nanoparticles, which increases the probability of sampling hot spots within a given area. Importantly, these substrates are easy to prepare, reproducible, and sensitive.

Carbonaceous contamination on the SERS surfaces can interfere with the spectra and increase the detection limits, thus hindering the analytical utility of SERS [173]. As shown in Figure (4.4a), the silver colloid prepared substrates have a considerable background spectrum in the region of 1100 and 1600 cm^{-1} , which is most likely due to Raman scattering from the residual citrate. Demonstrated by the SERS spectrum in Figure (4.4b), the background is reduced by submerging the substrate in water for ~ 15 minutes, presumably the excess citrate is dissolved from the surface. X-ray photoelectron spectroscopy was used to map the silicon, sodium, carbon, and silver before and after washing the substrate with water. As shown in Figure (4.5), after washing, the sodium and carbon decreased and the silver increased with no significant change in the silicon. It is very important to dry the substrate quickly with a large flow of inert gas. As illustrated in Figure (4.3d), if the water is allowed to dry slowly onto the substrate the silver nanoparticles fuse together changing their size and interstitial spacing. This results in a complete loss of the SERS signal.

a.



b.

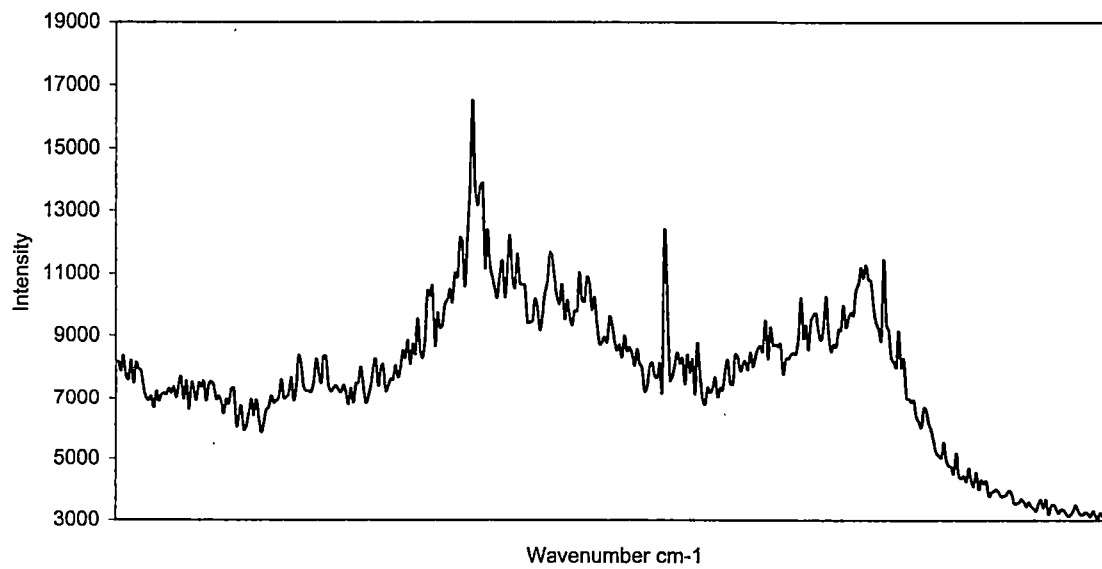


Figure 4.4 Background spectra of SERS substrate: (a) unwashed and (b) washed with water. Conditions are described in the experiment section.

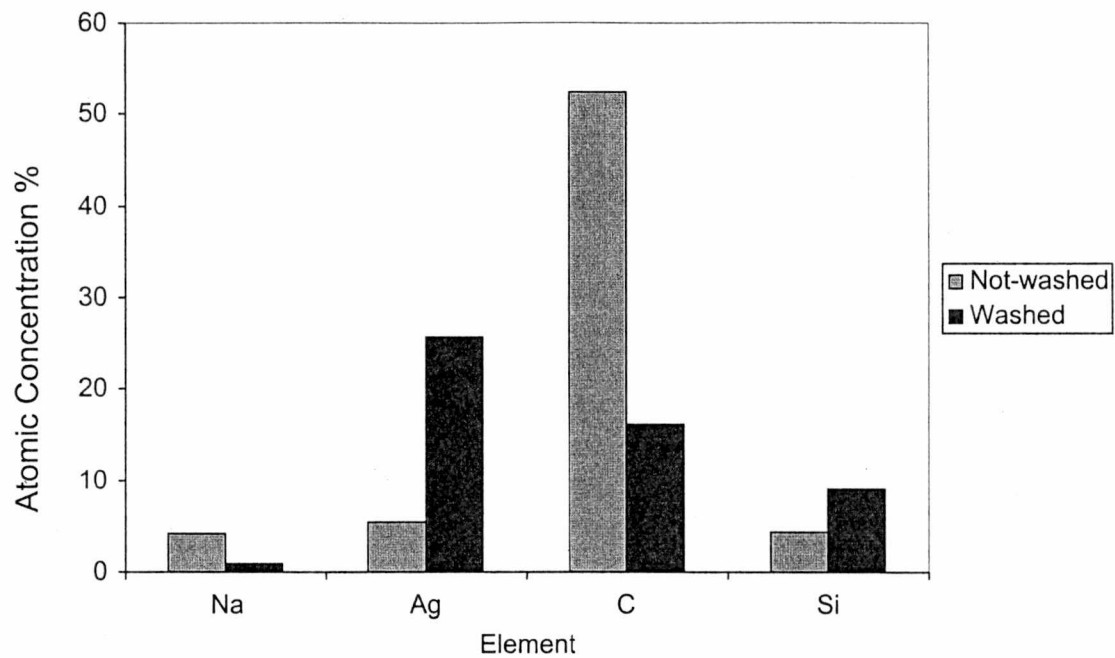


Figure 4.5 Graph showing XPS data before and after washing the SERS substrate with water.

Optimization of CE and Raman Conditions

Much effort has been put forth into developing surfaces that are SERS-active. However, the chemical states of the analyte and the sample matrix are equally important to obtaining quality SERS spectra [151]. Two effects, which could reduce the SERS signal by hindering the analyte molecules from coming into contact with the silver, are pH induced electrostatic interactions and matrix components that sterically hinder the analyte molecule-surface interactions. In CE, there are a large number of buffer solutions covering a wide range of pH values that can be employed to separate anionic, cationic, and neutral analytes. Hence, the CE buffer and its affect on the analyte need to be considered when developing a SERS method.

For the initial studies, a borate buffer was employed due to its wide range of applications in CE. In Figure (4.6a), the SERS spectrum is shown for a 10^{-5} M injection of erythrosin B obtained following electrophoresis using a 4 mM borate (pH ~ 9.3) running buffer. Erythrosin B is a negatively charged, fluorescent compound; when it is in contact with the silver nanoparticles the fluorescence is effectively quenched and the Raman signal is enhanced. The radiationless decay rate (quenching) decreases as d^3 (d is the distance measured from the metal surface to the molecule) [136]. Under the conditions of the borate buffer, the fluorescence is not adequately quenched; presumably, the erythrosin B is electrostatically repelled by borate on the surface of the silver nanoparticles. As demonstrated in Figure (4.6b), after the analytes have been EF deposited onto SERS-active substrates, washing the substrates with water can

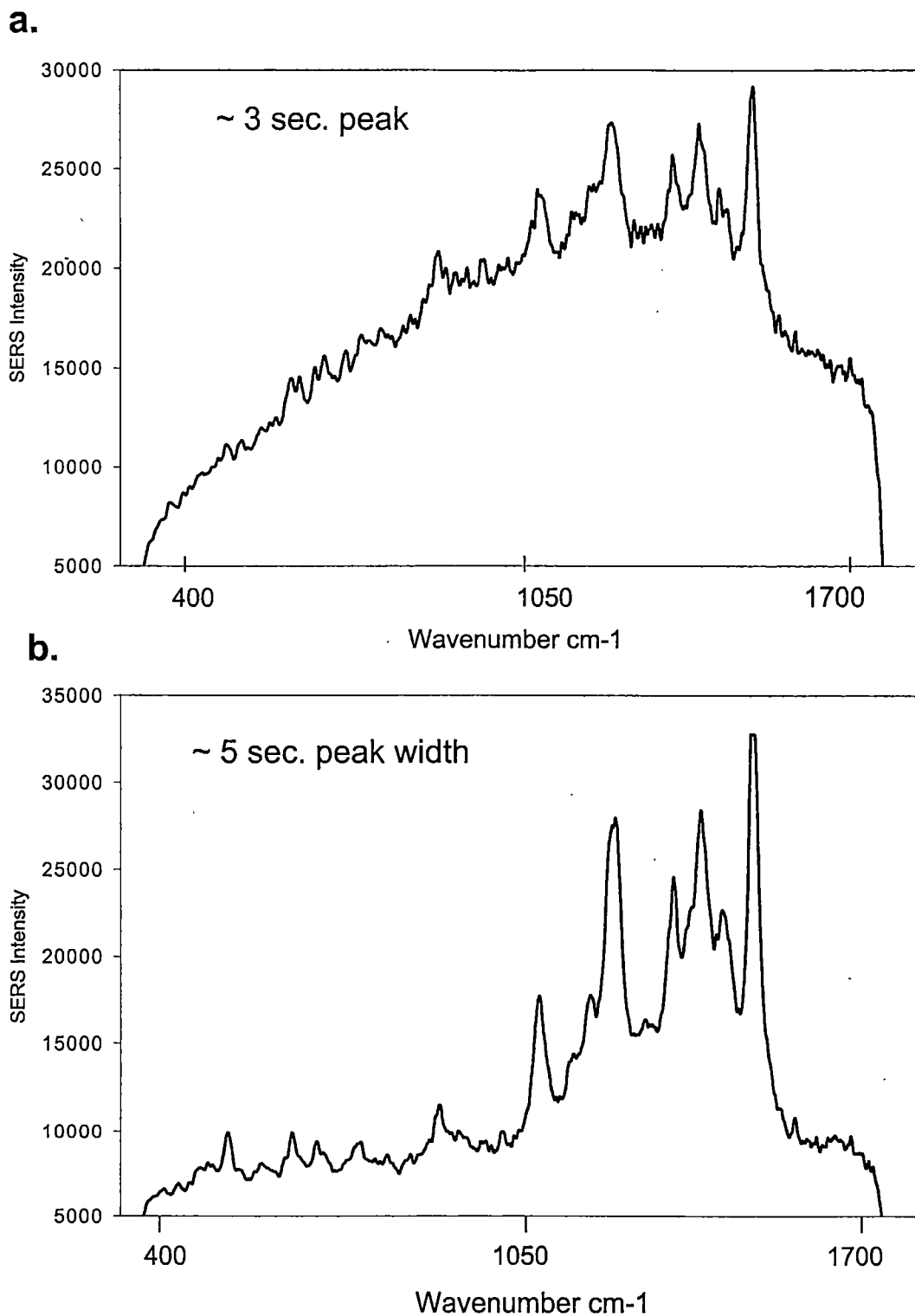


Figure 4.6 SERS spectra of 10^{-9} M erythrosin B injected and EF deposited onto the SERS-substrate; (a) before washing the deposited CE band with water and (b) after washing the deposited CE band with water. Conditions are described in the experimental section.

greatly improve the spectrum. Possibly, the dried running buffer is being preferentially dissolved into the water, allowing the erythrosin B molecules to be in close contact to the silver surface. The effective temporal width of the electropherogram peaks broadened from ~ 3 sec to ~ 5 sec after washing with water. A self-assembled monolayer (SAM) formed on the colloidal surface reduced the broadening. Although the running buffer does not affect the SERS signal of every compound, these effects should be further investigated considering the complexity of some CE separation buffers (e.g. micelle solutions and cyclodextrins).

The above experiments demonstrate one advantage of off-column detection; the separation and detection are separated in time and space, thus allowing the SERS-active substrate to be optimized after EF deposition. Additionally, the off-column detection permits the use of long exposure times, which will increase the signal-to-noise ratios. In SERS analyses, either increasing the laser power or increasing the exposure time of the detector can improve the signal-to-noise. As expected in Figure (4.7a), the signal-to-noise ratios of the Raman bands for the fluorescent dye Rhodamine 6G are increased with extended exposure times. However as shown in Figure (4.7b), as the laser power is increased the Raman spectrum degrades. Potentially at high laser powers, a carbon layer could be created by the photodecomposition of the analyte. Admittedly, photodecomposition is a greater problem for a compound like rhodamine 6G because of its high absorption coefficient at the laser wavelength. In solution work, due to constant replenishing of the molecules at the

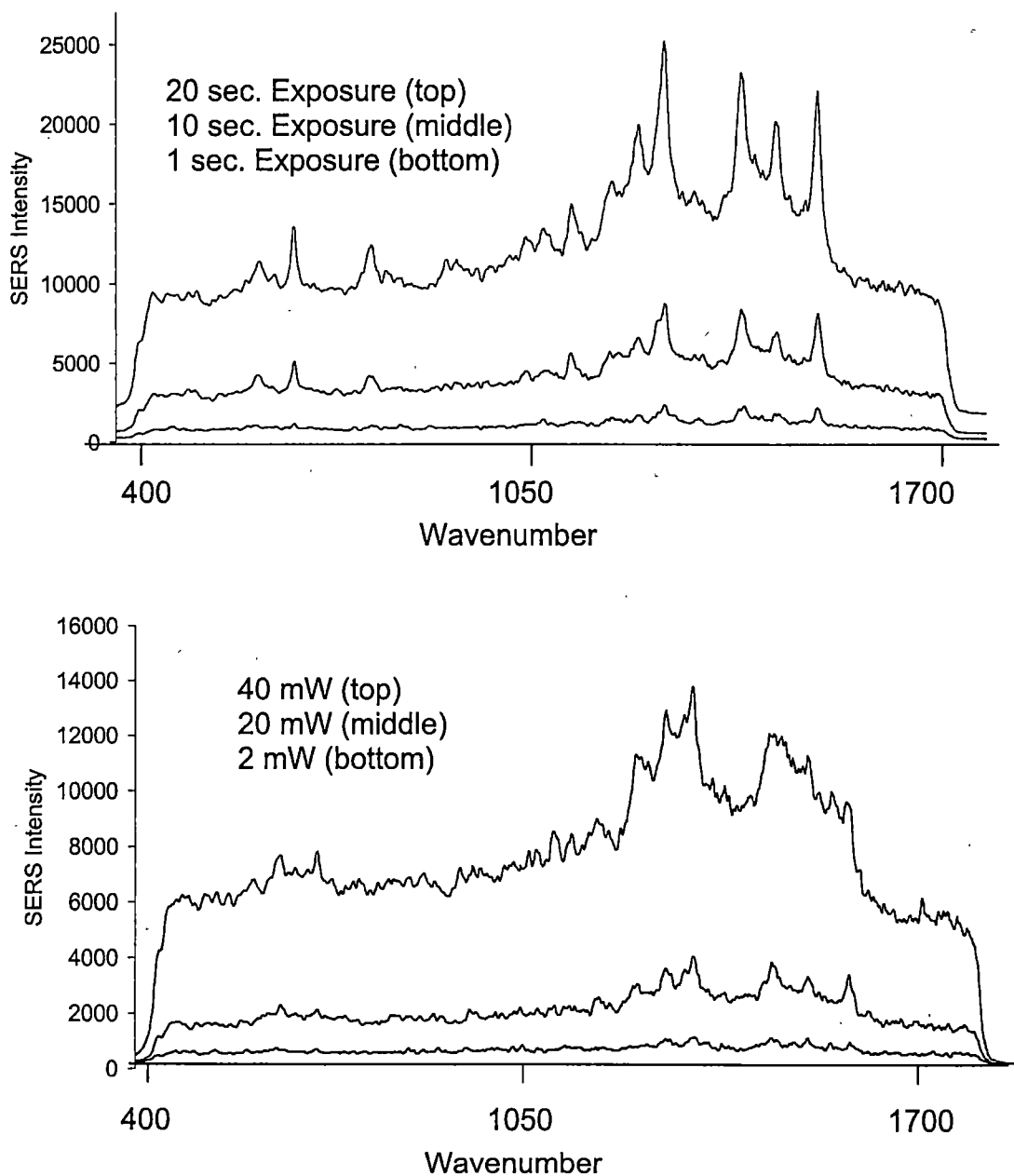


Figure 4.7 SERS spectra of rhodamine 6G: (a) showing the effects of increasing the diode-array exposure time and of (b) increasing the laser power. A solution of 10^{-8} M rhodamine 6G diluted in CE buffer was EF deposited onto the SERS substrate. Conditions are described in the experimental section.

colloid surface, higher laser powers can be used (e.g., our prior on-column CE-SERS report) [170]. Nevertheless, long exposure times are not an available option for on-column detection techniques.

Evaluation of CE/SERS Technique

The compounds that have been chosen to demonstrate the CE-SERS technique are compounds of biological significance: benzyloxyresorufin (BzRes), resorufin, and riboflavin. At the running buffer pH, BzRes is a neutral relatively non-fluorescent compound, whereas riboflavin and resorufin are negatively charged and exhibit good fluorescent quantum yields. For riboflavin and resorufin, the relevant excitation λ_{max} values are 475 and 565 nm and the emission λ_{max} values are 520 and 590 nm. Resonance enhanced Raman signals without interfering fluorescence may be achieved at the metal surface. Several examples of SERS spectra for riboflavin (vitamin B₂) appear in the literature [170,174]. BzRes and resorufin are the substrate/product pair used in enzyme-based assays. Their structures and fluorescence excitation/emission spectra are shown in Figure (4.8). To our knowledge, this is the first time that SERS spectra have been reported for these two compounds. Traditionally, fluorescence has been used to monitor the resorufin-based assay reactions, by detecting a highly fluorescent product (resorufin) that is produced from the reaction of an enzyme with a weakly fluorescent substrate (BzRes) [175].

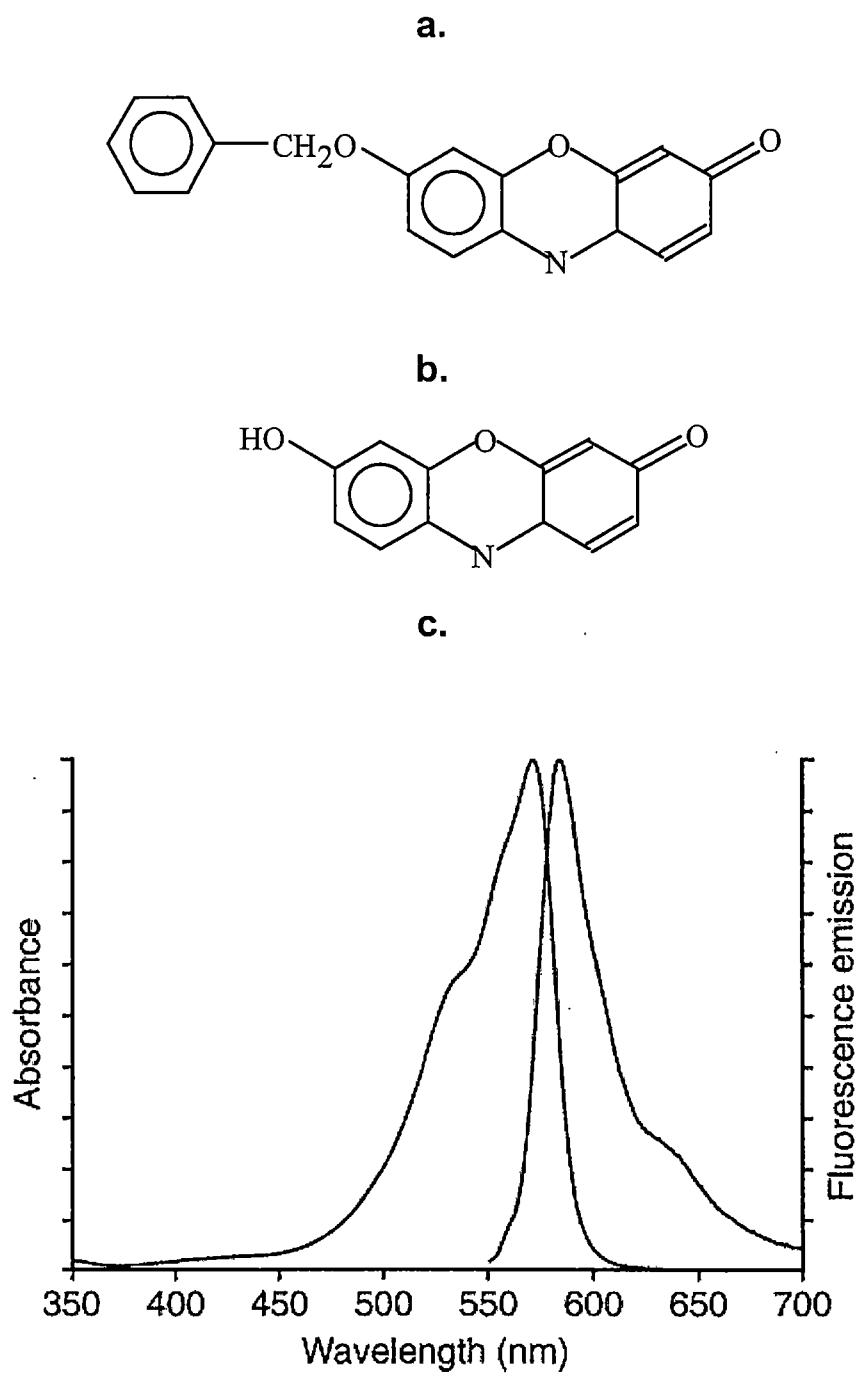


Figure 4.8 The structures of (a) benzyloxyresorufin and (b) resorufin used in the SERS experiments. The fluorescence emission and excitation spectra for resorufin.

Several examples of using CE with laser-induced fluorescence (LIF) and UV-Vis absorption detection for enzyme and enzyme-based assays appear in the literature [176,177]. Potentially, CE-SERS is an alternative technique that may provide unambiguous detection of reactants and products in complex-biological assays.

A 10^{-5} M test mixture was injected onto the CE column, separated, and EF deposited onto a plain-SERS-active substrate. In Figure (4.9), the on-column electropherogram and the off-column electropherogram bands are compared. The on-column electropherogram was measured at the LIF cell, whereas the off-column electropherogram bands were reconstructed by scanning across the SERS substrate. A specific Raman band, as specified in Figure (4.10), was plotted as a function of time to recreate the electropherogram from the EF deposited analytes. Due to the limitation of the data acquisition software, a 3-dimensional plot of time (or position on substrate) vs wavenumber vs intensity could not be obtained. Of course, an advantage of the off-column approach is that real time acquisition and storage of extensive amounts of spectral data, much of which is useless, is not required. The full SERS spectrum in Figure (4.10) was obtained only at the electropherogram peak maximum. For these experiments, the substrates were not washed with water after the analytes had been EF deposited. The average on-column efficiencies were 156,000 plates/m, compared to the average off-column efficiencies of 100,000 plates/m. The 36% decrease in efficiency is due to the EF process and to band broadening occurring

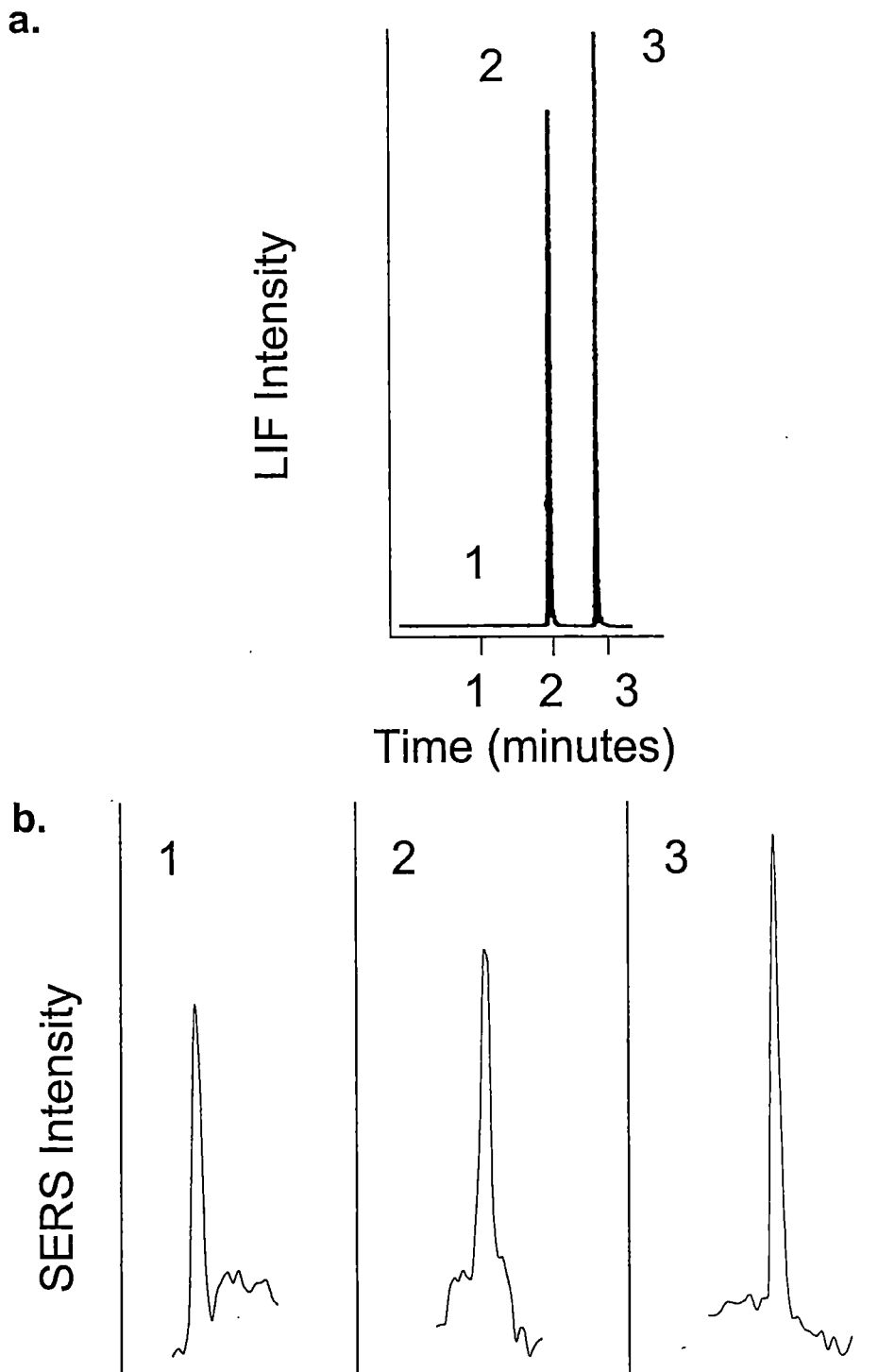


Figure 4.9 Electropherograms of a 10^{-5} M mixture of (1) BzRes, (2) riboflavin, and (3) resorufin: (a) the on-column LIF detection and (b) the off-column SERS detection. The wavenumber of the Raman band that was used to reconstruct the electropherograms is shown in Figure 4.10. Conditions are described in the experimental section.

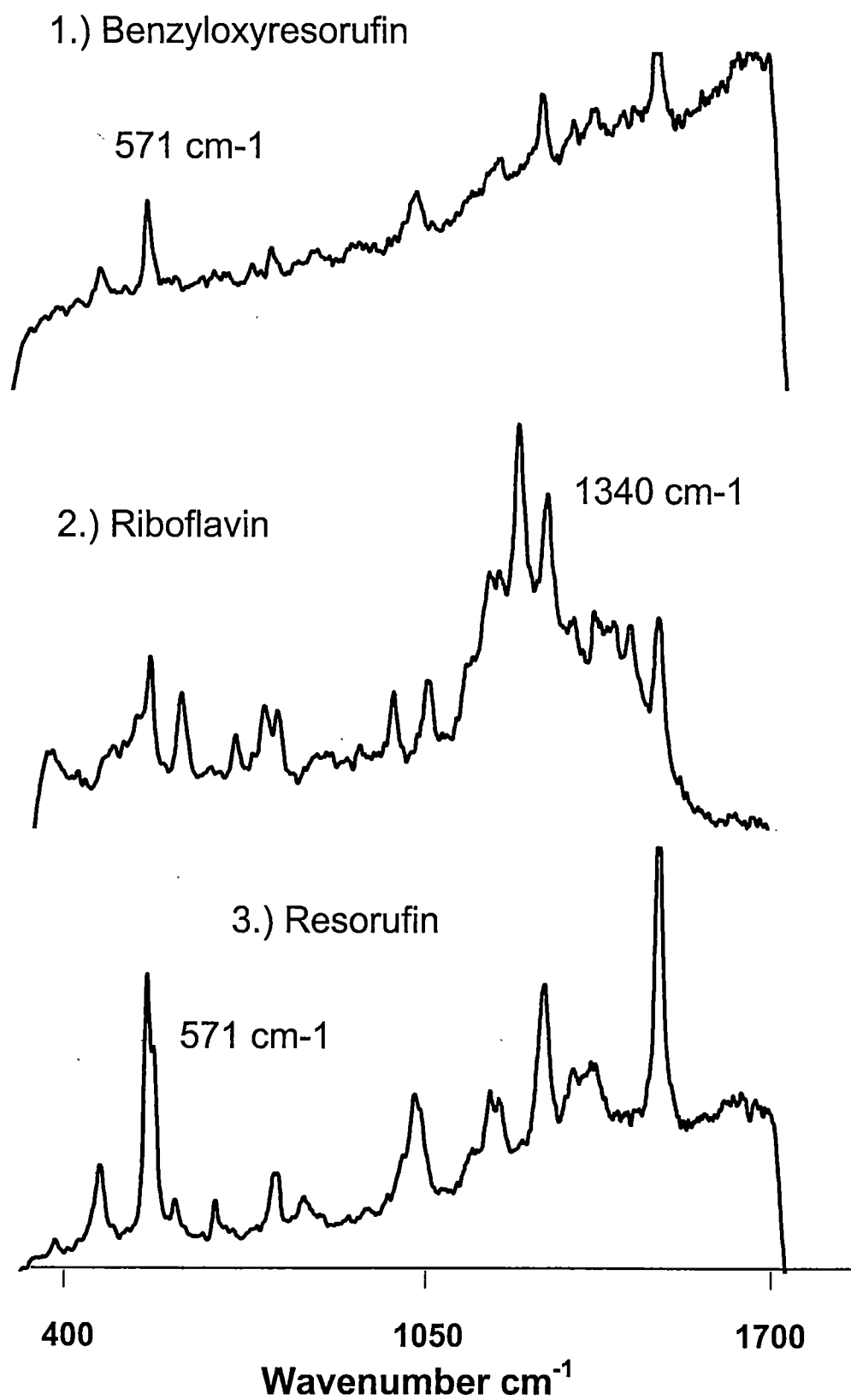


Figure 4.10 The full SERS spectra obtained at the maximum of the CE bands in Figure 4.9b. Conditions are described in the experimental section.

post deposition on the SERS substrate. In spite of that, the advantages of obtaining information-rich spectra greatly outweigh the loss of some separation efficiency. The reproducibility of the SERS signal measured at the 571 cm^{-1} Raman band was 11 % RSD for five injections of 10^{-5} M resorufin. This not only reflects the reproducibility of the SERS measurement, but also the CE and EF processes. For plain-SERS substrates, SERS spectra with major Raman bands exhibiting S/N ratios greater than 3 were obtained for a 3.2-nL injection of resorufin at a concentration of 10^{-6} M (706 fg).

In off-column SERS detection, a variety of substrates can be used to potentially improve the detection performance. For example, an organic layer formed by a self-assembled monolayer (SAM) could be used to concentrate the analyte on the SERS surface through selective absorption. Many examples of SAMs formed on gold and silver surfaces can be found in the literature [178-181]. For the following experiments, dodecanethiol was used to form a SAM on the deposited silver nanoparticles. The alkanethiols can easily form strong Ag-S bonds. Modification of the silver surface with a self-assembled monolayer (SAM) has the potential to improve the detection limits and reduce the on-substrate band broadening.

The dodecanethiol reaction with the silver substrates was optimized with respect to the dodecanethiol concentration and the reaction time. As shown in Figure (4.11), a maximum SERS intensity was achieved for substrates that were immersed for a time of 15 minutes in a 4-mM dodecanethiol solution. By changing the concentration and time of reaction, the surface density of the dodecanethiol

a.

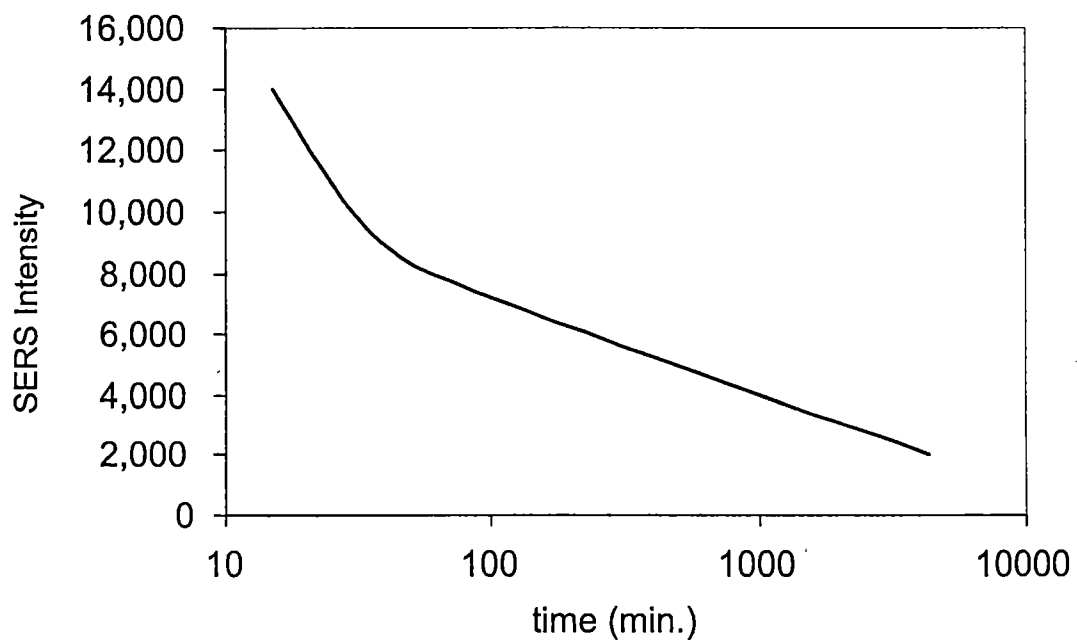
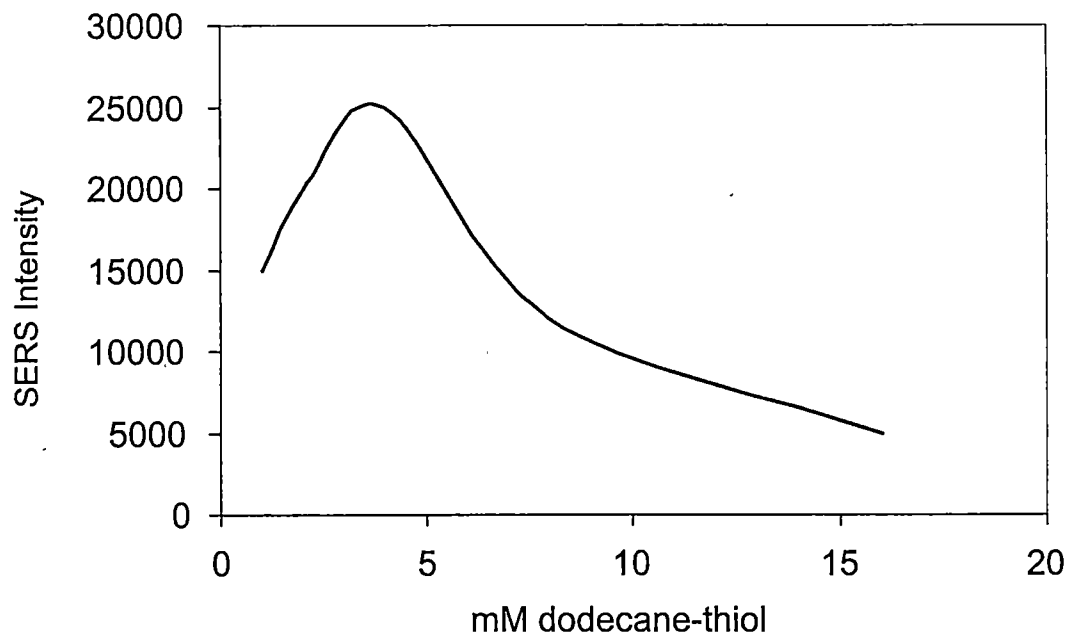


Figure 4.11 Plots of (a) concentration and (b) reaction time for the dodecanethiol self-assembled monolayer formation.

on the SERS substrate was optimized. At the previously specified conditions (4-mM for ~ 15 min.), the EF deposited analytes were effectively concentrated, as well as positioned in close proximity to the roughened SERS substrate. At lower surface densities, the SAM would not adequately concentrate the EF deposited analytes. At higher surface densities, the EF deposited analytes would be adequately concentrated, however their position relative to the roughened surface may not be optimized.

In Figure (4.12), calibration curves are demonstrated for the plain- and dodecane-SERS substrates. For these experiments, the analytes were diluted in CE buffer and EF deposited onto the SERS substrates at a translation rate of 1.0 cm/min. As can be inferred from the calibration curves, EF depositing the analyte onto a SAM resulted in improved sensitivity. The detection limits for resorufin EF deposited onto the plain- and dodecane-SERS substrates were 10^{-6} M and 10^{-7} M, respectively. The width of the deposited band for the plain-SERS substrate (no SAM) was ~ 375 μ m, which was decreased to ~ 175 μ m for the dodecane-SERS substrate. The analytes were more spatially focused (i.e. concentrated) on the SAM surface, which may have contributed to the increased sensitivity for the dodecane substrate. Additionally through selective absorption of the analytes by the SAM, improvements in sensitivity could be a result of reducing any detrimental electrostatic or steric interactions between the analyte, the buffer, and the silver surface. Furthermore, the properties of the SAM (e.g. the dielectric constant) could further enhance the local electric fields present at the surface of the colloidal silver, thus increasing the SERS signal [182]. After

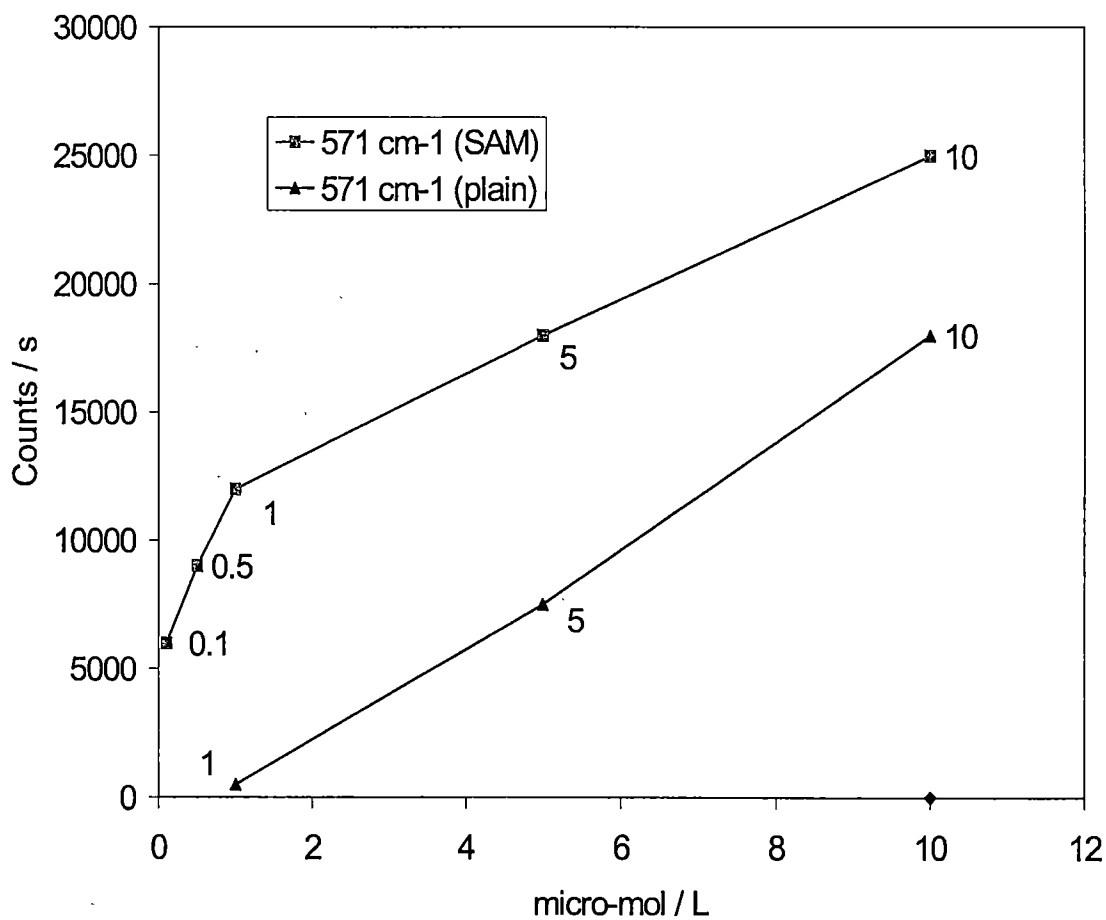


Figure 4.12 Calibration curves for resorufin EF deposited onto a plain-SERS substrate and onto a dodecane-SERS substrate. The resorufin Raman band at 571 cm^{-1} was used for calibration. Conditions are described in the experimental section.

deposition of the analytes, the SAM substrates were washed with water, which resulted in only a marginal increase in effective track width on the SERS substrate (from $\sim 175 \mu\text{m}$ to $\sim 200 \mu\text{m}$). This is a substantial improvement over the plain-SERS substrates. In addition to the above advantages, an added dimension of selectivity could be obtained by applying highly selective SAM, such as with thiolated cyclodextrins, to the substrate [183].

For the experimental set-up demonstrated in this paper, the on-column detection technique (either UV-Vis, LIF, or electrochemical methods) could provide quantitative analysis, whereas the off-column SERS technique could provide analyte identification. However, to reach its full analytical potential, quantitative and qualitative analysis should be accomplished simultaneously by SERS. For the dodecane-SERS substrate, the calibration has two distinct regions: one from 10^{-7} to 10^{-6} M, and a second one from 10^{-6} to 10^{-5} M. The first region may correspond to the distributed mass range leading up to the completion of a molecular monolayer on the SERS substrate or, more likely, occupation of the most SERS-active sites. The first layer of molecules would result in a more dramatic SERS effect, which is reflected in the steeper slope. The second region may result from molecules being distributed less optimally on the substrate [184]. If a wider dynamic range was achievable, it is expected that the plain-SERS substrate would also have two regions. Nevertheless, quantitative analysis should be possible for both types of substrates.

Chapter 5. SUMMARY AND FUTURE STUDIES

In many respects, CE has approached the mature stage of its development, however for CE to reach its full potential advances are needed in the development of more selective and sensitive detectors. A technique that efficiently preserves the separation on a planar substrate would result in opportunities for new detection strategies. In the work previously described, the electrofilament mode of electrospray was successfully developed to deposit the effluent from a CE column onto a planar substrate. This was the first time that ES conditions had been optimized to produce a liquid filament for the purpose of depositing spatially focused bands. With the application of the EF voltage, a decrease in on-column separation performance was observed. However, by raising the inlet of the CE column a hydrodynamic flow was generated that reduced the adverse EF effects. Under optimized conditions, the on-column CE separation was deposited with only a marginal decrease in the efficiency and resolution. Potentially, the advantages of an off-column technique would greatly outweigh this minimal loss of separation performance.

To demonstrate the usefulness of the EF technique, the CE effluent was deposited onto planar substrates; subsequently, two-dimensional separations and SERS-based detection was demonstrated. For the 2D separations, CE was combined with TLC for the first time to separate

the enantiomers of several amino acids. The off-column approach allowed independent optimization of the general and enantiomeric separation conditions, which was shown to be problematic with conventional one-dimensional CE. Additionally, when compared to one-dimensional CE there was a considerable increase in peak capacity. The CE-TLC technique offers an alternative approach to multidimensional separations when analyzing volume-limited complex samples.

Developing a SERS-based detection technique for CE, clearly demonstrated the advantages of the off-column approach. By employing EF deposition, the effluent from a CE column was efficiently transferred onto a SERS-active substrate, subsequently distinctive SERS spectra of the CE separated analytes were obtained. This was the first time that SERS was used as an off-column detection method for CE. Although very little effort was spent on assigning the observed bands to particular vibrational modes, clearly the information-rich spectra will be valuable for identifying peaks in complex samples. An advantage of the off-column approach is the separation and the detection techniques are de-coupled in time and space, which allows the SERS substrates and Raman conditions to be optimized independently to reduce the background and obtain the best SERS signals. Successfully separating, detecting, and obtaining distinctive spectra of biological-assay compounds, such as resorufin, demonstrates one of the many potential applications for the CE-SERS technique.

The author acknowledges that continued development of the EF deposition technique would be beneficial, for example monitoring of the EF current and better control of the sheath-solution flow rate. However, the more significant advances will occur through research and development of novel detection strategies. For SERS-based detection significant improvements could be realized by nano-fabricating substrates with the most SERS-active sizes, shapes, and interstitial spacing. Thus, generating a substrate with higher field enhancements that occur uniformly across the surface.

References

References

1. Pennisi E. *Science* **2000**, 290, 2220.
2. Kheterpal, I.; Mathies, R.A. *Anal. Chem.* **1999**, 71, 31A.
3. Krylov, S.N.; Dovichi, N.J. *Anal. Chem.* **2000**, 72, 111R.
4. Figeys, D.; Pinto, D. *Anal. Chem.* **2000**, 72, 330A.
5. Culbertson, C.T.; Jacobson, S.C.; Ramsey, J.M. *Anal. Chem.* **2000**, 72, 5814.
6. Meldrum, D. *Genome Res.* **2000**, 10, 1288.
7. Sanders, G.H.W.; Manz A. *Tract-Trend Anal. Chem.* **2000**, 19, 364.
8. Gaus, H.J.; Kung, P.P., Brooks, D., Cook P.D.; Cummins, L.L. *Biotech. Bioeng.* **1998**, 61, 169.
9. Venton, D.L.; Woodbury, C.P. *Chemomet. Intell. Lab. Sys.* **1999**, 48, 131.
10. Zander, C. *Fresen. J. Anal. Chem.* **2000**, 366, 745.
11. Michaelis, L. *Biochem. Z.* **1909**, 16, 81.
12. Tiselius, A. *Trans. Faraday Soc.* **1937**, 33, 524.
13. Oda, R.P.; Landers, J.P. *Handbook of Capillary Electrophoresis*, 2nd Ed; Landers, J.P. Ed.; CRC Press: Boca Raton, FL, **1997**, pp 14.
14. *Handbook of Instrumental Techniques for Analytical Chemistry*; Settle, F.A. Ed.; Prentice Hall: Upper Saddle River, NJ, **1997**, pp 165.
15. Csapo, Z.; Gerstner, A.; Sasvari-Szekely, M.; Gutman, A. *Anal. Chem.* **2000**, 72, 2519.

16. Studier, F.W. Trends Biochem. S. **2000**, 25, 588.
17. Hjertter, S. Chromatogr. Rev. **1967**, 9, 122.
18. Virtanen, R. Acta Polytechnica Scand. **1974**, 123, 1.
19. Mikkers, F.E.P.; Everaerts, F.M.; Verheggen, P.E.M. Chrom. 11, 442.
20. Jorgenson, J.W.; Lukacs, K.D. Anal. Chem. **1981**, 53, 1298.
21. Jorgenson, J.W.; Lukacs, K.D. Science **1983**, 222, 266.
22. Gordon, M.J.; Xiaohua, H.; Stephen, P.L.; Zare, R.N. Science **1988**, 242, 224.
23. Anon Science **1998**, 239, 1377.
24. Warner, M. Anal. Chem. **1988**, 60, 1159A.
25. Handbook of Capillary Electrophoresis, 2nd Ed; Landers, J.P. Ed.; CRC Press: Boca Raton, FL, **1997**.
26. High Performance Capillary Electrophoresis – An Introduction, 2nd Ed; Heiger, D.N. Ed.; Hewlett Packard Co.: France, **1992**.
27. Helmholtz, H.Z. Annal. Phys. Chem. **1879**, 7, 337.
28. Issaq, H.J. Electrophoresis **2000**, 21, 1921.
29. Terabe, S.T.; Otsuka, K.; Ando, T. Anal. Chem. **1985**, 57, 834.
30. Sepaniak, M.J.; Cole, R.O. Anal. Chem. **1987**, 59, 472.
31. Quirino, J.P.; Terabe, S. J. Chrom. A. **1999**, 856, 465.
32. Guttman, A., Handbook of Capillary Electrophoresis, 2nd Ed; Landers, J.P. Ed.; CRC Press: Boca Raton, FL, **1997**, pp 75.
33. Vespalec R.; Bocek, P. Chem. Rev. **2000**, 100, 3715.
34. Beckers, J.L.; Bocek, P. Electrophoresis **2000**, 21, 2747.

35. Osbourn, D.M.; Weiss, D.J.; Lunte, C.E. *Electrophoresis* **2000**, 21, 2768.
36. Swinney, K.; Bornhop, D. *Critical Rev. Anal. Chem.* **2000**, 30, 1.
37. Swinney, K.; Bornhop, D. *Electrophoresis* **2000**, 21, 1239.
38. Pentoney, S.L.; Sweedler, J.V., *Handbook of Capillary Electrophoresis*, 2nd Ed; Landers, J.P. Ed.; CRC Press: Boca Raton, FL, **1997**, pp 379.
39. Yeung, E.S. *Acc. Chem. Res.* **1989**, 22, 125.
40. Waldron, K.C.; Dovichi, N.J. *Anal. Chem.* **1992**, 64, 1396.
41. Swaile, D.F.; Sepaniak, M.J. *J. Liq. Chromatogr.* **1991**, 14, 869.
42. Craig, D.B.; Arriaga, E.; Wong, J.C.Y.; Lu, H.; Dovichi, N.J. *Anal. Chem.* **1998**, 70, 39A.
43. Craig, D.B.; Arriaga, E.; Wong, J.C.Y.; Lu, H.; Dovichi, N.J. *Am. Chem. Soc.* **1998**, 118, 5254.
44. Kuhr, W.G.; eung, E.S. *Anal. Chem.* **1988**, 60, 2642.
45. Nann, A.; Pretsch, E. *J. Chromatogr. A* **1994**, 676, 437.
46. Kar, S; Dasgupta, P.K.; Liu, H.; Hwang, H. *Anal. Chem.* **1994**, 66, 2537.
47. Lin, H.; Xu, D.K.; Chen, H.K. *J. Chromatogr. A* **1997**, 760, 227.
48. Swinney, K.; Bornhop, D.J. *J. Microcol. Sep.* **1999**, 11, 596.
49. Walker III, P.A.; Morris, M.D. *J. Chromatogr. A* **1998**, 805, 269.
50. Nirode, W.F.; DeVault, G.L.; Sepaniak, M.J.; Cole, R.O. *Anal. Chem.* **2000**, 72, 1866.
51. Olson, D.L.; Lacey, M.E.; Webb, A.G.; Sweedler, J.V. *Anal. Chem.* **1999**, 71, 3070.
52. Pentoney, S.L.; Zare, R.N.; Quint, J.F. *Anal. Chem.* **1989**, 61, 1642.

53. Odake, T.; Kitamori, T.; Sawada, T. *Anal. Chrm.* **1995**, 67, 145.
54. Severs, J.C.; Smith, R.D. *Handbook of Capillary Electrophoresis*, 2nd Ed; Landers, J.P. Ed.; CRC Press: Boca Raton, FL, **1997**, pp 791.
55. Preisler, J.; Hu, P.; Rejtar, T.; Karger, B.L. *Anal. Chem.* **2000**, 72, 4785.
56. Somsen, G.W., Coulter, S.K., Gooijer, C.; Velthorst, N.H.; Brinkman, U.A.Th. *Anal. Chim. Acta* **1997**, 349, 189.
57. *Handbook of Instrumental Techniques for Analytical Chemistry*; Settle, F.A. Ed.; Prentice Hall: Upper Saddle River, NJ, **1997**, pp 481.
58. Xu, X.; Koeijer, J.A.; Moel, J.J.M.; Logtenberg, H. *Int. J. Forensic Document Examiners* **1997**, 3, 240.
59. Waterval, J.C.M.; Lingeman, H.; Bult, A.; Underberg, W.J.M. *Electrophoresis* **2000**, 21, 4029.
60. Willard, H.H.; Merritt, L.L.; Dean, J.A.; Settle, F.A., *Instrumental Methods of Analysis*, 6th ed; D. Van Nostrand Co.: New York, NY, **1981**, pp 109.
61. Fuller, R.R.; Moroz, L.L.; Gillette, R.; Sweedler, J.V. *Neuron* **1998**, 20, 173.
62. Roberts, K.P.; Lin, C.H.; Jankowiak, R.; Small, G.J. *J. Chrom. A.* **1999**, 853, 159.
63. Campion, A.; Kambhampati, P. *Chem. Soc. Rev.* **1998**, 27, 241.
64. Ingle, J.D.; Crouch, S.R., *Spectrochemical Analysis*: Prentice-Hall Inc.: Englewood Cliffs, NJ, **1988**, pp 501.
65. Walker, P.A.; Burns, M.A.; Johnson, B.N.; Morris, M.D. *Anal. Chrm.* **1998**, 70, 3766.

66. Kowalchuk, W.K.; Walker, P.A.; Morris, M.D. *Applied Spec.* **1995**, 49, 1183.
67. Liu, K.L.K.; Davis, K.L.; Morris, M.D. *Anal. Chem.* **1994**, 66, 3744.
68. Stevenson, C.L.; Vo-Dinh, T. *Modern Techniques in Raman Spectroscopy*, Laserna, J.J. Ed., John Wiley and Sons, Chichester, **1996**, p 22.
69. Somsen, G.W.; Morden, W.; Wilson, I.D. *J. Chromatogr. A* **1995**, 703, 613.
70. Murray, K.K. *Mass spectrom. Rev.* **1997**, 16, 283.
71. Somsen, G.W.; Van De Nessee, R.J.; Gooijer, C.; Brinkman, U.A.T., Velthorst, N.H. *J. Chromatogr.* **1991**, 552, 635.
72. Tracht, S.E.; Cruz, L.; Stobba-Wiley, C.M.; Sweedler, J.V. *Anal. Chem.* **1996**, 68, 3922.
73. Shultz, L.L.; Shippy, S.; Nieman, T.A.; Sweedler, J.V. *J. Microcol. Sep.* **1998**, 10, 329.
74. Kok, S.J.; Posthumus, R.; Vakker, I.; Gooijer, C.; Brinkman, U.A.T.; Velthorst, N.H. *Anal. Chem. Acta* **1995**, 303, 3.
75. Uchiyama, K. *Bunsekikagaku* **1999**, 48, 737.
76. Banno, K.; Matsuoka, M.; Takahashi, R. *Chromatogr.* **1991**, 32, 179.
77. Chiu, R.W.; Walker, K.L.; Hagen, J.J.; Monnig, C.A.; Wilkins, C.L. *Anal. Chem.* **1995**, 67, 4190.
78. Huang, X.; Zare, R.N. *J. Chromatogr.* **1990**, 516, 185.
79. Tracht, S.; Toma, V.; Sweedler, J.V. *Anal. Chem.* **1994**, 66, 2382.
80. Preisler, J.; Foret, F.; Karger, B.L. *Anal. Chem.* **1998**, 70, 5278.

81. Shultz, L.L.; Shipy, S.; Nieman, T.A.; Swedler, J.V. *J. Microcol. Sep.* **1998**, 10, 329.
82. Bourne, S. *Am. Lab.* **1998**, 30, 17F.
83. Beavis, R.C.; Ens, W.; Main, D.E.; Standing, K.G. *Anal. Chem.* **1990**, 62, 1259.
84. McLeod, G.S.; Axelsson, J.; Self, R.; Derrick, P.J. *Rapid Commun. Mass Spectrom.* **1997**, 11, 214.
85. Kebarle, P.; Tang, L. *Anal. Chem.* **1993**, 65, 972A.
86. Dickens, J.; Sepaniak, M.J. *Environ. Monit.* **2000**, 2, 11.
87. Cai, J.; Henion, J. *J. Chromatogr. A* **1995**, 703, 667-692.
88. Ding, J.; Vouros, P. *Anal. Chem.* **1999**, 71, 378A.
89. Foret, F.; Thompson, T.J.; Vouros, P.; Karger, B.L.; Gebauer, P.; Bocek, P. *Anal. Chem.* **1994**, 66, 4450.
90. Corstjens, H.; Billiet, H.A.H.; Frank, J.; Luyben, K.C.A.M. *Electrophoresis* **1996**, 17, 137.
91. Bateman, K.P. *J. Am. Soc. Mass Spectrom.* **1999**, 10, 309.
92. Monini, M.; Cao, P.; Bard, A.J. *Anal. Chem.* **1999**, 71, 1658.
93. Lee, M.L.; Lazar, I.M. *J. Am. Soc. Mass Spectrom.* **1999**, 10, 261.
94. Smith, A.D.; Moini, M. *Anal. Chem.* **2001**, 73, 240.
95. Timperman, A.; Tracht, S.E.; Sweedler, J.V. *Anal. Chem.* **1996**, 68, 2693.
96. Van Berkel, G.J.; Zhou, F.; Aronson, J.T. *Int. J. Mass Spectrom. Ion Processes* **1997**, 162, 55.
97. Zhou, S.L.; Cook, K.D. *J. Am. Soc. Mass Spectr.* **2000**, 11, 961.

98. Keely, C.A.; Holloway, R.R.; vande Goor, T.; McManigill, D. J. *Chromatogr.* **1993**, 652, 283.
99. Datta, R.; Kotamarthi, V.R. *AiChE J.* **1990**, 916.
100. Rice, C.L.; Whitehead, R. *J. Phys. Chem.* **1965**, 69, 4017.
101. Poole, C.F.; Poole, S.K. *Chromatography Today*, Elsevier, New York **1991**, pp. 708.
102. Yang, L.; Harrata, A.K.; Lee, C.S. *Anal. Chem.* **1997**, 69, 1820.
103. Jeffery, D.J.; Hooker, T.F.; Jorgenson, J.W., *Handbook of Capillary Electrophoresis*, 2nd Ed; Landers, J.P. Ed.; CRC Press: Boca Raton, FL, **1997**, pp 768.
104. Davis, J.M.; Giddings, J.C. *Anal. Chem.* **1983**, 55, 418.
105. Giddings, J.C. *Anal. Chem.* **1984**, 56, 1258A.
106. Jeffery, D.J.; Hooker, T.F.; Jorgenson, J.W., *Handbook of Capillary Electrophoresis*, 2nd Ed; Landers, J.P. Ed.; CRC Press: Boca Raton, FL, **1997**, pp 771.
107. Bushey, M.M.; Jorgenson, J.W. *Anal. Chem.* **1990**, 62, 978.
108. Holland, L.A.; Jorgenson, J.W. *Anal. Chem.* **1995**, 67, 3275.
109. Moore, A.W., Jr.; Jorgenson, J.W. *Anal. Chem.* **1995**, 67, 3448.
110. Poole, C.F. *J. Chromatogr. A* **1999**, 856, 399.
111. Dunbar, B.S. *Two-Dimensional Electrophoresis and Immunological Techniques*; Plenum Press: New York, **1987**.
112. Poole, C.F.; Poole, S.K. *J. Chromatogr. A* **1995**, 703, 573.
113. Moore, A.W., Jr.; Jorgenson, J.W. *Anal. Chem.* **1995**, 67, 3456.

114. Roclin, R.D.; Ramsey, R.S.; Ramsey, J.M. *Anal. Chem.* **2000**, 72, 5244.
115. Somsen, G.W.; Gooijer, C.; Brinkman, U.A.Th. *Trends Anal. Chem.* **1998**, 17, 129.
116. Liu, Y.M.; Sweedler, J.V. *Anal. Chem.* **1996**, 68, 3928.
117. Shi, W.; Davis, J.M. *Anal. Chem.* **1993**, 65, 482.
118. *Selectivity and Optimization in Capillary Electrophoresis*; El Rassi, Z.; Giese, R.W., Eds.; Elsevier Science: Amsterdam, The Netherlands, **1998**; pp 179.
119. Smith, J.T. *Electrophoresis* **1997**, 18, 2377.
120. Terabe, S.; Miyashita, Y.; Ishihama, Y.; Shibata, O.J. *Chromatogr.* **1993**, 636, 47.
121. Cooper, C.L.; Davis, J.B.; Cole, R.O.; Sepaniak, M.J. *Electrophoresis* **1994**, 15, 785.
122. Aboul-Enein, H.Y.; El-Awady, M.I.; Heard, C.M.; Nicholls, P.J. *Biomedical Chromatography* **1999**, 13, 531.
123. Armstrong, D.W.; Feng-Ying, H.; Soon, M.H. *J. Chromatogr.* **1988**, 448, 345.
124. Lepri, L.; Coas, V.; Desideri, P.G.; Checchini, L. *J. Planar Chromatogr.* **1990**, 3, 311.
125. LeFevre, J.W. *J. Chromatogr. A* **1993**, 653, 293.
126. Armstrong, D.W.; Nome, F.; Sino, L.A.; Golden T. *J. Am. Chem. Soc.* **1986**, 108, 1418.

127. Giddings, J.C. Unified Separation Science; Wiley & Sons: New York, **1991**, Chap. 5.
128. Kok, S.J.; Velthorst, N.H.; Gooijer, C.; Brinkman, U.A.Th. Electrophoresis **1998**, 19, 2753.
129. Fleischmann, M.; Hendra, P.J.; McQuillan, A.J. chem. Phys. Lett. **1974**, 26, 163.
130. Mulvaney, S.P.; Keating, C.D. Anal. Chem. **2000**, 72, 145R.
131. Kneipp, K.; Kneipp, H.; Itzkan, I.; Dasari, R.R.; Feld, M.S. chem. Rev. **1999**, 99, 2957.
132. Campion, A.; Kambhampati, P. Chem. Soc. Rev. **1998**, 27, 241.
133. Somsen, G.W.; Coulter, S.K.; Gooijer, C.; Velthorst, N.H.; Brinkman, U.A.Th. Anal. Chim. Acta **1997**, 349, 189.
134. Beljebbar, A.; Sockalingum, G.D.; Angiboust, J.F.; Manfait, M. Spectrochim. Acta A **1995**, 51, 2083.
135. Hildebrandt, P.; Stockburger, M. J. Phys. Chem. **1984**, 88, 283.
136. Tarcha, P.J.; DESaja-Gonzalez, J.; Rodriguez-Llorente, S.; Aroca, R. Applied Spec. **1999**, 53, 43.
137. Pal, T.; Jana, N.R.; Sau, T. Radiat. Phys. Chem. **1997**, 49, 127.
138. Daffertshofer, M.; Port, H. Wolf, H.C. Chem. Phys. **1995**, 200, 225.
139. Zeisel, D.; Deckert, V.; Zenobi, R.; Vo-Dinh, T. Chem. Phys. Lett. **1998**, 283, 381.
140. Deckert, V.; Zeisel, D.; Zenobi, R.; Vo-Dinh, T. Anal. Chem. **1998**, 70, 2646.

141. Nie, S.; Emory, S.R. *Science* **1997**, 275, 1102.
142. Kneipp, K.; Wang, Y.; Kneipp, H.; Perelman, L.T.; Itzkan, I. Dasari, R.R.; Feld, M. *Phys. Rev. Lett.* **1997**, 78, 1667.
143. Vo-Dinh, T. *Trends Anal. Chem.* **1998**, 17, 557.
144. Norrod, K.L.; Sudnik, L.M.; Rousell, D.; Rowlen, K.L. *Applied spec.* **1997**, 51, 994.
145. Gunnarsson L.; Petronis, S.; Kasemo, B.; Xu, H.; Bjerneld, J.; Kall, M. *Nanostr. Mat.* **1999**, 12, 783.
146. Bright, R.M.; Musick, M.D.; Natan, M.J. *Langmuir* **1998**, 14, 5695.
147. Munro, C.H.; Smith, W.E.; Garner, M.; Clarkson, J.; White, P.C. *Langmuir* **1995**, 11, 3712.
148. Kneipp, K.; Kneipp, H.; Manoharan, R.; Hunion, E.B.; Itzkan, I.; Dasari, R.R.; Feld, M.S. *Applied Spec.* **1998**, 52, 1493.
149. Mosier-Boss, P.A.; Lieberman, S.H. *Applied Spec.* **1999**, 53, 862.
150. Dou, X.M.; Ozaki, Y. *Rev. Anal. Chem.* **1999**, 18, 285.
151. Dou, X.M.; Jung, Y.M.; Cao, Z.Q.; Wzaki, Y. *Applied Spec.* **1999**, 53, 1440.
152. Graham, D.; Smith, W.E.; Linacre, A.M.T.; Munro, C.H.; Watson, N.D.; White, P.C. *Anal. Chem.* **1997**, 69, 4703.
153. Kneipp, K.; Kneipp, H.; Dinum, G.; Itzkan, I.; Dasar, R.R.; Feld, M.S. *Applied Spec.* **1998**, 52, 175.
154. Michaels, A.M.; Jiang, J.; Brus, L. *J. Phys. Chem. B* **2000**, 104, 11965.
155. Horvath, E.; Mink, J.; Kristof, J. *Mikrochim. Acta* **1997**, 745.

156. Sockalingum, G.D.; Beljebbar, A.; Morjani, H.; Angiboust, J.F.; Manfait, M. *Biospec.* **1998**, 4, S71.
157. Lee, N.S.; Hsieh, Y.Z.; Paisley, R.F.; Morris, M.D. *Anal. Chem.* **1998**, 60, 442.
158. Xu, H.; Bjerneld, E.J.; Kall, M.; Bojesson, L. *Phy. Rev. Letters* **1999**, 83, 4357.
159. Stewart, S.; Fredericks, P.M. *Spectrochim. Acta Part A* **1999**, 55, 1641.
160. Sulk, R.; Chan, C.; Guicheteau, J.; Gomez, C.; Heyns, J.B.B.; Corcoran, R.; Carron, K. *J. Raman Spectrosc.* **1999**, 30, 853.
161. Vo-Dinh, T.; Stokes, D.L.; Griffin, G.B.; Volkan, M.; Kim, U.J.; Simon, M.I. *J. Raman Spec.* **1999**, 30, 785.
162. Graham, D.; Mallinder, B.J.; Smith, W.E. *Biopolymers* **2000**, 57, 85.
163. Ye, Y.; Hu, J.M.; He, L.; Zeng, Y.E. *Vibrational Spec.* **1999**, 20, 1.
164. Kocsis, L.; Horvath, E.; Kristof, J.; Frost, R.C.; Rede, A.; Mink, J. *J Chromatogr A* **1999**, 845, 197.
165. Horvath, E.; Katay, G.; Tyihak, E.; Kristof, J.; Redey, A. *Chromatogr* **2000**, 51, Part 2, S297.
166. Szabo, N.J.; Winefordner, J.D. *Appl. Spectrosc.* **1997**, 51, 965.
167. Roth, E.; Kiefer, W. *Applied Spec.* **1994**, 48, 1193.
168. Carron, K.T.; Kennedy, B.J. *Anal. Chem.* **1995**, 67, 3353.
169. Kennedy, B.J.; Milofsky, R.; Carron, K.T. *Anal. Chem.* **1997**, 69, 4708.
170. Nirode, W.f.; DeVault, G.L.; Sepaniak, M.J. *Anal. Chem.* **2000**, 72, 1866.
171. Lee, P.C.; Melsel, D. *J. Phys. Chem.* **1982**, 86, 3391.

172. Emory, S.R.; Nie, S. J. Phys. Chem. B **1998**, 102, 493.
173. Norrod, K.L.; Rowlen, K.L. Anal. Chem. **1998**, 70, 4218.
174. Wang, X.M.; Yan, M.D.; Zha, J.J.; Chen, H.Y. J. Electroanal. Chem. **1998**, 451, 187.
175. Crespi, C.L.; Miller, V.P.; Pernman, B.W. Anal. Biochem. **1997**, 248, 188.
176. Eggertson, M.J.; Craig, D.B. Biomed. Chromatogr. **1999**, 13, 516.
177. Bogan, D.P.; Deasy, B.; O'Kennedy, R.; Smyth, M.R. Xenobiotica **1996**, 26, 437.
178. Tsen, M.; Sun, L. Anal. Chim. Acta **1995**, 307, 333.
179. Grabar, K.C.; Freeman, R.G.; Hommer, M.B.; Natan, M.J. Anal. Chem. **1995**, 67, 735.
180. Wachter, E.A.; Storey, J.M.; Sharp, S.L.; Carron, K.T.; Jiang, X. Applied Spec. **1995**, 49, 193.
181. Deschaines, T.O.; Carron, K.T. Applied Spec. **1997**, 51, 1355.
182. Hinde, R.J.; Sepaniak, M.J.; Compton, R.N.; Nordling, J.; Lavrik, N., submitted for publication in Science.
183. Maeda, Y.; Kitano, H. J. Phys. Chem. **1995**, 99, 487.
184. Stokes, D.L., Ph.D. Dissertation, University of Tennessee, **1999**.

Vita

Gerald L. DeVault was born in Johnson City, Tennessee on August 24, 1969. He was raised in Gray Tennessee, where he graduated from Daniel Boone High School in 1987. Subsequently, he entered East Tennessee State University, where he was awarded a Bachelor of Science Degree in Chemistry in May of 1992. In that same month, he started work at Lockheed Martin in Oak Ridge as an analytical chemist. The majority of his time has been spent at the Y12 National Security Complex as an Analytical Development Chemist, where his efforts have been directed toward the development of a wide variety of analytical instruments and techniques. He started taking graduate classes in the spring of 1993 and officially entered the chemistry graduate program in the fall of 1995. While there, he majored in analytical chemistry as a part-time/full-time student under Professor Michael J. Sepaniak. His graduate work involved development of off-column technologies for capillary electrophoresis. He officially received his doctoral degree in analytical chemistry in August, 2001.